Progress In Electromagnetics Research, PIER 17, 91–183, 1997

THE DISCRETIZED MIE-FORMALISM FOR ELECTROMAGNETIC SCATTERING

T. Rother and K. Schmidt

German Aerospace Research Establishment
Remote Sensing Ground Station Neustrelitz
17235 Neustrelitz
Germany

1. Introduction
2. Formulation of the Scattering Problem
2.1 TE/TM-Decomposition in Cylindrical and Spherical Co-ordinates
2.2 Boundary and Continuity Conditions
3. The Method of Lines
3.1 Solution of the Helmholtz Equation in Cylindrical Co-ordinates
3.2 Solution of the Helmholtz Equation in Spherical Co-ordinates
3.3 The Discretized Mie-Formalism and the Rayleigh Hypothesis
4. Derivation of the Characteristic Equation System
4.1 The Discretized Mie-Formalism in Cylindrical Co-ordinates
4.1.1 The Limiting Case of Circular Cylinders
4.1.2 Non-Circular Cross-sections
4.2 The Discretized Mie-Formalism in Spherical Co-ordinates
4.2.1 The Limiting Case of Spheres
4.2.2 Axisymmetric Geometries
4.3 The Iterative Discretized Mie-Formalisms
5. Definition of Scattering Parameters
5.1 Polarimetric Differential Scattering Cross-sections in Cylindrical Co-ordinates
5.2 Polarimetric Differential Scattering Cross-sections in Spherical Co-ordinates

6. Applications
6.1 Circular Cylinders and Spheres
6.2 Non-circular Cylinder
6.3 Axisymmetric Scatterers
7. Conclusion
References

1. INTRODUCTION

Scattering of electromagnetic waves on dielectric structures is a basic physical process and plays an important role in different scientific and technical fields. Due to the increasing interest in remote sensing of the earth and its environment, scattering on objects in the atmosphere (aerosols, ice crystals in clouds) and on structures on the earth surface (ice, vegetation, geological structures) becomes more and more important [1–5]. In astrophysics, the analysis of light scattered by interplanetary and interstellar dust can improve our understanding of the cosmic evolution [6–8]. In biology and chemistry, the scattered light analysis is helpful for the investigation of macromolecules in solutions and, last not least, it's an important diagnostic method in medicine and technics [9–11]. These few examples demonstrate the necessity to deal with scattering in different frequency ranges and on different geometrical configurations. Scattering on spherical particles and infinitely extended circular cylinders can be treated analytically within the Mie theory (strictly speaking, "Mie theory" means scattering on spheres but, since the way of solution for an infinitely extended circular cylinder is very similar, this name will be used for both cases in this paper) [12–18]. Otherwise, numerical methods have to be applied. Unfortunately, there exist only few methods which offer a rigorous electromagnetic approach to this problem. Most of the methods start from assumptions resulting in a restriction of their applicability like the Discrete Dipole Approximation to lower frequencies and permittivities [19, 20], the Ray Tracing technique in the geometric optics approximation to higher frequencies [21, 22], and the perturbation approach to minute deviations from separable geometries [23].

Among the rigorous methods, a variety of Finite-Difference/Finite-Element techniques (FD/FE), the T-matrix approach and the Point Matching method are of special importance to deal with scattering on dielectric objects having a non-separable boundary surface. The common FD/FE techniques start from a complete discretization of the

scattering problem formulated by partial differential equations [24, 25]. This makes these techniques invariably simpler in concept and execution than integral equation approaches. FD/FE techniques are applicable to different geometries and are often the only possibility when dealing with strongly inhomogeneous scatterers. But they suffer from essential disadvantages. It is known that spurious solutions may occur which must be withdrawn by additional filtering procedures. Furthermore, the fulfillment of the radiation condition provides difficulties since the discretization can not be performed up to infinity. Sometimes, this results in very large matrices which must be handled. Due to these problems, computation in electromagnetic scattering has been pursued more often in terms of integral equations. At present, Waterman's T-matrix approach, which is based on the Extended Boundary Condition Method (EBCM), is the most powerful method to compute scattering on different geometries and over wide frequency ranges [26–30]. Since the radiation condition is analytically incorporated by use of the free space Green's function, the final calculation can be restricted to the scatterer surface, and much smaller matrices are obtained. On the other hand, the loss of conceptual simplicity (formulation of the EBCM, singular-kernel problem) requires a higher theoretical effort to derive appropriate convergency criteria. This makes it a difficult method for practitioners. The simplest method of all is Point Matching but, it has uncertain convergence and uses too much computer time. Only if combined with a least-square procedure this method becomes more practicable [17, 32–34]. Thus, the Mie theory for spheres is still the mostly used method in practical applications, and non-spherical particles are often considered by use of its equal-volume or equal-surface sphere although this approximation produces wrong results for the polarization behavior. With the Discretized Mie-Formalism (DMF) presented in this paper it becomes possible to integrate the advantages of the differential and integral equation approaches into one method [35–37]. The DMF can be considered as a numerical generalization of the Mie theory to structures with non-separable boundary surfaces. Therefore, this method is especially suitable for practical applications since the formulation is very similar to what is known from the conventional Mie theory. This is achieved by using the so called Method of Lines (MoL) to solve the basic Helmholtz equations of the scattering problem. The MoL is a special FD technique which allows the analytical incorporation of the radiation condition. In the

last years, this mathematical tool has been applied very successfully to guided wave problems with separable but inhomogeneous boundary conditions [38–42]. In this paper it is demonstrated that it can be used also for non-separable boundary value problems. This expands its range of applicability drastically.

In this contribution, a closed formulation of the DMF in cylindrical and spherical co-ordinates is given. Beside the direct DMF, we also discuss an iterative procedure which has an extended range of applicability and a higher numerical stability. This iterative version turns out to be nothing but a Method of Moment scheme. Finally, different applications are discussed with special emphasis on the derivation of an appropriate convergency criterion. This will demonstrate the usefulness of the proposed method. It's our hope that, with this method we can contribute to a better understanding of non-spherical scattering processes.

2. FORMULATION OF THE SCATTERING PROBLEM

Throughout this paper, we make the following assumptions to formulate the scattering problem:

(a) The medium is assumed to be homogeneous and isotropic inside and outside the scatterer.
(b) We assume a time dependence according to $\exp(-j\omega t)$. Thus, $\exp(jkz)$ describes a wave traveling along the positive z-direction.
(c) The permittivity of the scatterer is given by $\epsilon_s = \epsilon_s' + j\epsilon_s''$, where $\epsilon_s'' \geq 0$. The restriction to only positive imaginary parts of the permittivity is caused by our time dependence and the corresponding expression for the radiation condition. We assume free space outside the scatterer.
(d) We consider only source-free regions.

According to the Mie theory for spheres, the scattering problem is formulated by use of differential equations. For this, we choose the well-known decomposition of the electromagnetic fields into transverse electric (TE) and transverse magnetic (TM) parts with respect to a certain direction [49, 50]. This decomposition is given in cylindrical and spherical co-ordinates, as well.

2.1 TE/TM-Decomposition in Cylindrical and Spherical Coordinates

With the requirements given above the Maxwell's equations read as follows:

$$\nabla \times \vec{E} = j\omega\mu_0 \vec{H} \tag{2.1}$$
$$\nabla \times \vec{H} = -j\omega\epsilon \vec{E} \tag{2.2}$$
$$\nabla \cdot \vec{B} = 0 \tag{2.3}$$
$$\nabla \cdot \vec{D} = 0 \tag{2.4}$$
$$\vec{D} = \epsilon \vec{E} \tag{2.5}$$
$$\vec{B} = \mu_0 \vec{H} \ . \tag{2.6}$$

Due to assumption (d), we can define appropriate vector potentials by the relations

$$\vec{H}^e = \nabla \times \vec{A}_p \tag{2.7}$$
$$\vec{E}^m = \nabla \times \vec{F}_p \ . \tag{2.8}$$

In this way, (2.3) and (2.4) are satisfied automatically. For the vector potentials we get the vector Helmholtz equations

$$\nabla^2 \vec{A}_p + k^2 \vec{A}_p = 0 \tag{2.9}$$
$$\nabla^2 \vec{F}_p + k^2 \vec{F}_p = 0 \qquad \text{with} \qquad k^2 = \omega^2 \epsilon \mu_0 \ . \tag{2.10}$$

If these potentials are known, any field is given by a superposition of the fields belonging to each of these potentials [49], i.e.,

$$\vec{E} = \vec{E}^e + \vec{E}^m = \nabla \times \vec{F}_p + \frac{j}{\omega\epsilon}[\nabla\nabla \cdot \vec{A}_p + k^2 \vec{A}_p] \tag{2.11}$$
$$\vec{H} = \vec{H}^e + \vec{H}^m = \nabla \times \vec{A}_p - \frac{j}{\mu_0}[\nabla\nabla \cdot \vec{F}_p + k^2 \vec{F}_p] \ . \tag{2.12}$$

If choosing

$$\vec{A}_p = \hat{c}\Pi_e \qquad \text{and} \qquad \vec{F}_p = \hat{c}\Pi_m, \tag{2.13}$$

(2.11) and (2.12) describe the TE/TM-decomposition with respect to the direction given by the vector $\hat{c}$. From the vector Helmholtz equations (2.9) and (2.10) two scalar equations for the so-called Debye potentials Π_e and Π_m are obtained.

In the cylindrical co-ordinate system $\hat{c} = \hat{z}$ is used. The resulting components of the electric field are given by

$$E_z = \frac{j}{\omega\epsilon}\left[\frac{\delta^2\Pi_e}{\delta z^2} + k^2\Pi_e\right] \tag{2.14}$$

$$E_r = \frac{j}{\omega\epsilon}\frac{\delta^2\Pi_e}{\delta z \delta r} + \frac{1}{r}\frac{\delta\Pi_m}{\delta\phi} \tag{2.15}$$

$$E_\phi = \frac{j}{\omega\epsilon}\frac{1}{r}\frac{\delta^2\Pi_e}{\delta z\delta\phi} - \frac{\delta\Pi_m}{\delta r}\ , \tag{2.16}$$

and for the magnetic components we have

$$H_z = -\frac{j}{\omega\mu_0}\left[\frac{\delta^2\Pi_m}{\delta z^2} + k^2\Pi_m\right] \tag{2.17}$$

$$H_r = -\frac{j}{\omega\mu_0}\frac{\delta^2\Pi_m}{\delta z\delta r} + \frac{1}{r}\frac{\delta\Pi_e}{\delta\phi} \tag{2.18}$$

$$H_\phi = -\frac{j}{\omega\mu_0}\frac{1}{r}\frac{\delta^2\Pi_m}{\delta z\delta\phi} - \frac{\delta\Pi_e}{\delta r}\ . \tag{2.19}$$

The Helmholtz equation for the Debye potentials reads

$$\nabla^2\Pi_{e/m} + k^2 r^2\Pi_{e/m} = 0 \tag{2.20}$$

$$\nabla^2 = r\frac{\delta}{\delta r}r\frac{\delta}{\delta r} + r^2\frac{\delta^2}{\delta z^2} + \frac{\delta^2}{\delta\phi^2}\ . \tag{2.21}$$

We can see that equations (2.14)–(2.19) will indeed produce a transverse electric ($E_z = 0$) or transverse magnetic ($H_z = 0$) field if Π_e or Π_m is taken to be zero.

In spherical co-ordinates the vector $\hat{c}$ is chosen to be $\hat{c} = r\cdot\hat{r}$. This leads to the following expressions for the electromagnetic field components:

$$E_r = \frac{j}{\omega\epsilon}\left[\frac{\delta^2(r\Pi_e)}{\delta r^2} + k^2 r\Pi_e\right] \tag{2.22}$$

$$E_\theta = \frac{j}{\omega\epsilon}\frac{1}{r}\frac{\delta^2(r\Pi_e)}{\delta r\delta\theta} + \frac{1}{\sin\theta}\frac{\delta\Pi_m}{\delta\phi} \tag{2.23}$$

$$E_\phi = \frac{j}{\omega\epsilon}\frac{1}{r\sin\theta}\frac{\delta^2(r\Pi_e)}{\delta r\delta\phi} - \frac{\delta\Pi_m}{\delta\theta} \tag{2.24}$$

$$H_r = -\frac{j}{\omega\mu_0}\left[\frac{\delta^2(r\Pi_m)}{\delta r^2} + k^2 r\Pi_m\right] \tag{2.25}$$

$$H_\theta = -\frac{j}{\omega\mu_0}\frac{1}{r}\frac{\delta^2(r\Pi_m)}{\delta r\delta\theta} + \frac{1}{\sin\theta}\frac{\delta\Pi_e}{\delta\phi} \tag{2.26}$$

$$H_\phi = -\frac{j}{\omega\mu_0}\frac{1}{r\sin\theta}\frac{\delta^2(r\Pi_m)}{\delta r\delta\phi} - \frac{\delta\Pi_e}{\delta\theta}\ . \tag{2.27}$$

Now the Helmholtz equation for the Debye potentials is given by

$$\nabla^2\Pi_{e/m} + k^2\Pi_{e/m} = 0 \tag{2.28}$$

$$\nabla^2 = \frac{1}{r}\frac{\delta^2}{\delta r^2}r + \frac{1}{r^2\sin\theta}\frac{\delta}{\delta\theta}\sin\theta\frac{\delta}{\delta\theta} + \frac{1}{r^2\sin^2\theta}\frac{\delta^2}{\delta\phi^2}\ . \tag{2.29}$$

It's our essential problem to solve these scalar Helmholtz equations for the Debye potentials for cases in which the boundary surface of the scatterer doesn't coincide with a co-ordinate line, i.e., the boundary has an angular dependence in the corresponding co-ordinate system. That's what is called a non-separable boundary value problem in scattering.

To find the complete and unique solution of the internal and scattered field, additional boundary and continuity conditions are needed. These conditions will be discussed in the next section.

2.2 Boundary and Continuity Conditions

First, let's have a look at the conditions for the radial part of the solutions. Inside the scatterer (especially at the origin $r = 0$) the fields must behave regular, i.e., there should be no singularities since a source-free region is assumed. In the far field region outside the scatterer the radiation condition has to be fulfilled. This condition states that no energy may be radiated from infinity into the direction of the scatterer. Mathematically, this requirement is given by the equation [51]

$$\lim_{r\to\infty} r\left[\frac{d\Pi(r)}{dr} - jk\Pi(r)\right] = 0\ . \tag{2.30}$$

As we will see later, the application of this radiation condition will withdraw one of the linearly independent solutions of the ordinary differential equations depending only on the radial co-ordinate.

For the ϕ-dependence the periodicity condition holds in both co-ordinate systems, i.e., the following relation is valid:

$$\Pi(\phi) = \Pi(\phi + 2\pi)\ . \tag{2.31}$$

Additional conditions are needed for the θ-dependence of the potentials in the spherical coordinate system. These are linked to the azimuthal modes of the ϕ-dependence in the following manner [51,53]:

$$\text{azimuthal mode } l = 0: \quad \frac{d\Pi(\theta)}{d\theta} = 0 \quad \text{if } \theta = 0,\, \pi \quad \text{(Neumann)} \tag{2.32}$$

$$\text{azimuthal mode } l \neq 0: \quad \Pi(\theta = 0) = \Pi(\theta = \pi) \equiv 0 \text{ (Dirichlet)} \tag{2.33}$$

All these conditions are valid for both potentials Π_e and Π_m, of course.

To derive the characteristic equation system of the DMF, the continuity conditions for the tangential electromagnetic field components are of special importance. These conditions can be derived from the integral representation of Maxwell's equation. In the boundary layer between different dielectric regions we get [49, 50]

$$\vec{n} \times (\vec{E}_1 - \vec{E}_2) = 0 \tag{2.34}$$

$$\vec{n} \times (\vec{H}_1 - \vec{H}_2) = 0\ . \tag{2.35}$$

In what follows, we generally consider two different regions which are separated by the boundary layers $r = r(\theta)$ and $r = r(\phi)$, respectively. This means that we restrict ourselves to non-spherical but axisymmetric scatterers (NAS) in spherical co-ordinates and to non-circular but infinitely extended cylinders (NIC) within the cylindrical co-ordinate system. Inside the scatterer (Figs. 2 and 3, region 1) we have the internal field $\vec{E}^{int.}$, $\vec{H}^{int.}$. In the outer region (Figs. 2 and 3, region 2), the total field is given by a superposition of the incident and the scattered field $\vec{E}^t = \vec{E}^{inc.} + \vec{E}^s$ and $\vec{H}^t = \vec{H}^{inc.} + \vec{H}^s$. The tangential components have to be continuous across the boundary layer. For this, we need the angle of the tangential plane in each point (r_i, θ_i) of the scatterer surface (see Fig. 1) which is given in spherical co-ordinates by the expression

$$\alpha_i = \arctan\left(\frac{1}{r(\theta)}\frac{dr(\theta)}{d\theta}\right)_{\theta_i}\ . \tag{2.36}$$

Due to the above mentioned restriction to axisymmetric structures, the ϕ-component of the electromagnetic field is always a tangential component. The remaining tangential contribution is obtained by a

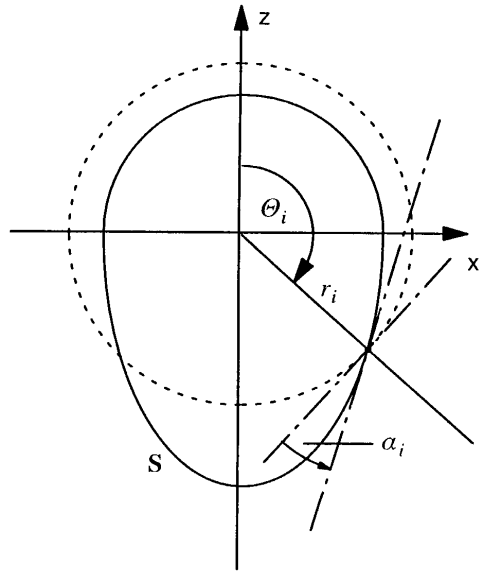

Figure 1. Angle of the tangential plane in (r_i, θ_i) at the scatterer surface S.

combination of the r- and θ-components. Applying this to the continuity conditions (2.34) and (2.35) yields

$$E_\phi^{int.} = E_\phi^{inc.} + E_\phi^s \tag{2.37}$$
$$E_\theta^{int.} + \tan(\alpha_i) \cdot E_r^{int.} = E_\theta^{inc.} + E_\theta^s + \tan(\alpha_i) \cdot [E_r^{inc.} + E_r^s] \tag{2.38}$$
$$H_\phi^{int.} = H_\phi^{inc.} + H_\phi^s \tag{2.39}$$
$$H_\theta^{int.} + \tan(\alpha_i) \cdot H_r^{int.} = H_\theta^{inc.} + H_\theta^s + \tan(\alpha_i) \cdot [H_r^{inc.} + H_r^s] \ . \tag{2.40}$$

For the NIC in cylindrical co-ordinates we have to replace θ by ϕ in (2.36). Now the z-component is already a tangential one, and the other is obtained by combining the ϕ- and r-components of the electromagnetic field:

$$E_z^{int.} = E_z^{inc.} + E_z^s \tag{2.41}$$
$$E_\phi^{int.} + \tan(\alpha_i) \cdot E_r^{int.} = E_\phi^{inc.} + E_\phi^s + \tan(\alpha_i) \cdot [E_r^{inc.} + E_r^s] \tag{2.42}$$
$$H_z^{int.} = H_z^{inc.} + H_z^s \tag{2.43}$$
$$H_\phi^{int.} + \tan(\alpha_i) \cdot H_r^{int.} = H_\phi^{inc.} + H_\phi^s + \tan(\alpha_i) \cdot [H_r^{inc.} + H_r^s] \ . \tag{2.44}$$

Finally, some of the boundary surfaces to which the DMF will be applied are given explicitly.

(a) sphere:

$$r = \text{constant} \tag{2.45}$$

(b) sphere which is shifted by ε on the z-axis:

$$r(\theta) = r_{sphere} \cdot \left[p\cos\theta + (1 - p^2 \sin^2\theta)^{1/2} \right] \tag{2.46}$$

$$\frac{dr(\theta)}{d\theta} = -r_{sphere}\, p \sin\theta \left[1 + \frac{p\cos\theta}{(1 - p^2\sin^2\theta)^{1/2}} \right] \tag{2.47}$$

$$p = \frac{\varepsilon}{r_{sphere}} \ . \tag{2.48}$$

(c) prolate and oblate spheroid:

$$r(\theta) = a \cdot \left[\cos^2\theta + \left(\frac{a}{b}\right)^2 \sin^2\theta \right]^{-1/2} \tag{2.49}$$

$$\frac{dr(\theta)}{d\theta} = -a \sin\theta\cos\theta \cdot \left[\left(\frac{a}{b}\right)^2 - 1 \right] \cdot \left[\cos^2\theta + \left(\frac{a}{b}\right)^2 \sin^2\theta \right]^{-3/2} \tag{2.50}$$

a : semi-axis on the z-axis

b : semi-axis on the x-axis

(d) Chebyshev particle of n-th order:

$$r(\theta) = r_{sphere} \cdot [1 + \varepsilon \cos(n\theta)] \tag{2.51}$$

$$\frac{dr(\theta)}{d\theta} = -n r_{sphere}\, \varepsilon \sin(n\theta) \tag{2.52}$$

ε : deformation parameter

We will use these boundaries also as cross-sections for the infinitely extended cylinders. Additionally, hexagonal cross-sections are treated as basic structures of ice crystals in cirrus clouds.

With the equations discussed in this section, the scattering problem is formulated. In the next chapter we want to derive the solution of the Helmholtz equations (2.20) and (2.28) if non-separable boundary layers are given.

3. THE METHOD OF LINES

From FD-methods the MoL differs in the fact that only one of the independent variables is discretized to reduce the original partial differential equation to a system of ordinary differential equations. For

the geometries which we want to consider in this paper, a discretization with respect to ϕ in cylindrical and θ in spherical co-ordinates, respectively, has to be chosen. This discretzation must be performed in such a way that the lateral boundary conditions are taken into account. An equidistant discretization scheme in the interval $[a_1, a_2]$ is exclusively used throughout this paper. Of course, this restriction is not necessary but it reduces the numerical effort to solve the related eigenvalue problem. How a non-equidistant discretization can be performed is discussed in detail in [38].

Because of the equations (2.31), (2.32) and (2.33) the following variations have to be taken into account:

(a) homogeneous Dirichlet condition in a_1 and a_2 (DC):

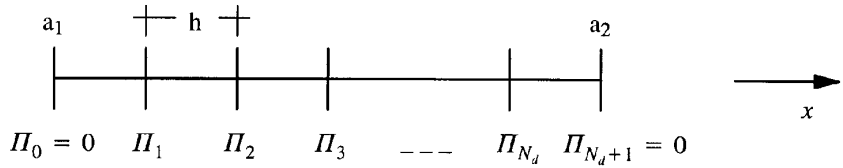

(b) homogeneous Neumann condition in a_1 and a_2 (NC):

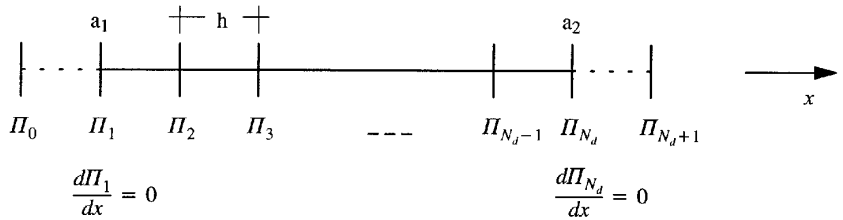

(c) periodicity condition (PC):

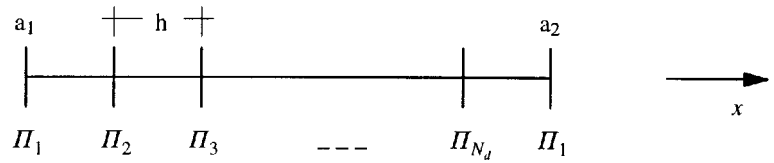

Now the first and second derivatives with respect to ϕ or θ can be replaced by an appropriate left hand side, right hand side or centered

difference operator (subscript l, r, c or z).

$$\frac{\delta}{\delta x} \quad \Longrightarrow \quad \frac{1}{h}\overleftrightarrow{D}_l^{(\alpha)} \quad \Longrightarrow \quad \frac{1}{h}\overleftrightarrow{D}_r^{(\alpha)} \quad \Longrightarrow \quad \frac{1}{2h}\overleftrightarrow{D}_c^{(\alpha)} \tag{3.1}$$

$$\frac{\delta^2}{\delta x^2} \quad \Longrightarrow \quad -\frac{1}{h^2}\overleftrightarrow{D}_z^{(\alpha)} \tag{3.2}$$

$\alpha = \text{DC, NC, PC}$

These difference operators are matrices of the order $(N_d \times N_d)$, where N_d denotes the number of discretization lines in the interval $[a_1, a_2]$, and read as follows:

$$\overleftrightarrow{D}_l^{(\alpha)} = \begin{pmatrix} l_1 & 0 & \cdots & \cdots & \cdots & \cdots & 0 & l_2 \\ -1 & 1 & 0 & \cdots & \cdots & \cdots & \cdots & 0 \\ 0 & -1 & 1 & 0 & \cdots & \cdots & \cdots & 0 \\ \vdots & 0 & \ddots & \ddots & \ddots & \vdots & \vdots & \vdots \\ \vdots & \vdots & \ddots & \ddots & \ddots & 0 & \vdots & \vdots \\ 0 & \cdots & \cdots & 0 & -1 & 1 & 0 & 0 \\ 0 & \cdots & \cdots & \cdots & 0 & -1 & 1 & 0 \\ 0 & \cdots & \cdots & \cdots & \cdots & 0 & l_3 & l_4 \end{pmatrix} \tag{3.3}$$

with

	DC	NC	PC
l_1	1	0	1
l_2	0	0	-1
l_3	-1	0	-1
l_4	1	0	1

(3.4)

$$\overleftrightarrow{D}_r^{(\alpha)} = \begin{pmatrix} r_1 & r_2 & 0 & \cdots & \cdots & \cdots & \cdots & 0 \\ 0 & -1 & 1 & 0 & \cdots & \cdots & \cdots & 0 \\ 0 & 0 & -1 & 1 & 0 & \cdots & \cdots & 0 \\ \vdots & \vdots & 0 & \ddots & \ddots & \ddots & \vdots & \vdots \\ \vdots & \vdots & \vdots & \ddots & \ddots & \ddots & 0 & \vdots \\ 0 & \cdots & \cdots & \cdots & 0 & -1 & 1 & 0 \\ 0 & \cdots & \cdots & \cdots & \cdots & 0 & -1 & 1 \\ r_3 & 0 & \cdots & \cdots & \cdots & \cdots & 0 & r_4 \end{pmatrix} \tag{3.5}$$

with

	DC	NC	PC
r_1	1	0	1
r_2	0	0	-1
r_3	-1	0	-1
r_4	1	0	1

(3.6)

$$\overleftrightarrow{D}_c^{(\alpha)} = \begin{pmatrix} 0 & c_1 & 0 & \cdots & \cdots & \cdots & \cdots & c_2 \\ -1 & 0 & 1 & 0 & \cdots & \cdots & \cdots & 0 \\ 0 & -1 & 0 & 1 & 0 & \cdots & \cdots & 0 \\ \vdots & 0 & \ddots & \ddots & \ddots & \ddots & \vdots & \vdots \\ \vdots & \vdots & \ddots & \ddots & \ddots & \ddots & 0 & \vdots \\ 0 & \cdots & \cdots & 0 & -1 & 0 & 1 & 0 \\ 0 & \cdots & \cdots & \cdots & 0 & -1 & 0 & 1 \\ c_3 & 0 & \cdots & \cdots & \cdots & 0 & c_4 & 0 \end{pmatrix} \tag{3.7}$$

with

	DC	NC	PC
c_1	1	0	1
c_2	0	0	-1
c_3	0	0	1
c_4	-1	0	-1

(3.8)

$$\overleftrightarrow{D}_z^{(\alpha)} = \begin{pmatrix} 2 & z_1 & 0 & \cdots & \cdots & \cdots & 0 & z_2 \\ -1 & 2 & -1 & 0 & \cdots & \cdots & \cdots & 0 \\ 0 & -1 & 2 & -1 & 0 & \cdots & \cdots & 0 \\ \vdots & 0 & \ddots & \ddots & \ddots & \ddots & \vdots & \vdots \\ \vdots & \vdots & \ddots & \ddots & \ddots & \ddots & 0 & \vdots \\ 0 & \cdots & \cdots & 0 & -1 & 2 & -1 & 0 \\ 0 & \cdots & \cdots & \cdots & 0 & -1 & 2 & -1 \\ z_3 & 0 & \cdots & \cdots & \cdots & 0 & z_4 & 2 \end{pmatrix} \tag{3.9}$$

with

	DC	NC	PC
z_1	-1	-2	-1
z_2	0	0	-1
z_3	0	0	-1
z_4	-1	-2	-1

(3.10)

Next we apply this discretization scheme to solve the Helmholtz equation in cylindrical and spherical co-ordinates.

3.1 Solution of the Helmholtz Equation in Cylindrical Co-ordinates

In this chapter we want to treat the infinitely extended cylinder having a non-circular cross-section which does not change along the z-direction. This restriction is not necessary but it reduces the scattering problem to a two-dimensional one by making it possible to separate the z-dependence of the Debye potentials in the following way:

$$\Pi_e(r,\phi,z) = -\frac{j}{\omega\mu_0} E_0 \tilde{\Pi}_e(r,\phi)\cdot\exp(jhz) \tag{3.11}$$

$$\Pi_m(r,\phi,z) = -\frac{j}{k} E_0 \tilde{\Pi}_m(r,\phi)\cdot\exp(jhz)\ . \tag{3.12}$$

Here we have the parameter h which will be determined later by the incident field (see chapter 4.1, Eq. (4.16)). Upon substituting these equations into (2.20) and (2.21), a modified Helmholtz equation results:

$$\begin{aligned} &\tilde{\nabla}^2\tilde{\Pi}_{e/m} + r^2(k^2-h^2)\tilde{\Pi}_{e/m} = 0 \\ &\tilde{\nabla}^2 = r\frac{\delta}{\delta r} r\frac{\delta}{\delta r} + \frac{\delta^2}{\delta\phi^2} \end{aligned} \tag{3.13}$$

The discretization is performed with respect to the ϕ-co-ordinate in the interval $[0, 2\pi]$. The corresponding discretization scheme is shown in Fig. 2.

h_ϕ denotes the discretization angle given by

$$h_\phi = \frac{2\pi}{N_d} \quad \text{and} \quad \phi_i = (i-1)h_\phi;\ i = 1,\ldots,N_d\ . \tag{3.14}$$

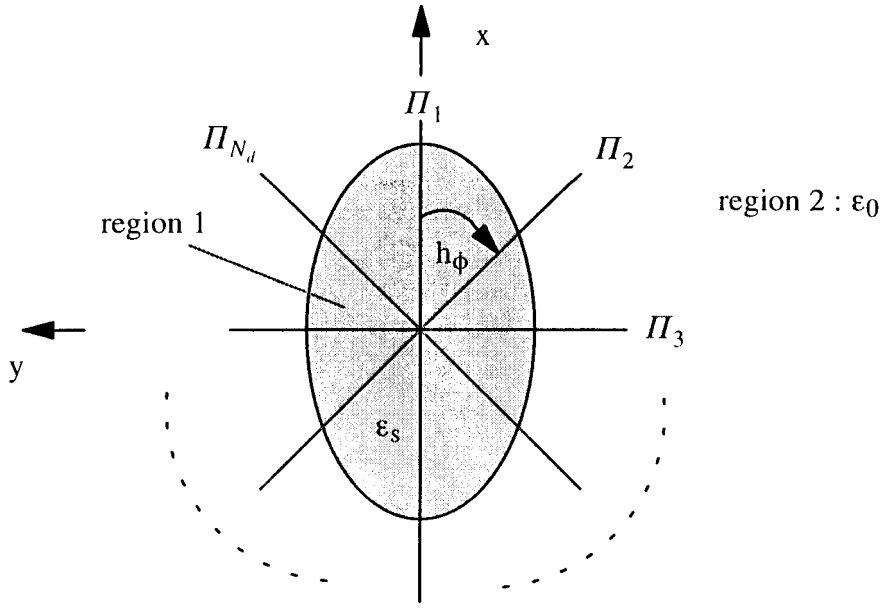

Figure 2. Equidistant discretization of the cylindrical cross-section taking periodicity into account.

Applying the replacement

$$\frac{\delta^2}{\delta\phi^2} \quad \Longrightarrow \quad -\frac{1}{h_\phi^2}\overleftrightarrow{D}_z^{(PC)}$$

to (3.13) yields the algebraic version of the modified Helmhotz equation

$$\begin{aligned} &\left\{h_\phi^2\left[r\frac{d}{dr}r\frac{d}{dr}+(k^2-h^2)r^2\right]\overleftrightarrow{E}-\overleftrightarrow{P}_z\right\}\cdot|\Pi^t\rangle=|0\rangle \\ &\overleftrightarrow{P}_z=\overleftrightarrow{D}_z^{(PC)}, \qquad \overleftrightarrow{E}: \text{ unit matrix} \end{aligned} \tag{3.15}$$

$$|\Pi^t\rangle=\left(\tilde{\Pi}_{e/m}(\phi_1),\ldots,\tilde{\Pi}_{e/m}(\phi_{N_d})\right)^t\,, \tag{3.16}$$

where we use the "bra ($\langle\ldots|$)" and "ket ($|\ldots\rangle$)" notation to indicate the algebraic character of the field components and potentials. This notation is well-known from Quantum Mechanics [54], and it is

also used in Electrodynamics to formulate the Generalized Method of Moments [55].

(3.15) is nothing but a coupled system of ordinary differential equations. The potentials $\tilde{\Pi}_{e/m}(\phi_i)$ given on each discretization line depend only on r.

We are able to decouple this system by solving the corresponding eigenvalue problem

$$(\overleftrightarrow{P}_z - \lambda\vec{E}) \cdot |x\rangle = |0\rangle \ . \tag{3.17}$$

As demonstrated in [56], this can be done analytically resulting in

$$x_i^{(\alpha)} = \frac{1}{\sqrt{N_d}}[\sin\beta_{i\alpha} + \cos\beta_{i\alpha}] \tag{3.18}$$

$$\lambda_\alpha = 4 \cdot \sin^2\left(\frac{\beta_\alpha}{2}\right) \tag{3.19}$$

$$\beta_{i\alpha} = h_\phi \cdot (\alpha - 1) \cdot (i - 1)$$

$$\beta_\alpha = h_\phi \cdot (\alpha - 1) \quad \text{with } \alpha,\, i = 1, \ldots, N_d \ .$$

The eigenvectors $|x_\alpha\rangle$ form the columns of the orthogonal transformation matrix $\overleftrightarrow{T}$ for which the relations

$$\overleftrightarrow{T}^{-1} \cdot \overleftrightarrow{T} = \overleftrightarrow{E} \tag{3.20}$$

and

$$\overleftrightarrow{T}^{-1} \cdot \overleftrightarrow{P}_z \cdot \overleftrightarrow{T} = diag\{\lambda_i\}; \quad i = 1, \ldots, N_d \tag{3.21}$$

are valid. Introducing transformed potentials by the definition

$$|U\rangle = \overleftrightarrow{T}^{-1} \cdot |\Pi\rangle \ , \tag{3.22}$$

we get from (3.15) the following system of uncoupled ordinary differential equations:

$$\left\{\left[r\frac{d}{dr}r\frac{d}{dr} + (k^2 - h^2)r^2\right]\overleftrightarrow{E} - \frac{1}{h_\phi^2}diag\{\lambda_i\}\right\} \cdot |U^t\rangle = |0\rangle \ . \tag{3.23}$$

If substituting

$$\rho = (k^2 - h^2)^{1/2} \cdot r \tag{3.24}$$

into (3.23), we obtain Bessels's differential equation for each component of the transformed potential

$$\frac{d^2U_i(\rho)}{d\rho^2} + \frac{1}{\rho}\frac{dU_i(\rho)}{d\rho} + \left[1 - \frac{\nu_i^2}{\rho^2}\right] U_i(\rho) = 0 \tag{3.25}$$

$$\nu_i^2 = \frac{\lambda_i}{h_\phi^2} \ . \tag{3.26}$$

Since (3.25) must be solved in each homogeneous subregion by taking the regularity and the radiation condition into account, we finally have

$$U_{e_i}^{int.} = a_i \cdot J_{\nu_i}(\rho_s) \qquad U_{m_i}^{int.} = b_i \cdot J_{\nu_i}(\rho_s) \tag{3.27}$$

inside the scatterer (region 1) and

$$U_{e_i}^{s} = c_i \cdot H_{\nu_i}^{(1)}(\rho_0) \qquad U_{m_i}^{s} = d_i \cdot H_{\nu_i}^{(1)}(\rho_0) \tag{3.28}$$

in the outer region (region 2). The coefficients a_i, b_i, c_i and d_i are unknown, to the present. Obviously, with the eigenvectors $|x_\alpha\rangle$ a space is given in which we can always find a solution of the algebraic Helmholtz equation, no matter whether the cross-section is circular or not. Since the solutions given in (3.27) and (3.28) are very similar to what is known from the conventional Mie theory, this space is called the Discretized Mie Space (DMS). As we will see later, it has its own meaning if dealing with the separable limiting case of a circular cylinder at vertical incidence with respect to the cylindrical axis. The essential difference of (3.27) and (3.28) compared to the analytical solution of the circular cylinder is the order of the Bessel and Hankel functions which are now calculated by use of the eigenvalues of equation (3.17).

In the case of non-circular cross-sections we have to go back to the physical space by taking the inversion of (3.22), i.e., we have to calculate

$$|\Pi\rangle = \overleftrightarrow{T} \cdot |U\rangle \ . \tag{3.29}$$

By simple manipulations this transformation can be put into the form

$$|\Pi\rangle = \sum_{\alpha=1}^{N_d} \kappa_\alpha \overleftrightarrow{\Pi}_\alpha \cdot |x_\alpha\rangle \tag{3.30}$$

κ_α : unknown coefficients

$\overleftrightarrow{\Pi}_\alpha$: matrix operator

This describes an expansion of $|\Pi\rangle$ with respect to the eigenvectors $|x_\alpha\rangle$, where we have a different matrix operator for each of the expansion coefficients. For the discussion of the Rayleigh hypothesis and the derivation of the iteration procedure of the DMF, this reformulation will become a crucial step in our analysis. Additionally, it reveals some interesting features of the MoL.

Thus, using (3.11) and (3.12), the Debye potentials in each homogeneous subregion are given by the expansions:

$$|\Pi_e^s\rangle = -\frac{j}{\omega\mu_0} E_0 e^{jhz} \sum_{\alpha=1}^{N_d} c_\alpha \overleftrightarrow{\Pi}{}^s_\alpha \cdot |x_\alpha\rangle \tag{3.31}$$

$$|\Pi_m^s\rangle = -\frac{j}{k_0} E_0 e^{jhz} \sum_{\alpha=1}^{N_d} d_\alpha \overleftrightarrow{\Pi}{}^s_\alpha \cdot |x_\alpha\rangle \tag{3.32}$$

$$|\Pi_e^{int.}\rangle = -\frac{j}{\omega\mu_0} E_0 e^{jhz} \sum_{\alpha=1}^{N_d} a_\alpha \overleftrightarrow{\Pi}{}^{int.}_\alpha \cdot |x_\alpha\rangle \tag{3.33}$$

$$|\Pi_m^{int.}\rangle = -\frac{j}{k_0} E_0 e^{jhz} \sum_{\alpha=1}^{N_d} b_\alpha \overleftrightarrow{\Pi}{}^{int.}_\alpha \cdot |x_\alpha\rangle \tag{3.34}$$

where

$$\overleftrightarrow{\Pi}{}^s_\alpha = diag\{H^{(1)}_{\nu_\alpha}(\rho_{0_i})\}, \quad i = 1, \ldots, N_d \tag{3.35}$$

$$\overleftrightarrow{\Pi}{}^{int.}_\alpha = diag\{J_{\nu_\alpha}(\rho_{s_i})\}, \quad i = 1, \ldots, N_d \tag{3.36}$$

The situation will become a little bit more complicated if dealing with the NAS in spherical co-ordinates.

3.2 Solution of the Helmholtz Equation in Spherical Co-ordinates

Due to the restriction to axisymmetric scatterers we are able to separate the ϕ-dependence which again results in a reduction of the scattering problem to a two-dimensional one. The corresponding *ansatz* for the Debye potentials reads as follows:

$$\Pi_e(r, \theta, \phi) = -\frac{k}{\omega\mu_0} E_0 \sum_l \tilde{\Pi}_e^{(l)}(r, \theta) \cdot \exp(jl\phi) \tag{3.37}$$

$$\Pi_e(r, \theta, \phi) = E_0 \sum_l \tilde{\Pi}_m^{(l)}(r, \theta) \cdot \exp(jl\phi) \tag{3.38}$$

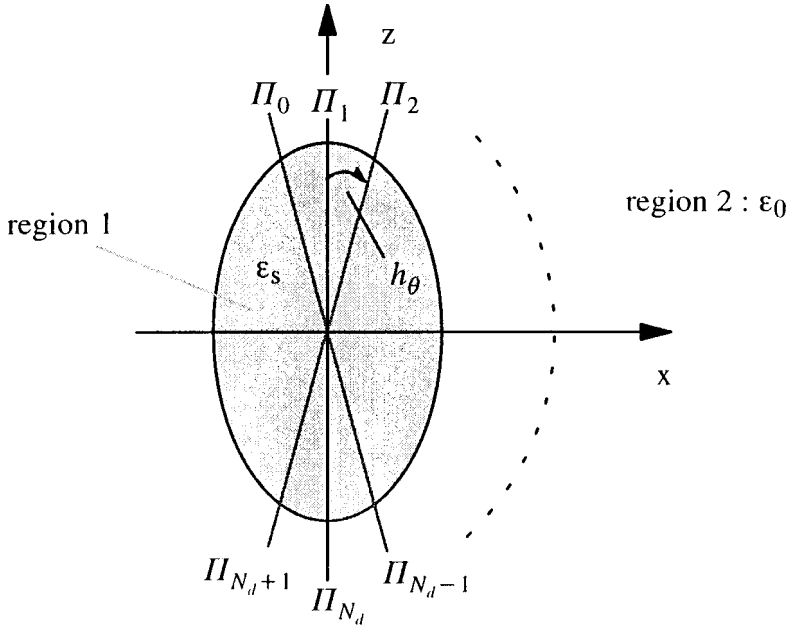

Figure 3. Equidistant discretization of the NAS for $l = 0$, i.e., taking the Neumann condition at $\theta = 0,\ \pi$ into account.

Inserting these equations into (2.28) and (2.29) provides the modified Helmholtz equation

$$\begin{aligned} &\tilde{\nabla}^2 \tilde{\Pi}_{e/m}^{(l)} + k^2 r^2 \tilde{\Pi}_{e/m}^{(l)} = 0 \\ &\tilde{\nabla}^2 = r \frac{\delta^2}{\delta r^2} r + \frac{1}{\sin\theta} \frac{\delta}{\delta\theta} \sin\theta \frac{\delta}{\delta \sin\theta} - \frac{l^2}{\sin^2\theta} \ . \end{aligned} \tag{3.39}$$

The discretization is performed with respect to θ in the interval $[0, \pi]$. According to (2.32) and (2.33), the dependence on the azimuthal modes has to be taken into account. For $l = 0$ we choose

$$h_\theta = \frac{\pi}{N_d - 1} \quad \text{and} \quad \theta_i = (i-1)h_\theta;\ i = 1, \ldots, N_d \ . \tag{3.40}$$

The corresponding discretization scheme is shown in Fig. 3. Applying this to (3.39) results in the following system of coupled ordinary differential equations:

$$\left\{ h_\theta^2 \left[r\frac{d^2}{dr^2}r + k^2 r^2 \right] \overleftrightarrow{E} - \overleftrightarrow{P}_z^{(0)} \right\} \cdot |\Pi^{(0)^t}\rangle \tag{3.41}$$

$$|\Pi^{(0)^t}\rangle = \left(\tilde{\Pi}_{e/m}^{(0)}(\theta_1), \ldots, \tilde{\Pi}_{e/m}^{(0)}(\theta_{N_d}) \right)^t$$

with

$$\overleftrightarrow{P}_z^{(0)} = \overleftrightarrow{D}_z^{(NC)} - diag\{\kappa_i\} \cdot \overleftrightarrow{D}_r^{(NC)} \quad \text{and} \tag{3.42}$$

$$\kappa_i = h_\theta \cot\theta_i \ .$$

In matrix notation, the expression (3.42) is given by

$$\overleftrightarrow{P}_z^{(0)} =$$

$$\begin{pmatrix} 2 & -2 & 0 & \cdots & \cdots & 0 \\ -1 & (2+\kappa_2) & -(1+\kappa_2) & 0 & \cdots & \vdots \\ 0 & -1 & (2+\kappa_3) & -(1+\kappa_3) & \ddots & \vdots \\ \vdots & 0 & \ddots & \ddots & \ddots & 0 \\ \vdots & \vdots & \ddots & -1 & (2+\kappa_{N_d-1}) & -(1+\kappa_{N_d-1}) \\ 0 & \cdots & \cdots & 0 & -2 & 2 \end{pmatrix}$$

If $l \neq 0$ is considered the discretization is somewhat different. We choose (compare Fig. 4)

$$h_\theta = \frac{\pi}{N_d + 1} \quad \text{and} \quad \theta_i = i h_\theta;\ i = 1, \ldots, N_d \tag{3.43}$$

and get from (3.39)

$$\left\{ h_\theta^2 \left[r\frac{d^2}{dr^2}r + k^2 r^2 \right] \overleftrightarrow{E} - \overleftrightarrow{P}_z^{(l)} \right\} \cdot |\Pi^{(l)^t}\rangle = |0\rangle \tag{3.44}$$

$$|\Pi^{(l)^t}\rangle = \left(\tilde{\Pi}_{e/m}^{(l)}(\theta_1), \ldots, \tilde{\Pi}_{e/m}^{(l)}(\theta_{N_d}) \right)^t$$

$$\overleftrightarrow{P}_z^{(l)} = \overleftrightarrow{D}_z^{(DC)} - diag\{\kappa_i\} \cdot \overleftrightarrow{D}_r^{(DC)} + diag\{\gamma_i\} \tag{3.45}$$

$$\gamma_i = \frac{h_\theta^2 l^2}{\sin^2\theta_i} \ . \tag{3.46}$$

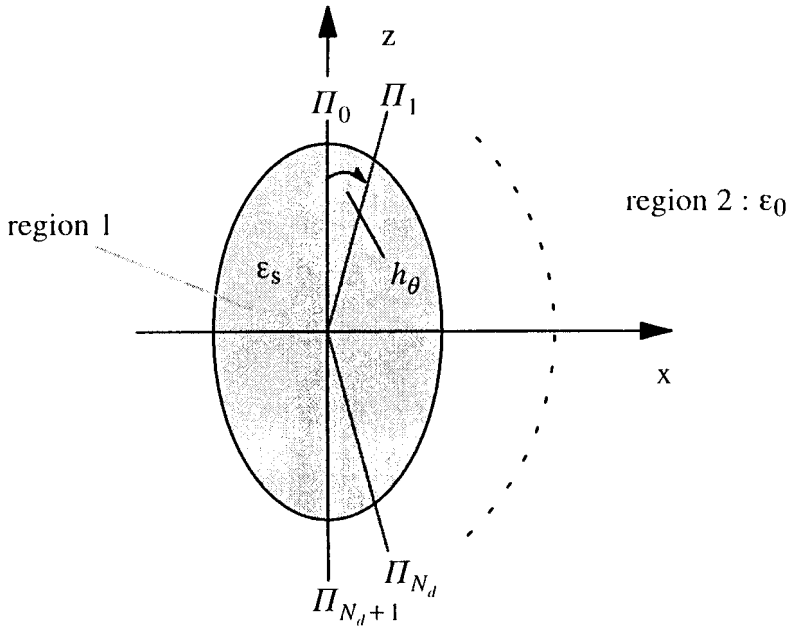

Figure 4. Equidistant discretization of the NAS for $l \neq 0$, i.e., taking the Dirichlet condition at $\theta = 0, \pi$ into account.

Again, let's present (3.45) in matrix notation which reads

$$\overleftrightarrow{P}_z^{(l)} = \begin{pmatrix} (2+\kappa_1 & -(1+\kappa_1) & 0 & \cdots & \cdots & 0 \\ +\gamma_1) & & & & & \\ -1 & (2+\kappa_2 & -(1+\kappa_2) & 0 & \cdots & \vdots \\ & +\gamma_2) & & & & \\ 0 & -1 & (2+\kappa_3 & -(1+\kappa_3) & \ddots & \vdots \\ & & +\gamma_3) & & & \\ \vdots & 0 & \ddots & \ddots & \ddots & 0 \\ \vdots & \vdots & \ddots & -1 & (2+\kappa_{N_d-1} & -(1+\kappa_{N_d-1}) \\ & & & & +\gamma_{N_d-1}) & \\ 0 & \cdots & \cdots & 0 & -1 & (2+\kappa_{N_d} \\ & & & & & +\gamma_{N_d}) \end{pmatrix}$$

In the following analysis both cases are summarized by the superscript (l), i.e., $l = 0$ is included.

In contrast to what we have got in the case of cylindrical co-ordinates, $\overleftrightarrow{P}_z^{(l)}$ is now a non-symmetric matrix. Fortunately, it's known that each matrix of the form

$$\overleftrightarrow{P}_{unsymm.} = \begin{pmatrix} \alpha_1 & -\beta_2 & 0 & \cdots & \cdots & 0 \\ -\gamma_2 & \alpha_2 & -\beta_3 & 0 & \cdots & \vdots \\ 0 & -\gamma_3 & \alpha_3 & -\beta_4 & \ddots & \vdots \\ \vdots & 0 & \ddots & \ddots & \ddots & 0 \\ \vdots & \vdots & \ddots & -\gamma_{N_d-1} & \alpha_{N_d-1} & -\beta_{N_d} \\ 0 & \cdots & \cdots & 0 & -\gamma_{N_d} & \alpha_{N_d} \end{pmatrix} \tag{3.47}$$

with $\alpha_i \in \mathbf{R}$ and $\gamma_i \cdot \beta_i > 0$ can be transformed into a real symmetric matrix by means of a similarity transformation [57]

$$\overleftrightarrow{P}_{symm.} = \overleftrightarrow{Z}^{-1} \cdot \overleftrightarrow{P} \cdot \overleftrightarrow{Z} \tag{3.48}$$

with a diagonal matrix $\overleftrightarrow{Z}$, where

$$z_{1,1} = 1; \qquad z_{ii} = \left(\frac{\gamma_2 \cdot \ldots \cdot \gamma_i}{\beta_2 \cdot \ldots \cdot \beta_i} \right)^{\frac{1}{2}} . \tag{3.49}$$

This results in the following elements of the symmetric matrix:

$$p_{symm.\,i,i} = \alpha_i; \quad p_{symm.\,i,i+1} = p_{symm.\ i+1,i} = -(\beta_{i+1} \cdot \gamma_{i+1})^{\frac{1}{2}} . \tag{3.50}$$

As in cylindrical co-ordinates, we have to solve the eigenvalue problem

$$\left(\overleftrightarrow{P}_{z\,symm.}^{(l)} - \lambda^{(l)} \overleftrightarrow{E} \right) \cdot |x^{(l)}\rangle = |0\rangle \tag{3.51}$$

to get the orthogonal transformation matrix $\overleftrightarrow{T}^{(l)}$ for which the relations

$$\overleftrightarrow{T}^{(l)\,-1} \cdot \overleftrightarrow{T}^{(l)} = \overleftrightarrow{E} \tag{3.52}$$

and

$$\overleftrightarrow{T}^{(l)^{-1}} \cdot \overleftrightarrow{P}^{(l)}_{z\,symm.} \cdot \overleftrightarrow{T}^{(l)} = diag\{\lambda_i^{(l)}\}; \quad i = 1, \ldots, N_d \tag{3.53}$$

are valid. This solution can be found only numerically but without any difficulties. Now we are able to decouple the equations (3.41) and (3.44) by introducing the transformed potentials according to

$$|U^{(l)}\rangle = \overleftrightarrow{Tr}^{(l)^{-1}} \cdot |\Pi^{(l)}\rangle \ , \tag{3.54}$$

where

$$\begin{aligned} \overleftrightarrow{Tr}^{(l)} &= \overleftrightarrow{Z}^{(l)} \cdot \overleftrightarrow{T}^{(l)} \\ \overleftrightarrow{Tr}^{(l)^{-1}} &= \overleftrightarrow{T}^{(l)^{-1}} \cdot \overleftrightarrow{Z}^{(l)^{-1}} \ . \end{aligned} \tag{3.55}$$

Substituting

$$\rho = k \cdot r \quad \text{and} \quad U_i^{(l)} = \frac{1}{\sqrt{\rho}} \cdot Z_i^{(l)}(\rho) \ , \tag{3.56}$$

we obtain the following ordinary differential equations in the DMS defined by $\overleftrightarrow{Tr}^{(l)^{-1}}$:

$$\frac{d^2 Z_i^{(l)}(\rho)}{d\rho^2} + \frac{1}{\rho}\frac{dZ_i^{(l)}(\rho)}{d\rho} + \left[1 - \frac{{\nu_i^{(l)}}^2}{\rho^2}\right] Z_i^{(l)}(\rho) = 0 \tag{3.57}$$

$${\nu_i^{(l)}}^2 = \frac{\lambda_i^{(l)}}{h_\theta^2} + \frac{1}{4} \ . \tag{3.58}$$

Taking the regularity and the radiation condition into account the components of the transformed potentials are given by

$$U_{e_i}^{(l)_{int.}} = a_i^{(l)} \cdot \frac{J_{\nu_i^{(l)}}(\rho_s)}{\sqrt{\rho_s}} \qquad U_{m_i}^{(l)_{int.}} = b_i^{(l)} \cdot \frac{J_{\nu_i^{(l)}}(\rho_s)}{\sqrt{\rho_s}} \tag{3.59}$$

inside the scatterer, and by

$$U_{e_i}^{(l)_s} = c_i^{(l)} \cdot \frac{H^{(1)}_{\nu_i^{(l)}}(\rho_0)}{\sqrt{\rho_0}} \qquad U_{m_i}^{(l)_s} = d_i^{(l)} \cdot \frac{H^{(1)}_{\nu_i^{(l)}}(\rho_0)}{\sqrt{\rho_0}} \tag{3.59}$$

outside. $a_i^{(l)}$, $b_i^{(l)}$, $c_i^{(l)}$ and $d_i^{(l)}$ are the unknown coefficients.

Since we have to go back to the physical space if dealing with non-spherical scatterers the expressions of the inversion of (3.54) are needed, i.e.,

$$|\Pi^{(l)}\rangle = \overleftrightarrow{Tr}^{(l)} \cdot |U^{(l)}\rangle \ . \tag{3.61}$$

Taking equations (3.37) and (3.38) into account, (3.61) can be reformulated to get the following expressions for each of the Debye potentials:

$$|\Pi_e^s\rangle = -\frac{k_0}{\omega\mu_0} E_0 \sum_l e^{jl\phi} \sum_{\alpha=1}^{N_d} c_\alpha^{(l)} \overleftrightarrow{\Pi}_\alpha^{(l)_s} \cdot |x_\alpha^{(l)}\rangle \tag{3.62}$$

$$|\Pi_m^s\rangle = E_0 \sum_l e^{jl\phi} \sum_{\alpha=1}^{N_d} d_\alpha^{(l)} \overleftrightarrow{\Pi}_\alpha^{(l)_s} \cdot |x_\alpha^{(l)}\rangle \tag{3.63}$$

$$|\Pi_e^{int.}\rangle = -\frac{k_0}{\omega\mu_0} E_0 \sum_l e^{jl\phi} \sum_{\alpha=1}^{N_d} a_\alpha^{(l)} \overleftrightarrow{\Pi}_\alpha^{(l)_{int.}} \cdot |x_\alpha^{(l)}\rangle \tag{3.64}$$

$$|\Pi_m^{int.}\rangle = E_0 \sum_l e^{jl\phi} \sum_{\alpha=1}^{N_d} b_\alpha^{(l)} \overleftrightarrow{\Pi}_\alpha^{(l)_{int.}} \cdot |x_\alpha^{(l)}\rangle \tag{3.65}$$

where

$$\overleftrightarrow{\Pi}_\alpha^{(l)_s} = diag\left\{ \frac{H^{(1)}_{\nu_\alpha^{(l)}}(\rho_{0_i})}{\sqrt{\rho_{0_i}}} \right\}, \quad i = 1, \ldots, N_d \tag{3.66}$$

$$\overleftrightarrow{\Pi}_\alpha^{(l)_{int.}} = diag\left\{ \frac{J_{\nu_\alpha^{(l)}}(\rho_{0_i})}{\sqrt{\rho_{0_i}}} \right\}, \quad i = 1, \ldots, N_d \tag{3.67}$$

It can be seen again that the column vectors $|x_\alpha^{(l)}\rangle$ of the transformation matrix $\overleftrightarrow{Tr}^{(l)}$ serve as an orthogonal basis in this expansion.

With (3.62)–(3.65), the solution of the algebraic Helmholtz equation in spherical co-ordinates has been found. Before deriving the characteristic equation system of the DMF to determine the unknown expansion coefficients, we want to discuss a problem which is known as the Rayleigh hypothesis. The point of view of the DMF to this problem is presented here since it belongs to the representation given in (3.31)–(3.34) and (3.62)–(3.65).

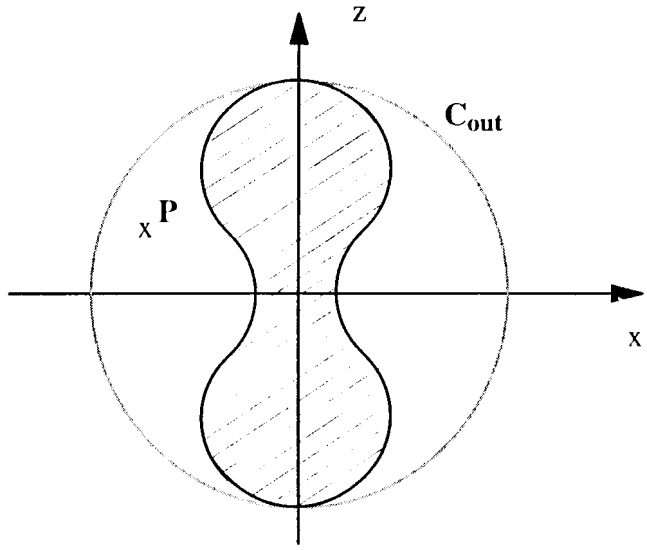

Figure 5. Non-spherical scattering geometry and Rayleigh hypothesis.

3.3 The Discretized Mie-Formalism and the Rayleigh Hypothesis

Originally, this hypothesis was related to plane wave scattering from sinusoidal surfaces. Rayleigh assumed that only upgoing wave eigenfunctions need be considered above the surface but between its peaks. This assumption became a point of controversy when applied to scattering on finite objects [43–48]. The question is the following:

Consider a scatterer with a non-spherical boundary surface as depicted in Fig. 5. At any point outside the circumscribing sphere $\mathbf{C_{out}}$, there exist only outgoing waves. But what happens at any point inside $\mathbf{C_{out}}$ but outside the scatterer? Do we have to take into account incoming waves or, mathematically speaking, is the expansion which is used outside $\mathbf{C_{out}}$ incomplete and non-unique in this region? Especially if we think of concave boundaries, this last question seems to be answered with 'yes'.

Different methods have given different answers to this question. Especially the EBCM has been originally developed to circumvent this discussion [26]. For the original problem, Millar has estimated the upper limit of validity of the Rayleigh hypothesis. If the surface can be described by $f(x) = a\cos(kx)$, then, this hypothesis is valid for

$ka < 0.448$ [44]. Curiously, Wiscombe and Mugnai have found a correspondence with this value in EBCM convergency considerations for Chebyshev particles [32]. It is assumed, however, that the validity depends on which functional basis is used for the expansion of the potentials or fields, and on the location of the origin of the co-ordinate system.

If we want to answer this question from the point of view of the DMF for NAS, we must look at the equations (3.62)–(3.67). In contrast to other methods (EBCM, Method of Moments, Point Matching) which start from an appropriate ansatz, the basic partial differential equations are solved within the DMF by use of the above described algebraization scheme to get the eigenvectors and eigenvalues of the expansion, as it is known from the separation of variable method. The final solution of the ordinary differential equation, depending only on the radial co-ordinate, is uniquely determined by the radiation condition outside the scatterer as long as the boundary intersects each discretization line only into two parts. Therefore, we can give the following answer:

If we can find a co-ordinate system with its origin inside the scatterer and in which each possible discretization line intersects the boundary surface only once, then, in the outer section of each discretization line (i.e., in each point outside the scatterer) the radial solution is uniquely given by (3.66) which represents outgoing waves, due to the fulfillment of the radiation condition in the far field. This means that the boundary surface $r = r(\theta)$ must be a single-valued function with respect to θ in this co-ordinate system. If this requirement is violated, the DMF in its present form can not be applied.

From this point of view we may state that scattering on Chebyshev particles is not influenced by the Rayleigh hypothesis since their boundary surfaces are always single-valued. Nevertheless, there can exist limitations in size parameter and geometry caused by numerical problems.

Obviously, our answer to the Rayleigh hypothesis is in contradiction to the result of Millar since his estimation is a condition of roughness of the boundary surface. We believe that this contradiction is caused by the different approaches which are used to formulate the scattering problem. Millar starts from an expansion of the scattering coefficients for which the so-called requirement of finality [51] is fulfilled. On the other hand, the DMF leads to an equation system for the determination

of the expansion coefficients which do not satisfy such an requirement. The derivation of this characteristic equation system is of our interest in the next chapter.

4. DERIVATION OF THE CHARACTERISTIC EQUATION SYSTEM

Now we want to calculate the unknown coefficients of the general solutions (3.31)–(3.34) and (3.62)–(3.65), respectively. As in the case of the separable scatterer geometries, the continuity conditions of the tangential field components at the scatterer surface are used for this purpose. These are given by (2.37)–(2.44). In this way an inhomogeneous equation system

$$\overleftrightarrow{A} \circ \vec{x} = \vec{I}_{inc.} \tag{4.1}$$

is obtained the inhomogeneity $\vec{I}_{inc.}$ of which depends only on the incident field. The characteristic coefficient matrix $\overleftrightarrow{A}$ for axisymmetric scatterers is solely determined by their geometries and the size parameter. In the following derivations of these equation systems in the different co-ordinates the separable limiting cases are treated in extra sections. Though this is not necessary because the equations of the form (4.1) are generally valid, essentially simpler expressions can be obtained for separable geometries which give the justification for the name **Discretized Mie-Formalism**.

Of course, the reproduction of the separable limiting cases is a touchstone for every numerical algorithm. This test, however, is of special importance for the DMF. As we have seen in the preceding chapter, the eigenvalues and eigenvectors of the eigenvalue problems (3.17) and (3.51) do not depend on a special scatterer geometry but only on the angular boundary conditions and the number of discretization lines. A correspondence of the results obtained by means of both methods, the DMF and the well-known Mie theory for separable structures, will demonstrate the quality of these eigenvalues and eigenvectors which are of decisive importance in formulating the DMF. As it will be discussed later, appropriate convergency criteria can be derived from this property.

4.1 The Discretized Mie-Formalism in Cylindrical Co-ordinates

First of all, the representation of the incident field must be discussed in order to derive the characteristic equation system. The xz-plane is assumed to be the incident plane. We consider two different polarization states. In the TE case (vertical polarization), the $\vec{E}$-vector lies in y-direction whereas in the TM case (horizontal polarization) it oscillates in $\hat{z}'$-direction (see Fig. 6). Therefore it holds

TE:

$$\vec{E}^{inc.} = \hat{y} \cdot E_0 \cdot \exp(-jk_0 x') \tag{4.2}$$

$$\vec{H}^{inc.} = -\hat{z}' \cdot \frac{k_0}{\omega\mu_0} \cdot E_0 \cdot \exp(-jk_0 x') \tag{4.3}$$

TM:

$$\vec{E}^{inc.} = \hat{z}' \cdot E_0 \cdot \exp(-jk_0 x') \tag{4.4}$$

$$\vec{H}^{inc.} = \hat{y} \cdot \frac{k_0}{\omega\mu_0} \cdot E_0 \cdot \exp(-jk_0 x') \ . \tag{4.5}$$

The system $\{\hat{x}', \hat{y}, \hat{z}'\}$ results from a rotation of the system $\{\hat{x}, \hat{y}, \hat{z}\}$ in mathematically negative sense around the $\hat{y}$-axis which leads to the relation

$$\begin{aligned} \hat{x}' &= \cos\delta \cdot \hat{x} - \sin\delta \cdot \hat{z} \\ \hat{z}' &= \sin\delta \cdot \hat{x} + \cos\delta \cdot \hat{z} \ , \end{aligned} \tag{4.6}$$

where the rotation angle δ is just the tilt angle of the incident wave vector towards the xy-plane. Inserting of (4.6) into (4.2)–(4.5) and transforming the system $\{\hat{x}, \hat{y}, \hat{z}\}$ to cylindrical co-ordinates by means of

$$\begin{aligned} \hat{x} &= \hat{r} \cdot \cos\phi - \hat{\phi} \cdot \sin\phi \\ \hat{y} &= \hat{r} \cdot \sin\phi + \hat{\phi} \cdot \cos\phi \\ \hat{z} &= \hat{z} \end{aligned} \tag{4.7}$$

yield the following expressions for the corresponding incident field components.

TE:

$${}^{(TE)}E_r^{inc.} = E_0 \cdot \sin\phi \cdot \exp(-j \cdot \{\phi\delta\}) \tag{4.8}$$

$${}^{(TE)}E_\phi^{inc.} = E_0 \cdot \cos\phi \cdot \exp(-j \cdot \{\phi\delta\}) \tag{4.9}$$

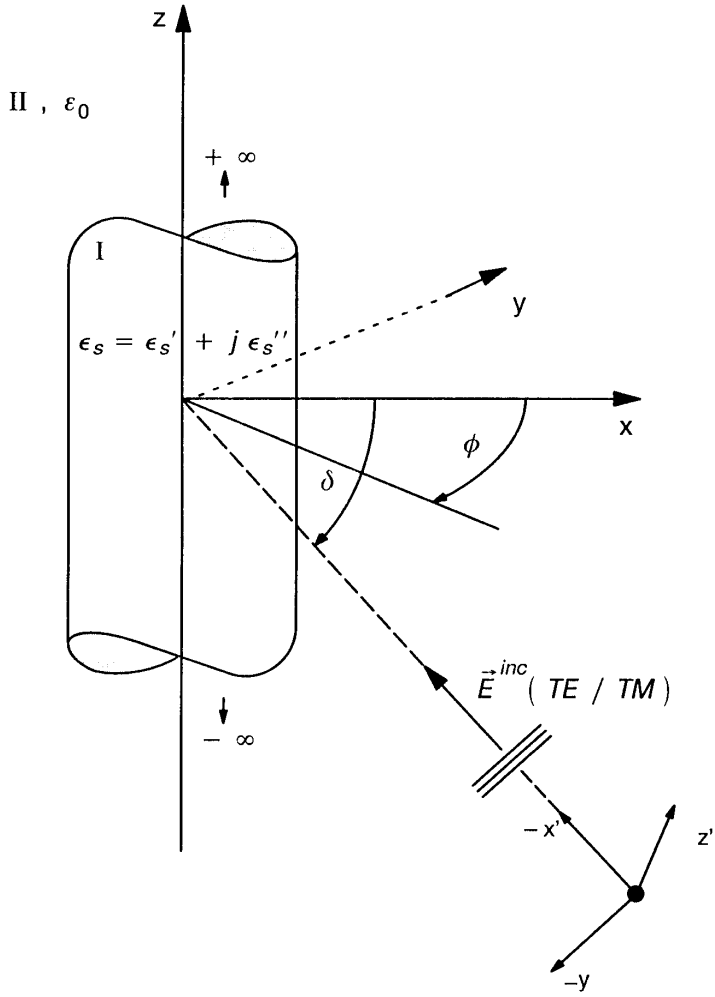

Figure 6. Geometry of the scattering problem in cylindrical coordinates.

$$ {}^{(TE)}E_z^{inc.} = 0 \tag{4.10} $$

$$ {}^{(TE)}H_r^{inc.} = -\frac{k_0}{\omega\mu_0} \cdot E_0 \cdot \sin\delta\cos\phi \cdot \exp(-j \cdot \{\phi\delta\}) \tag{4.11} $$

$$ {}^{(TE)}H_\phi^{inc.} = \frac{k_0}{\omega\mu_0} \cdot E_0 \cdot \sin\delta\sin\phi \cdot \exp(-j \cdot \{\phi\delta\}) \tag{4.12} $$

$$ {}^{(TE)}H_z^{inc.} = -\frac{k_0}{\omega\mu_0} \cdot E_0 \cdot \cos\delta \cdot \exp(-j \cdot \{\phi\delta\}) \tag{4.13} $$

TM:

$$ {}^{(TM)}\vec{E}^{inc.} = -\frac{\omega\mu_0}{k_0} \cdot {}^{(TE)}\vec{H}^{inc.} \tag{4.14} $$

$$ {}^{(TM)}\vec{H}^{inc.} = \frac{k_0}{\omega\mu_0} \cdot {}^{(TE)}\vec{E}^{inc.} \tag{4.15} $$

with

$$ \{\phi\delta\} = k_0 \cdot (r \cdot \cos\phi \cdot \cos\delta - z \cdot \sin\delta) = \rho_0 \cdot \cos\phi - h \cdot z \tag{4.16} $$
$$ \rho_0 = k_0 \cdot r \cdot \cos\delta $$
$$ h = k_0 \cdot \sin\delta $$

4.1.1 The Limiting Case of Circular Cylinders

The relations become especially simple if the cylinder exhibits a circular cross-section $(\tan\alpha_i = 0, \forall\, i)$ and if the incident field impinges perpendicularly on the cylindrical axis $(\delta = 0°)$. Then, the expressions for the incident field can be reduced to

$$ \begin{aligned} {}^{(TE)}\vec{E}_r^{inc.} &= E_0 \cdot \sin\phi \cdot \exp(-j\rho_0 \cos\phi) \\ {}^{(TE)}\vec{E}_\phi^{inc.} &= E_0 \cdot \cos\phi \cdot \exp(-j\rho_0 \cos\phi) \\ {}^{(TE)}\vec{H}_z^{inc.} &= -\frac{k_0}{\omega\mu_0} \cdot E_0 \cdot \exp(-j\rho_0 \cos\phi) \\ {}^{(TE)}\vec{E}_z^{inc.} &= {}^{(TE)}\vec{H}_r^{inc.} = {}^{(TE)}\vec{H}_\phi^{inc.} = 0 \end{aligned} \tag{4.17} $$

and

$$ \begin{aligned} {}^{(TM)}\vec{E}_z^{inc.} &= E_0 \cdot \exp(-j\rho_0 \cos\phi) \\ {}^{(TM)}\vec{H}_r^{inc.} &= \frac{k_0}{\omega\mu_0} \cdot E_0 \cdot \sin\phi \cdot \exp(-j\rho_0 \cos\phi) \\ {}^{(TM)}\vec{H}_\phi^{inc.} &= \frac{k_0}{\omega\mu_0} \cdot E_0 \cdot \cos\phi \cdot \exp(-j\rho_0 \cos\phi) \\ {}^{(TM)}\vec{E}_r^{inc.} &= {}^{(TM)}\vec{E}_\phi^{inc.} = {}^{(TM)}\vec{H}_z^{inc.} = 0 \end{aligned} \tag{4.18} $$

In this case, the expressions (3.35) and (3.36) take an especially simple form. The diagonal matrices change to simple functions in terms of r.

In order to fulfill the continuity conditions, the corresponding internal and scattered fields have to possess an analog structure. This is achieved by means of

$$\text{TE}: \quad a_i = c_i = 0 \tag{4.19}$$

$$\text{TM}: \quad b_i = d_i = 0 \tag{4.20}$$

The following equation systems for the different polarizations of the incident field arise from the continuity conditions (2.41)–(2.44) in using the potentials (3.31)–(3.36) and fields (2.14)–(2.19).

TE:

$$-|\frac{d}{d\rho_0}\Pi_m^s\rangle + |\frac{d}{d\rho_s}\Pi_m^{int.}\rangle = |\frac{d}{d\rho_0}\Pi^{inc.}\rangle \tag{4.21}$$

$$-|\Pi_m^s\rangle + \frac{k_s}{k_0}\cdot|\Pi_m^{int.}\rangle = |\Pi^{inc.}\rangle \tag{4.22}$$

TM:

$$-|\Pi_e^s\rangle + |\Pi_e^{int.}\rangle = |\Pi^{inc.}\rangle \tag{4.23}$$

$$-|\frac{d}{d\rho_0}\Pi_e^s\rangle + \frac{k_s}{k_0}\cdot|\frac{d}{d\rho_s}\Pi_e^{int.}\rangle = |\frac{d}{d\rho_0}\Pi^{inc.}\rangle \tag{4.24}$$

with

$$\begin{aligned} |\Pi^{inc.}\rangle &= \left(\Pi^{inc.}(\phi_1), \ldots, \Pi^{inc.}(\phi_{N_d})\right) \\ \Pi^{inc.}(\phi_i) &= \exp(-j\rho_0\cos\phi_i) \\ \rho_s &= k_s r \end{aligned} \tag{4.25}$$

These equations can be transformed into the DMS by multiplying the system from the left by the transformation matrix $\overleftrightarrow{T}^{-1}$. In this space, the contribution of the incident field reads as follows.

$$u_i = \sum_{k=1}^{N_d} t_{ik}^{-1}\cdot\Pi^{inc.}(\phi_k) \tag{4.26}$$

$$u_i' = \sum_{k=1}^{N_d} t_{ik}^{-1}\cdot\frac{d}{d\rho_0}\Pi^{inc.}(\phi_k) \tag{4.27}$$

From the resulting equations the following scattering coefficients are obtained:

$$\begin{aligned} &\text{TE}: \quad c_i \equiv 0 \\ &d_i = -\frac{J_{\nu_i}'(\rho_s)\cdot u_i(\rho_0) - \sqrt{\epsilon_s}J_{\nu_i}(\rho_s)\cdot u_i'(\rho_0)}{J_{\nu_i}'(\rho_s)\cdot H_{\nu_i}^{(1)}(\rho_0) - \sqrt{\epsilon_s}J_{\nu_i}(\rho_s)\cdot H_{\nu_i}^{(1)'}(\rho_0)} \end{aligned} \tag{4.28}$$

$$\text{TM}: \quad d_i \equiv 0$$
$$c_i = -\frac{\sqrt{\epsilon_s} J'_{\nu_i}(\rho_s) \cdot u_i(\rho_0) - J_{\nu_i}(\rho_s) \cdot u'_i(\rho_0)}{\sqrt{\epsilon_s} J'_{\nu_i}(\rho_s) \cdot H^{(1)}_{\nu_i}(\rho_0) - J_{\nu_i}(\rho_s) \cdot H^{(1)'}_{\nu_i}(\rho_0)} \tag{4.29}$$

The primes at the Bessel and Hankel functions denote differentiation with respect to their arguments.

Obviously, the limiting case can be treated simply within the DMS and leads to expressions for the scattering coefficients which are identical in structure to those of the analytical solution (compare with [15]). This identity is the decisive reason for calling this space the **Discretized Mie-Space**. There are, however, two essential differences between (4.28) and (4.29) on the one hand and the analytical expressions on the other hand.

1. The contributions of the incident field, which provide the inhomogeneities of the equation system, have to be calculated also within the DMS according to (4.26) and (4.27). These two equations describe the expansion of $|\Pi^{inc.}\rangle$ and $|\frac{d}{d\rho_0}\Pi^{inc.}\rangle$ with respect to the eigenvectors $|x_\alpha\rangle$, i.e., it holds:

$$|\Pi^{inc.}\rangle = \sum_{\alpha=1}^{N_d} u_\alpha \cdot |x_\alpha\rangle \tag{4.30}$$

$$|\frac{d}{d\rho_0}\Pi^{inc.}\rangle = \sum_{\alpha=1}^{N_d} u'_\alpha \cdot |x_\alpha\rangle \tag{4.31}$$

   From these equations, it follows directly for the expansion coefficients:

$$\langle x_\alpha|\Pi^{inc.}\rangle = u_\alpha \tag{4.32}$$

$$\langle x_\alpha|\frac{d}{d\rho_0}\Pi^{inc.}\rangle = u'_\alpha \ . \tag{4.33}$$

   (4.32) and (4.33) represent, however, only another formulation of (4.26) and (4.27).
2. The orders ν_i of the Bessel and Hankel functions in (4.28) and (4.29) result from the eigenvalues λ_i of the eigenvalue problem (3.17).

As we will see later in the numerical considerations, the results obtained by means of (4.28) and (4.29) converge very rapidly to the known solutions of the Mie theory.

4.1.2 Non-circular Cross-sections

We are now considering the case of non-circular cross-sections and obliquely incident fields. Though the calculation proceeds analogously to the limiting case just considered, it can not any longer be carried out in the DMS. First of all, we calculate the internal and scattered fields by using the potentials (3.31)–(3.36) and the equations (3.11), (3.12). In doing so, the differential quotient $\frac{\delta}{\delta\phi}$ occurring in equations (2.14)–(2.19) is replaced by the difference operator $1/2h_\phi \cdot \overleftrightarrow{D}_c^{(PC)}$ according to (3.7) and (3.8). Due to the discretization with respect to ϕ, the fields are then given in an algebraic form and read as follows:

$$|e_z^s\rangle = E_0 \cdot e^{jhz} \cdot \sum_{\alpha=1}^{N_d} c_\alpha \cdot {}^s\overleftrightarrow{\Pi}_\alpha^{(z)} \cdot |x_\alpha\rangle \tag{4.34}$$

$$\begin{aligned} |e_r^s\rangle = {} & E_0 \cdot j \cdot \left(\frac{h}{k_0}\right) \cdot \cos\delta \cdot e^{jhz} \cdot \sum_{\alpha=1}^{N_d} c_\alpha \cdot {}^s\overleftrightarrow{\Pi}_\alpha^{(r_e)} \cdot |x_\alpha\rangle \\ & - E_0 \cdot j \cdot \cos\delta \cdot e^{jhz} \cdot \sum_{\alpha=1}^{N_d} d_\alpha \cdot {}^s\overleftrightarrow{\Pi}_\alpha^{(r_m)} \cdot |x_\alpha\rangle \end{aligned} \tag{4.35}$$

$$\begin{aligned} |e_\phi^s\rangle = {} & E_0 \cdot j \cdot \left(\frac{h}{k_0}\right) \cdot \cos\delta \cdot e^{jhz} \cdot \sum_{\alpha=1}^{N_d} c_\alpha \cdot {}^s\overleftrightarrow{\Pi}_\alpha^{(r_m)} \cdot |x_\alpha\rangle \\ & + E_0 \cdot j \cdot \cos\delta \cdot e^{jhz} \cdot \sum_{\alpha=1}^{N_d} d_\alpha \cdot {}^s\overleftrightarrow{\Pi}_\alpha^{(r_e)} \cdot |x_\alpha\rangle \end{aligned} \tag{4.36}$$

$$|h_z^s\rangle = -\frac{k_0}{\omega\mu_0} \cdot E_0 \cdot e^{jhz} \cdot \sum_{\alpha=1}^{N_d} d_\alpha \cdot {}^s\overleftrightarrow{\Pi}_\alpha^{(z)} \cdot |x_\alpha\rangle \tag{4.37}$$

$$\begin{aligned} |h_r^s\rangle = {} & -\frac{k_0}{\omega\mu_0} \cdot E_0 \cdot j \cdot \left(\frac{h}{k_0}\right) \cdot \cos\delta \cdot e^{jhz} \cdot \sum_{\alpha=1}^{N_d} d_\alpha \cdot {}^s\overleftrightarrow{\Pi}_\alpha^{(r_e)} \cdot |x_\alpha\rangle \\ & - \frac{k_0}{\omega\mu_0} \cdot E_0 \cdot j \cdot \cos\delta \cdot e^{jhz} \cdot \sum_{\alpha=1}^{N_d} c_\alpha \cdot {}^s\overleftrightarrow{\Pi}_\alpha^{(r_m)} \cdot |x_\alpha\rangle \end{aligned} \tag{4.38}$$

$$|h_\phi^s\rangle = -\frac{k_0}{\omega\mu_0} \cdot E_0 \cdot j \cdot \left(\frac{h}{k_0}\right) \cdot \cos\delta \cdot e^{jhz} \cdot \sum_{\alpha=1}^{N_d} d_\alpha \cdot {}^s\overleftrightarrow{\Pi}_\alpha^{(r_m)} \cdot |x_\alpha\rangle$$

$$+\frac{k_0}{\omega\mu_0}\cdot E_0\cdot j\cdot\cos\delta\cdot e^{jhz}\cdot\sum_{\alpha=1}^{N_d}c_\alpha\cdot{}^{s}\overleftrightarrow{\Pi}_{\alpha}^{(r_e)}\cdot|x_\alpha\rangle \tag{4.39}$$

with

$${}^{s}\overleftrightarrow{\Pi}_{\alpha}^{(z)}=\cos^2\delta\cdot diag\left\{H_{\nu_\alpha}^{(1)}(\rho_{0_i})\right\};\quad i=1,\ldots,N_d \tag{4.40}$$

$${}^{s}\overleftrightarrow{\Pi}_{\alpha}^{(r_e)}=diag\left\{\frac{d}{d\rho_0}\left[H_{\nu_\alpha}^{(1)}(\rho_0)\right]_{\rho_{0_i}}\right\};\quad i=1,\ldots,N_d \tag{4.41}$$

$${}^{s}\overleftrightarrow{\Pi}_{\alpha}^{(r_m)}=diag\left\{\frac{1}{\rho_{0_i}}\cdot H_{\nu_\alpha}^{(1)}(\rho_{0_i})\right\}\frac{1}{2h_\phi}\cdot\overleftrightarrow{D}_{c}^{(PC)};\quad i=1,\ldots,N_d \tag{4.42}$$

and

$$|e_z^{int.}\rangle=E_0\cdot e^{jhz}\cdot\sum_{\alpha=1}^{N_d}a_\alpha\cdot{}^{int.}\overleftrightarrow{\Pi}_{\alpha}^{(z)}\cdot|x_\alpha\rangle \tag{4.43}$$

$$\begin{aligned}|e_r^{int.}\rangle=&E_0\cdot j\cdot\left(\frac{h}{k_s}\right)\cdot\kappa_\delta\cdot e^{jhz}\cdot\sum_{\alpha=1}^{N_d}a_\alpha\cdot{}^{int.}\overleftrightarrow{\Pi}_{\alpha}^{(r_e)}\cdot|x_\alpha\rangle\\&-E_0\cdot j\cdot\kappa_\delta\cdot e^{jhz}\cdot\sum_{\alpha=1}^{N_d}b_\alpha\cdot{}^{int.}\overleftrightarrow{\Pi}_{\alpha}^{(r_m)}\cdot|x_\alpha\rangle\end{aligned} \tag{4.44}$$

$$\begin{aligned}|e_\phi^{int.}\rangle=&E_0\cdot j\cdot\left(\frac{h}{k_s}\right)\cdot\kappa_\delta\cdot e^{jhz}\cdot\sum_{\alpha=1}^{N_d}a_\alpha\cdot{}^{int.}\overleftrightarrow{\Pi}_{\alpha}^{(r_m)}\cdot|x_\alpha\rangle\\&+E_0\cdot j\cdot\kappa_\delta\cdot e^{jhz}\cdot\sum_{\alpha=1}^{N_d}b_\alpha\cdot{}^{int.}\overleftrightarrow{\Pi}_{\alpha}^{(r_e)}\cdot|x_\alpha\rangle\end{aligned} \tag{4.45}$$

$$|h_z^{int.}\rangle=-\frac{k_s}{\omega\mu_0}\cdot E_0\cdot e^{jhz}\cdot\sum_{\alpha=1}^{N_d}b_\alpha\cdot{}^{int.}\overleftrightarrow{\Pi}_{\alpha}^{(z)}\cdot|x_\alpha\rangle \tag{4.46}$$

$$\begin{aligned}|h_r^{int.}\rangle=&-\frac{k_s}{\omega\mu_0}\cdot E_0\cdot j\cdot\left(\frac{h}{k_s}\right)\cdot\kappa_\delta\cdot e^{jhz}\cdot\sum_{\alpha=1}^{N_d}b_\alpha\cdot{}^{int.}\overleftrightarrow{\Pi}_{\alpha}^{(r_e)}\cdot|x_\alpha\rangle\\&-\frac{k_s}{\omega\mu_0}\cdot E_0\cdot j\cdot\kappa_\delta\cdot e^{jhz}\cdot\sum_{\alpha=1}^{N_d}a_\alpha\cdot{}^{int.}\overleftrightarrow{\Pi}_{\alpha}^{(r_m)}\cdot|x_\alpha\rangle\end{aligned} \tag{4.47}$$

$$|h_\phi^{int.}\rangle = -\frac{k_s}{\omega\mu_0}\cdot E_0\cdot j\cdot\left(\frac{h}{k_s}\right)\cdot\kappa_\delta\cdot e^{jhz}\cdot\sum_{\alpha=1}^{N_d} b_\alpha\cdot {}^{int.}\overleftrightarrow{\Pi}_\alpha^{(r_m)}\cdot|x_\alpha\rangle + \frac{k_s}{\omega\mu_0}\cdot E_0\cdot j\cdot\kappa_\delta\cdot e^{jhz}\cdot\sum_{\alpha=1}^{N_d} a_\alpha\cdot {}^{int.}\overleftrightarrow{\Pi}_\alpha^{(r_e)}\cdot|x_\alpha\rangle \tag{4.48}$$

with

$$\kappa_\delta = \left(1-\frac{h^2}{k_s^2}\right)^{\frac{1}{2}} \tag{4.49}$$

$$\rho_s = \kappa_\delta\cdot k_s\cdot r \tag{4.50}$$

$${}^{int.}\overleftrightarrow{\Pi}_\alpha^{(z)} = \kappa_\delta^2\cdot diag\left\{J_{\nu_a}(\rho_{s_i})\right\}\quad i=1,\ldots,N_d \tag{4.51}$$

$${}^{int.}\overleftrightarrow{\Pi}_\alpha^{(r_e)} = diag\left\{\frac{d}{d\rho_s}[J_{\nu_a}(\rho_s)]_{\rho_{s_i}}\right\}\quad i=1,\ldots,N_d \tag{4.52}$$

$${}^{int.}\overleftrightarrow{\Pi}_\alpha^{(r_m)} = diag\left\{\frac{1}{\rho_{s_i}}[J_{\nu_a}(\rho_{s_i})]\cdot\frac{1}{2h_\phi}\cdot\overleftrightarrow{D}_c^{(PC)}\right\}\quad i=1,\ldots,N_d \tag{4.53}$$

The corresponding algebraic components of the incident field result from (4.8)–(4.16) by inserting of ϕ_i, $i=1,\ldots,N_d$. Then, the following equation system from the continuity conditions (2.41)–(2.44) can be obtained:

$$\sum_{\alpha=1}^{N_d} a_\alpha\overleftrightarrow{M}_\alpha\cdot|x_\alpha\rangle + \sum_{\alpha=1}^{N_d} c_\alpha\overleftrightarrow{O}_\alpha\cdot|x_\alpha\rangle = -\frac{1}{E_0}e^{-jhz}\cdot|e_z^{inc.}\rangle_{TE/TM} \tag{4.54}$$

$$\begin{aligned}&\sum_{\alpha=1}^{N_d} a_\alpha\overleftrightarrow{Q}_\alpha\cdot|x_\alpha\rangle + \sum_{\alpha=1}^{N_d} b_\alpha\overleftrightarrow{R}_\alpha\cdot|x_\alpha\rangle\\ &+\sum_{\alpha=1}^{N_d} c_\alpha\overleftrightarrow{S}_\alpha\cdot|x_\alpha\rangle + \sum_{\alpha=1}^{N_d} d_\alpha\overleftrightarrow{T}_\alpha\cdot|x_\alpha\rangle\\ &= -\frac{j}{E_0}e^{-jhz}\cdot\left\{|e_\phi^{inc.}\rangle_{TE/TM} + diag[\tan\alpha_i]\cdot|e_r^{inc.}\rangle_{TE/TM}\right\}\\ &-\left(\frac{k_s}{k_0}\right)\sum_{\alpha=1}^{N_d} b_\alpha\overleftrightarrow{M}_\alpha\cdot|x_\alpha\rangle - \sum_{\alpha=1}^{N_d} d_\alpha\overleftrightarrow{O}_\alpha\cdot|x_\alpha\rangle\end{aligned} \tag{4.55}$$

$$= -\frac{\omega\mu_0}{E_0 k_0} e^{-jhz} \cdot |h_z^{inc.}\rangle_{TE/TM} \tag{4.56}$$

$$-\left(\frac{k_s}{k_0}\right)\sum_{\alpha=1}^{N_d} a_\alpha \overleftrightarrow{R}_\alpha \cdot |x_\alpha\rangle + \left(\frac{k_s}{k_0}\right)\sum_{\alpha=1}^{N_d} b_\alpha \overleftrightarrow{Q}_\alpha \cdot |x_\alpha\rangle$$

$$-\sum_{\alpha=1}^{N_d} c_\alpha \overleftrightarrow{T}_\alpha \cdot |x_\alpha\rangle + \sum_{\alpha=1}^{N_d} d_\alpha \overleftrightarrow{S}_\alpha \cdot |x_\alpha\rangle$$

$$= \frac{j}{E_0}\frac{\omega\mu_0}{k_0} e^{-jhz} \cdot \left\{|h_\phi^{inc.}\rangle_{TE/TM} + diag[\tan\alpha_i] \cdot |h_r^{inc.}\rangle_{TE/TM}\right\} \tag{4.57}$$

with

$$\overleftrightarrow{M}_\alpha = -^{int.}\overleftrightarrow{\Pi}_\alpha^{(z)} \tag{4.58}$$

$$\overleftrightarrow{O}_\alpha = {}^{s}\overleftrightarrow{\Pi}_\alpha^{(z)} \tag{4.59}$$

$$\overleftrightarrow{Q}_\alpha = \left(\frac{h}{k_s}\right)\kappa_\delta \left\{{}^{int.}\overleftrightarrow{\Pi}_\alpha^{(r_m)} + diag[\tan\alpha_i] \cdot {}^{int.}\overleftrightarrow{\Pi}_\alpha^{(r_e)}\right\} \tag{4.60}$$

$$\overleftrightarrow{R}_\alpha = \kappa_\delta \left\{{}^{int.}\overleftrightarrow{\Pi}_\alpha^{(r_e)} - diag[\tan\alpha_i] \cdot {}^{int.}\overleftrightarrow{\Pi}_\alpha^{(r_m)}\right\} \tag{4.61}$$

$$\overleftrightarrow{S}_\alpha = \left(\frac{h}{k_s}\right)\cos\delta \left\{{}^{s}\overleftrightarrow{\Pi}_\alpha^{(r_m)} + diag[\tan\alpha_i] \cdot {}^{s}\overleftrightarrow{\Pi}_\alpha^{(r_e)}\right\} \tag{4.62}$$

$$\overleftrightarrow{T}_\alpha = -\cos\delta \left\{{}^{s}\overleftrightarrow{\Pi}_\alpha^{(r_e)} - diag[\tan\alpha_i] \cdot {}^{s}\overleftrightarrow{\Pi}_\alpha^{(r_m)}\right\} \tag{4.63}$$

Equations (4.54)–(4.57) can be transformed by simple manipulation into the form

$$\begin{aligned} &\overleftrightarrow{A} \circ \vec{x}^t = \vec{I}_{inc.} \\ &\vec{x} = (\vec{a}, \vec{b}, \vec{c}, \vec{d}) \ , \end{aligned} \tag{4.64}$$

where the coefficient matrix $\overleftrightarrow{A}$ is of the size $(4N_d \times 4N_d)$. The unknown coefficients a_i, b_i, c_i, and d_i are then computed from this equation system.

Beside the inhomogeneity at the right hand side of (4.64), $\overleftrightarrow{A}$ also depends on the scatterer orientation with respect to the incident field. This results from the infinite cylinder extension and the corresponding separation of the z-variable.

Now we want to deal with the derivation of the corresponding equation system in spherical co-ordinates.

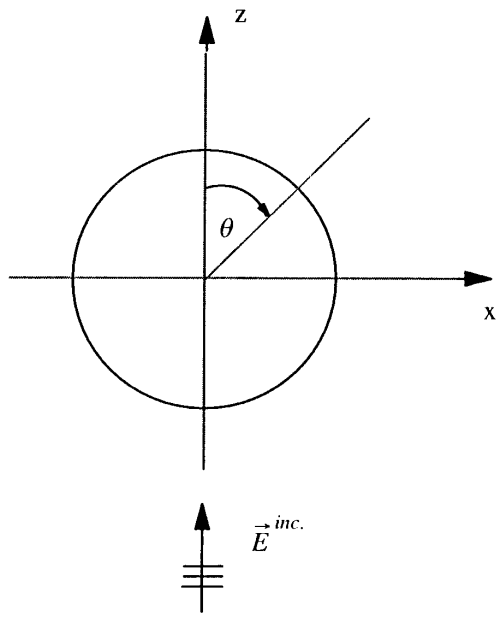

Figure 7. Scattering on a dielectric sphere.

4.2 The Discretized Mie-Formalism in Spherical Co-ordinates

4.2.1 The Limiting Case of Spheres

Plane wave scattering on dielectric spheres represents the limiting case (see Fig. 7). As for circular cylinders, the calculations simplify considerably. First of all, the expression (2.36) for α_i vanishes identically. We can, furthermore, restrict the consideration to the azimuthal mode $l = 1$. Thus, only the Dirichlet condition must be taken into account in the discretization with respect to θ. Consequently, Eqs. (3.37) and (3.38) can be reduced to

$$\Pi_e(r,\theta,\phi) = -\frac{k}{\omega\mu_0} E_0 \cos\phi \cdot \tilde{\Pi}_e(r,\theta) \tag{4.65}$$

$$\Pi_m(r,\theta,\phi) = E_0 \sin\phi \cdot \tilde{\Pi}_m(r,\theta)\ . \tag{4.66}$$

This form is caused by the simpler representation of the incident field. Under the assumption that it propagates along the positive z-direc-

tion, it reads as follows.

$$\vec{E}^{inc.} = \hat{x} \cdot E_0 \cdot \exp(jk_0 z) \tag{4.67}$$

$$\vec{H}^{inc.} = \hat{y} \cdot \frac{k_0}{\omega\mu_0} \cdot E_0 \cdot \exp(jk_0 z) \tag{4.68}$$

After choosing spherical co-ordinates we get the expressions

$$E_r^{inc.} = E_0 \cdot \cos\phi \cdot \sin\theta \cdot \exp(j\rho_0 \cdot \cos\theta) \tag{4.69}$$

$$E_\theta^{inc.} = E_0 \cdot \cos\phi \cdot \cos\theta \cdot \exp(j\rho_0 \cdot \cos\theta) \tag{4.70}$$

$$E_\phi^{inc.} = -E_0 \cdot \sin\phi \cdot \exp(j\rho_0 \cdot \cos\theta) \tag{4.71}$$

and

$$H_r^{inc.} = \frac{k_0}{\omega\mu_0} E_0 \cdot \sin\phi \cdot \sin\theta \cdot \exp(j\rho_0 \cdot \cos\theta) \tag{4.72}$$

$$H_\theta^{inc.} = \frac{k_0}{\omega\mu_0} E_0 \cdot \sin\phi \cdot \cos\theta \cdot \exp(j\rho_0 \cdot \cos\theta) \tag{4.73}$$

$$H_\phi^{inc.} = \frac{k_0}{\omega\mu_0} E_0 \cdot \cos\phi \cdot \exp(j\rho_0 \cdot \cos\theta) \tag{4.74}$$

with $\rho_0 = k_0 r$. In this way, both polarization contributions can be taken into account. Additionally, the diagonal matrices (3.66) and (3.67) become simple functions with respect to r. From the Mie theory it is known that the continuity conditions (2.37)–(2.40) can be reduced to corresponding continuity conditions for the Debye potentials in the case of a spherical geometry. In the algebraic form, they read as follows:

$$|\frac{d}{d\rho_0}(\rho_0 \cdot \Pi_e^{inc.})\rangle + |\frac{d}{d\rho_0}(\rho_0 \cdot \Pi_e^{s})\rangle = \frac{\epsilon_0}{\epsilon_s}|\frac{d}{d\rho_s}(\rho_s \cdot \Pi_e^{int.})\rangle \tag{4.75}$$

$$|\frac{d}{d\rho_0}(\rho_0 \cdot \Pi_m^{inc.})\rangle + |\frac{d}{d\rho_0}(\rho_0 \cdot \Pi_m^{s})\rangle = |\frac{d}{d\rho_s}(\rho_s \cdot \Pi_m^{int.})\rangle \tag{4.76}$$

$$|\Pi_e^{inc.}\rangle + |\Pi_e^{s}\rangle = |\Pi_e^{int.}\rangle \tag{4.77}$$

$$|\Pi_m^{inc.}\rangle + |\Pi_m^{s}\rangle = |\Pi_m^{int.}\rangle \tag{4.78}$$

The corresponding potentials of the incident field (4.69)–(4.74) are given by (compare, e.g., with [50, 58]):

$$\Pi_e^{inc.}(r,\theta,\phi) = -\frac{k_0}{\omega\mu_0} E_0 \cdot \cos\phi \cdot \tilde{\Pi}^{inc.}(r,\theta) \tag{4.79}$$

$$\Pi_m^{inc.}(r,\theta,\phi) = E_0 \cdot \sin\phi \cdot \tilde{\Pi}^{inc.}(r,\theta) \tag{4.80}$$

$$\tilde{\Pi}^{inc.} = \frac{1}{\rho_0} \sum_{n=1}^{\infty} \frac{(-j)^{-n}(2n+1)}{n(n+1)} \cdot j_n(\rho_0) \cdot P_n^1(\cos\theta) \tag{4.81}$$

j_n – Riccatti-Bessel functions
P_n^1 – Associated Legendre functions .

The components $\tilde{\Pi}_i^{inc.}$ of the algebraization result from (4.81) with $\Theta = \Theta_i$, $i = 1, \ldots, N_d$. Inserting these expressions and the relations (3.62)–(3.65) into the above mentioned continuity condition and multiplying the resulting equations by $\overleftrightarrow{Tr}^{-1}$ from the left yield a decoupled equation system for determining the unknown expansion coefficients. Note that, $\exp(j1\phi)$ is replaced by '$\sin\phi$' or '$\cos\phi$' according to (4.65)/(4.66). In eliminating a_i and b_i, we finally obtain the following expressions for the scattering coefficients c_i and d_i.

$$c_i = \frac{\epsilon_0 J_i' U_i - \epsilon_s J_i U_i'}{\epsilon_s H_i' J_i - \epsilon_0 H_i J_i'} \tag{4.82}$$

$$d_i = \frac{J_i' U_i - J_i U_i'}{H_i' J_i - H_i J_i'} \ , \tag{4.83}$$

where

$$J_i = \frac{1}{\sqrt{\rho_{s_i}}} \cdot J_{\nu_i}(\rho_{s_i}) \ ; \quad J_i' = \frac{d}{d\rho_s}[\sqrt{\rho_s} \cdot J_{\nu_i}(\rho_s)]_{\rho_{s_i}} \tag{4.84}$$

$$H_i = \frac{1}{\sqrt{\rho_{0_i}}} \cdot H_{\nu_i}^{(1)}(\rho_{0_i}) \ ; \quad H_i' = \frac{d}{d\rho_0}[\sqrt{\rho_0} \cdot H_{\nu_i}^{(1)}(\rho_0)]_{\rho_{0_i}} \tag{4.85}$$

$$U_i = \sum_{k=1}^{N_d} tr_{ik}^{-1} \cdot \tilde{\Pi}_k^{inc.} \ ; \quad U_i' = \frac{d}{d\rho_0}[\rho_0 \cdot U_i(\rho_0)]_{\rho_{0_i}} \ . \tag{4.86}$$

(4.82) and (4.83) show clearly the analogy to the Mie theory. But again, the differences to the known rigorous solutions which have already been stated in the discussion of (4.28) and (4.29) hold. The convergency behavior of the differential scattering cross-sections calculated by means of these scattering coefficients will be discussed in the numerical considerations of chapter 6.

4.2.2 Axisymmetric Geometries

The limitation to the azimuthal mode $l = 1$ and, consequently, to the modified *ansatz* (4.65)/(4.66) can also be maintained in the case where the incident field propagates along the symmetry axis (z-axis) of an axisymmetric scatterer. This would considerably simplify the

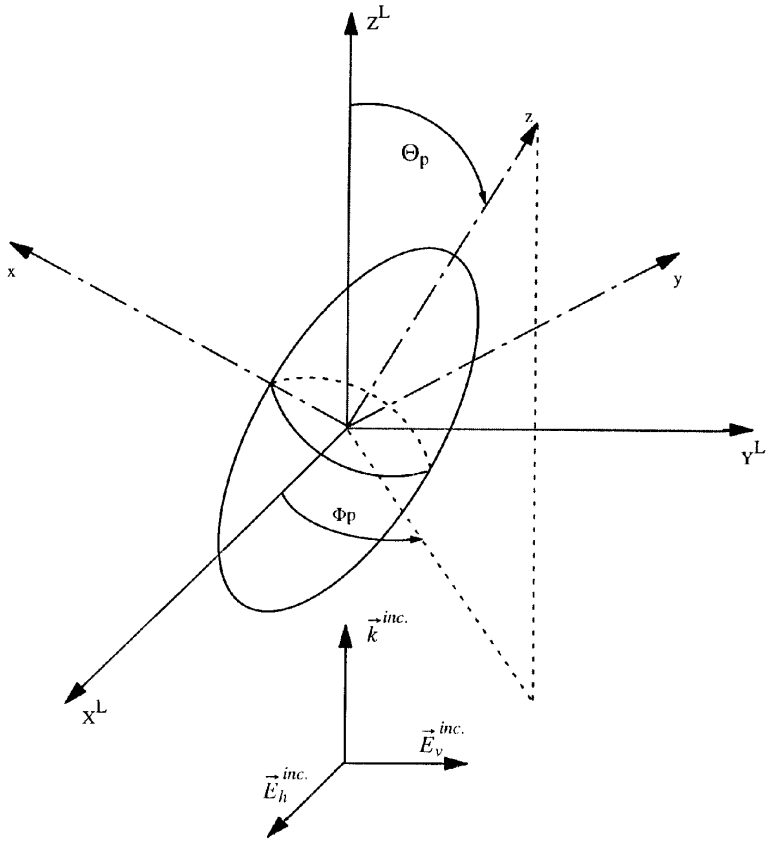

Figure 8. Orientation of the NAS in the laboratory frame.

derivation of the characteristic equation system which can, however, no longer be done in the DMS. Otherwise, since we want to allow a random scatterer orientation with respect to the incident field, this general case should be considered at once. Of course, it contains the limitation mentioned above as a special case, but in a more complicated form.

We go back to the *ansatz* (3.37)/(3.38) and deal first with the scatterer orientation with respect to the incident field. This can be done in a way which is known from the T-matrix approach [28]. The geometry is depicted in Fig. 8. The incident field may propagate, without loss of generality, along the positive z-axis of the laboratory frame

$\{X^L, Y^L, Z^L\}$, The scattering plane is chosen to be the $X^L Z^L$-plane. With respect to this plane, the incident field can be decomposed into a vertical and a horizontal part, i.e., it is $\vec{E}_h^{inc.} = E_h^{inc.} \cdot \hat{x}^L$ and $\vec{E}_v^{inc.} = E_v^{inc.} \cdot \hat{y}^L$.

It holds for the several contributions:

$$\vec{E}_v^{inc.} = \hat{Y}^L \cdot E_0 \cdot \exp(jk_0 Z^L) \tag{4.87}$$

$$\vec{H}_v^{inc.} = -\hat{X}^L \frac{k_0}{\omega\mu_0} \cdot E_0 \cdot \exp(jk_0 Z^L) \tag{4.88}$$

$$\vec{E}_h^{inc.} = -\frac{\omega\mu_0}{k_0} \cdot \vec{H}_v^{inc.} \tag{4.89}$$

$$\vec{H}_h^{inc.} = \frac{k_0}{\omega\mu_0} \cdot \vec{E}_v^{inc.} \tag{4.90}$$

The relationship between the vertical and the horizontal fields given by (4.89) and (4.90) is also valid for all further derivations. Therefore, we can restrict ourselves to the vertical contributions in the following considerations.

The orientation of the NAS in the laboratory frame is described by the 3 Eulerian angles Φ_p, Θ_p and Ψ_p. The rotational symmetry provides the freedom to choose any value for the angle Ψ_p but, for comparison purposes with Barber and Hill [28], $\Psi_p = 180°$ is taken in this paper. We want to formulate the DMF in the body frame $\{x, y, z\}$ since only there the simplifications which result from the rotational symmetry can be used. The transformation of the incident field into the body frame is given by:

$$\begin{pmatrix} \hat{X}^L \\ \hat{Y}^L \\ \hat{Z}^L \end{pmatrix} = \overleftrightarrow{A}_E^{-1} \circ \begin{pmatrix} \hat{x} \\ \hat{y} \\ \hat{z} \end{pmatrix} \tag{4.91}$$

with

$$\overleftrightarrow{A}_E^{-1} = \begin{pmatrix} -\cos\Phi_p \cdot \cos\Theta_p & \sin\Phi_p & \cos\Phi_p \cdot \sin\Theta_p \\ -\sin\Phi_p \cdot \cos\Theta_p & -\cos\Phi_p & \sin\Phi_p \cdot \sin\Theta_p \\ \sin\Theta_p & 0 & \cos\Theta_p \end{pmatrix} . \tag{4.92}$$

Applying the transformation to the incident field and choosing spherical co-ordinates in the body frame yield the following expressions:

$$
\begin{aligned}
{}^{(v)}E_r^{inc.} &= E_0 \cdot e^{j(s_b \cdot \cos\phi + c_b)} \cdot [\sin\Phi_p \cdot \sin\Theta_p \cdot \cos\theta \\
&\quad - \cos\Phi_p \cdot \sin\theta \cdot \sin\phi - \sin\Phi_p \cdot \cos\Theta_p \cdot \sin\theta \cdot \cos\phi] \qquad (4.93)\\
{}^{(v)}E_\phi^{inc.} &= E_0 \cdot e^{j(s_b \cdot \cos\phi + c_b)} \cdot [\sin\Phi_p \cdot \cos\Theta_p \cdot \sin\phi - \cos\Phi_p \cdot \cos\phi] \qquad (4.94)\\
{}^{(v)}E_\theta^{inc.} &= -E_0 \cdot e^{j(s_b \cdot \cos\phi + c_b)} \cdot [\cos\Phi_p \cdot \cos\theta \cdot \sin\phi \\
&\quad + \sin\Phi_p \cdot \cos\theta_p \cdot \cos\theta \cdot \cos\phi + \sin\Phi_p \cdot \sin\Theta_p \cdot \sin\theta] \qquad (4.95)
\end{aligned}
$$

$$
\begin{aligned}
{}^{(v)}H_r^{inc.} &= -\frac{k_0}{\omega\mu_0} \cdot E_0 \cdot e^{j(s_b \cdot \cos\phi + c_b)} \cdot [\sin\Phi_p \cdot \sin\theta \cdot \sin\phi \\
&\quad - \cos\Phi_p \cdot \cos\Theta_p \cdot \sin\theta \cdot \cos\phi + \cos\Phi_p \cdot \sin\Theta_p \cdot \cos\theta] \qquad (4.96)\\
{}^{(v)}H_\phi^{inc.} &= -\frac{k_0}{\omega\mu_0} \cdot E_0 \cdot e^{j(s_b \cdot \cos\phi + c_b)} \cdot [\sin\Phi_p \cdot \cos\phi \\
&\quad + \cos\Phi_p \cdot \cos\Theta_p \cdot \sin\phi] \qquad (4.97)\\
{}^{(v)}H_\theta^{inc.} &= -\frac{k_0}{\omega\mu_0} \cdot E_0 \cdot e^{j(s_b \cdot \cos\phi + c_b)} \cdot [\sin\Phi_p \cdot \cos\theta \cdot \sin\phi \\
&\quad - \cos\Phi_p \cdot \cos\Theta_p \cdot \cos\theta \cdot \cos\phi - \cos\Phi_p \cdot \sin\Theta_p \cdot \sin\theta] \qquad (4.98)
\end{aligned}
$$

$$
\begin{aligned}
s_b &= \rho_0 \cdot \sin\Theta_p \cdot \sin\theta \\
c_b &= \rho_0 \cdot \cos\Theta_p \cdot \cos\theta \qquad (4.99)\\
\rho_0 &= k_0 \cdot r
\end{aligned}
$$

In order to achieve the same functional dependence with respect to ϕ as in the relations (3.37) and (3.38) we apply a Fourier transformation to the incident field components in the body frame. This will enable an azimuthal decoupling of the characteristic equation system as discussed later (compare also with [34]). The following integrals are needed in performing the Fourier tranformation:

$$e_1^{(l)}(r,\theta) = \frac{1}{2\pi}\int_0^{2\pi} e^{js_b\cos\phi} \cdot e^{jl\phi} d\phi = j^l \cdot J_l(s_b) \qquad (4.100)$$

$$e_2^{(l)}(r,\theta) = \frac{1}{2\pi}\int_0^{2\pi} \sin\phi \cdot e^{js_b\cos\phi} \cdot e^{jl\phi} d\phi = -j^l \cdot l \cdot \frac{J_l(s_b)}{s_b} \qquad (4.101)$$

$$e_3^{(l)}(r,\theta) = \frac{1}{2\pi}\int_0^{2\pi} \cos\phi \cdot e^{js_b\cos\phi} \cdot e^{jl\phi} d\phi = -j^{l+1} \cdot \frac{dJ_l(s_b)}{ds_b} \qquad (4.102)$$

By this, the expressions for the Fourier transforms of the vertically polarized incident field components in the body frame are obtained.

$$
\begin{aligned}
{}^{(v)}E_r^{inc.} &= E_0 \cdot e^{jc_b} \sum_l e^{jl\phi} \cdot [\sin\Phi_p \cdot \sin\Theta_p \cdot \cos\theta \cdot e_1^{(l)} \\
&\quad - \cos\Phi_p \cdot \sin\theta \cdot e_2^{(l)} - \sin\Phi_p \cdot \cos\Theta_p \cdot \sin\theta \cdot e_3^{(l)}] \qquad (4.103)\\
{}^{(v)}E_\phi^{inc.} &= E_0 \cdot e^{jc_b} \sum_l e^{jl\phi} \cdot [\sin\Phi_p \cdot \cos\Theta_p \cdot e_2^{(l)} - \cos\Phi_p \cdot e_3^{(l)}] \qquad (4.104)\\
{}^{(v)}E_\theta^{inc.} &= -E_0 \cdot e^{jc_b} \sum_l e^{jl\phi} \cdot [\sin\Phi_p \cdot \sin\Theta_p \cdot \sin\theta \cdot e_1^{(l)} \\
&\quad + \cos\Phi_p \cdot \cos\theta \cdot e_2^{(l)} + \sin\Phi_q \cdot \cos\Theta_p \cdot \cos\theta \cdot e_3^{(l)}] \qquad (4.105)
\end{aligned}
$$

$$
\begin{aligned}
{}^{(v)}H_r^{inc.} &= -\frac{k_0}{\omega\mu_0} \cdot E_0 \cdot e^{jc_b} \sum_l e^{jl\phi} \cdot [\cos\Phi_q \cdot \sin\Theta_p \cdot \cos\theta \cdot e_1^{(l)} \\
&\quad + \sin\Phi_p \cdot \sin\theta \cdot e_2^{(l)} - \cos\Phi_p \cdot \cos\Theta_p \cdot \sin\theta \cdot e_3^{(l)}] \qquad (4.106)\\
{}^{(v)}H_\phi^{inc.} &= -\frac{k_0}{\omega\mu_0} \cdot E_0 \cdot e^{jc_b} \sum_l e^{jl\phi} \cdot [\cos\Phi_p \cdot \cos\Theta_p \cdot e_2^{(l)} + \sin\Phi_p \cdot e_3^{(l)}] \qquad (4.107)\\
{}^{(v)}H_r^{inc.} &= -\frac{k_0}{\omega\mu_0} \cdot E_0 \cdot e^{jc_b} \sum_l e^{jl\phi} \cdot [-\cos\Phi_p \cdot \sin\Theta_p \cdot \sin\theta \cdot e_1^{(l)} \\
&\quad + \sin\Phi_p \cdot \cos\theta \cdot e_2^{(l)} - \cos\Phi_p \cdot \cos\Theta_p \cdot \cos\theta \cdot e_3^{(l)}] \qquad (4.108)
\end{aligned}
$$

As already mentioned, the special case of propagation of the incident field along the symmetry axis, i.e., $\Phi_p = \Theta_p = 0$, leads to essential simplifications. Because of

$$
\begin{aligned}
\sin\phi &= \frac{j}{2} \cdot [e^{-j\phi} - e^{+j\phi}] \\
\cos\phi &= \frac{1}{2} \cdot [e^{-j\phi} + e^{+j\phi}] \; .
\end{aligned} \qquad (4.109)
$$

only the azimuthal modes $l = \pm 1$ need to be considered. Furthermore, the calculation has to be performed only for $l = +1$ since the scattering coefficients for $l = -1$ are related to those of $l = +1$. For the Fourier

integrals (4.100)–(4.102) it holds:

$$\begin{aligned} e_1^{(\pm 1)} &= 0 \\ e_2^{(\pm 1)} &= \mp\frac{j}{2} \\ e_3^{(\pm 1)} &= \frac{1}{2} \end{aligned} \tag{4.110}$$

This way is described in detail in [35].

The components of the internal and scattered field discretized with respect to θ result from equations (2.22)–(2.27) and the expressions (3.62)–(3.65) for the potentials. Again, the differential quotient $\delta/\delta\theta$ is replaced by the difference operator $1/(2h_\theta) \cdot \overleftrightarrow{D}_c^{(DC/NC)}$ (DC or NC according to the azimuthal mode l) defined in (3.7) and (3.8). We get:

$$|e_r^s\rangle = -E_0 \sum_l e^{jl\phi} \sum_{\alpha=1}^{N_d} c_\alpha^{(l)} \cdot {}^s\overleftrightarrow{\Pi}_\alpha^{r^{(l)}} \cdot |x_\alpha^{(l)}\rangle \tag{4.111}$$

$$\begin{aligned} |e_\theta^s\rangle = &-E_0 \sum_l e^{jl\phi} \sum_{\alpha=1}^{N_d} c_\alpha^{(l)} \cdot {}^s\overleftrightarrow{\Pi}_\alpha^{\theta_e^{(l)}} \cdot |x_\alpha^{(l)}\rangle \\ &+ E_0 \sum_l l \cdot e^{jl\phi} \sum_{\alpha=1}^{N_d} d_\alpha^{(l)} \cdot {}^s\overleftrightarrow{\Pi}_\alpha^{\theta_m^{(l)}} \cdot |x_\alpha^{(l)}\rangle \end{aligned} \tag{4.112}$$

$$\begin{aligned} |e_\phi^s\rangle = &E_0 \sum_l l \cdot e^{jl\phi} \sum_{\alpha=1}^{N_d} c_\alpha^{(l)} \cdot {}^s\overleftrightarrow{\Pi}_\alpha^{\phi_e^{(l)}} \cdot |x_\alpha^{(l)}\rangle \\ &- E_0 \sum_l e^{jl\phi} \sum_{\alpha=1}^{N_d} d_\alpha^{(l)} \cdot {}^s\overleftrightarrow{\Pi}_\alpha^{\phi_m^{(l)}} \cdot |x_\alpha^{(l)}\rangle \end{aligned} \tag{4.113}$$

$$|h_r^s\rangle = -\frac{k_0}{\omega\mu_0} \cdot E_0 \sum_l e^{jl\phi} \sum_{\alpha=1}^{N_d} d_\alpha^{(l)} \cdot {}^s\overleftrightarrow{\Pi}_\alpha^{r^{(l)}} \cdot |x_\alpha^{(l)}\rangle \tag{4.114}$$

$$\begin{aligned} |h_\theta^s\rangle = &-\frac{k_0}{\omega\mu_0} \cdot E_0 \sum_l e^{jl\phi} \sum_{\alpha=1}^{N_d} d_\alpha^{(l)} \cdot {}^s\overleftrightarrow{\Pi}_\alpha^{\theta_e^{(l)}} \cdot |x_\alpha^{(l)}\rangle \\ &- \frac{k_0}{\omega\mu_0} \cdot E_0 \sum_l l \cdot e^{jl\phi} \sum_{\alpha=1}^{N_d} c_\alpha^{(l)} \cdot {}^s\overleftrightarrow{\Pi}_\alpha^{\theta_m^{(l)}} \cdot |x_\alpha^{(l)}\rangle \end{aligned} \tag{4.115}$$

$$|h_\phi^s\rangle = \frac{k_0}{\omega\mu_0}\cdot E_0 \sum_l l\cdot e^{jl\phi}\sum_{\alpha=1}^{N_d} d_\alpha^{(l)}\cdot {}^s\overleftrightarrow{\Pi}_\alpha^{\phi_e^{(l)}}\cdot |x_\alpha^{(l)}\rangle + \frac{k_0}{\omega\mu_0}\cdot E_0\sum_l e^{jl\phi}\sum_{\alpha=1}^{N_d} c_\alpha^{(l)}\cdot {}^s\overleftrightarrow{\Pi}_\alpha^{\phi_m^{(l)}}\cdot |x_\alpha^{(l)}\rangle \tag{4.116}$$

with

$${}^s\overleftrightarrow{\Pi}_\alpha^{r^{(l)}} = j\cdot diag\left\{\left[\sqrt{\rho_0}\cdot H^{(1)}_{\nu_\alpha^{(l)}}(\rho_0)\right]''_{\rho_{0_i}}\right\} + j\cdot diag\left\{\sqrt{\rho_0}\cdot H^{(1)}_{\nu_\alpha^{(l)}}(\rho_{0_i})\right\} \tag{4.117}$$

$${}^s\overleftrightarrow{\Pi}_\alpha^{\theta_e^{(l)}} = j\cdot diag\left\{\frac{1}{\rho_{0_i}}\cdot\left[\sqrt{\rho_0}\cdot H^{(1)}_{\nu_\alpha^{(l)}}(\rho_0)\right]'_{\rho_{0_i}}\right\}\cdot\frac{1}{2h_\theta}\cdot\overleftrightarrow{D}_c^{(l)} \tag{4.118}$$

$${}^s\overleftrightarrow{\Pi}_\alpha^{\theta_m^{(l)}} = j\cdot diag\left\{\frac{1}{\sqrt{\rho_{0_i}}}\cdot H^{(1)}_{\nu_\alpha^{(l)}}(\rho_{0_i})\right\}\cdot diag[\sin^{-1}\theta_i] \tag{4.119}$$

$${}^s\overleftrightarrow{\Pi}_\alpha^{\phi_e^{(l)}} = diag\left\{\frac{1}{\rho_{0_i}}\cdot\left[\sqrt{\rho_0}\cdot H^{(1)}_{\nu_\alpha^{(l)}}(\rho_0)\right]'_{\rho_{0_i}}\right\}\cdot diag[\sin^{-1}\theta_i] \tag{4.120}$$

$${}^s\overleftrightarrow{\Pi}_\alpha^{\phi_m^{(l)}} = diag\left\{\frac{1}{\sqrt{\rho_{0_i}}}\cdot H^{(1)}_{\nu_\alpha^{(l)}}(\rho_{0_i})\right\}\cdot\frac{1}{2h_\theta}\cdot\overleftrightarrow{D}_c^{(l)} \tag{4.121}$$

and

$$|e_r^{int.}\rangle = -E_0\sum_l e^{jl\phi}\sum_{\alpha=1}^{N_d} a_\alpha^{(l)}\cdot {}^{int.}\overleftrightarrow{\Pi}_\alpha^{r^{(l)}}\cdot |x_\alpha^{(l)}\rangle \tag{4.122}$$

$$|e_\theta^{int.}\rangle = -E_0\sum_l e^{jl\phi}\sum_{\alpha=1}^{N_d} a_\alpha^{(l)}\cdot {}^{int.}\overleftrightarrow{\Pi}_\alpha^{\theta_e^{(l)}}\cdot |x_\alpha^{(l)}\rangle + E_0\sum_l l\cdot e^{jl\phi}\sum_{\alpha=1}^{N_d} b_\alpha^{(l)}\cdot {}^{int.}\overleftrightarrow{\Pi}_\alpha^{\theta_m^{(l)}}\cdot |x_\alpha^{(l)}\rangle \tag{4.123}$$

$$|e_\phi^{int.}\rangle = E_0\sum_l l\cdot e^{jl\phi}\sum_{\alpha=1}^{N_d} a_\alpha^{(l)}\cdot {}^{int.}\overleftrightarrow{\Pi}_\alpha^{\phi_e^{(l)}}\cdot |x_\alpha^{(l)}\rangle - E_0\sum_l e^{jl\phi}\sum_{\alpha=1}^{N_d} b_\alpha^{(l)}\cdot {}^{int.}\overleftrightarrow{\Pi}_\alpha^{\phi_m^{(l)}}\cdot |x_\alpha^{(l)}\rangle \tag{4.124}$$

$$|h_r^{int.}\rangle = -\frac{k_s}{\omega\mu_0}\cdot E_0 \sum_l e^{jl\phi} \sum_{\alpha=1}^{N_d} b_\alpha^{(l)} \cdot {}^{int.}\overleftrightarrow{\Pi}_\alpha^{r^{(l)}} \cdot |x_\alpha^{(l)}\rangle \tag{4.125}$$

$$\begin{aligned}|h_\theta^{int.}\rangle = &-\frac{k_s}{\omega\mu_0}\cdot E_0 \sum_l e^{jl\phi} \sum_{\alpha=1}^{N_d} b_\alpha^{(l)} \cdot {}^{int.}\overleftrightarrow{\Pi}_\alpha^{\theta_e^{(l)}} \cdot |x_\alpha^{(l)}\rangle \\ &-\frac{k_s}{\omega\mu_0}\cdot E_0 \sum_l l\cdot e^{jl\phi} \sum_{\alpha=1}^{N_d} a_\alpha^{(l)} \cdot {}^{int.}\overleftrightarrow{\Pi}_\alpha^{\theta_m^{(l)}} \cdot |x_\alpha^{(l)}\rangle\end{aligned} \tag{4.126}$$

$$\begin{aligned}|h_\phi^{int.}\rangle = &\frac{k_s}{\omega\mu_0}\cdot E_0 \sum_l l\cdot e^{jl\phi} \sum_{\alpha=1}^{N_d} b_\alpha^{(l)} \cdot {}^{int.}\overleftrightarrow{\Pi}_\alpha^{\phi_e^{(l)}} \cdot |x_\alpha^{(l)}\rangle \\ &+\frac{k_s}{\omega\mu_0}\cdot E_0 \sum_l e^{jl\phi} \sum_{\alpha=1}^{N_d} a_\alpha^{(l)} \cdot {}^{int.}\overleftrightarrow{\Pi}_\alpha^{\phi_m^{(l)}} \cdot |x_\alpha^{(l)}\rangle\end{aligned} \tag{4.127}$$

with

$${}^{int.}\overleftrightarrow{\Pi}_\alpha^{r^{(l)}} = j\cdot diag\left\{\left[\sqrt{\rho_s}\cdot J_{\nu_\alpha^{(l)}}(\rho_s)\right]''_{\rho_{s_i}}\right\} + j\cdot diag\left\{\sqrt{\rho_{s_i}}\cdot J_{\nu_\alpha^{(l)}}(\rho_{s_i})\right\} \tag{4.128}$$

$${}^{int.}\overleftrightarrow{\Pi}_\alpha^{\theta_e^{(l)}} = j\cdot diag\left\{\frac{1}{\rho_{s_i}}\cdot\left[\sqrt{\rho_s}\cdot J_{\nu_\alpha^{(l)}}(\rho_s)\right]'_{\rho_{s_i}}\right\}\cdot\frac{1}{2h_\theta}\cdot\overleftrightarrow{D}_c^{(l)} \tag{4.129}$$

$${}^{int.}\overleftrightarrow{\Pi}_\alpha^{\theta_m^{(l)}} = j\cdot diag\left\{\frac{1}{\sqrt{\rho_{s_i}}}\cdot J_{\nu_\alpha^{(l)}}(\rho_{s_i})\right\}\cdot diag[\sin^{-1}\theta_i] \tag{4.130}$$

$${}^{int.}\overleftrightarrow{\Pi}_\alpha^{\phi_e^{(l)}} = diag\left\{\frac{1}{\rho_{s_i}}\cdot\left[\sqrt{\rho_s}\cdot J_{\nu_\alpha^{(l)}}(\rho_s)\right]'_{\rho_{s_i}}\right\}\cdot diag[\sin^{-1}\theta_i] \tag{4.131}$$

$${}^{int.}\overleftrightarrow{\Pi}_\alpha^{\phi_m^{(l)}} = diag\left\{\frac{1}{\sqrt{\rho_{s_i}}}\cdot J_{\nu_\alpha^{(l)}}(\rho_{s_i})\right\}\cdot\frac{1}{2h_\theta}\cdot\overleftrightarrow{D}_c^{(l)} \tag{4.132}$$

The primes at the brackets denote differentiation with respect to the arguments of the Bessel and Hankel functions, respectively. The index i is always running from 1 to N_d. Inserting of these relations into the continuity conditions (2.37)–(2.40) and integrating each of the four equations with $\int_0^{2\pi} e^{-jl'\phi}d\phi$ yield a characteristic equation system for each azimuthal mode l of the form

$$\sum_{\alpha=1}^{N_d} a_\alpha^{(l)} \overleftrightarrow{M}_\alpha^{(l)} \cdot |x_\alpha^{(l)}\rangle + \sum_{\alpha=1}^{N_d} b_\alpha^{(l)} l \cdot \overleftrightarrow{N}_\alpha^{(l)} \cdot |x_\alpha^{(l)}\rangle$$
$$+ \sum_{\alpha=1}^{N_d} c_\alpha^{(l)} \overleftrightarrow{O}_\alpha^{(l)} \cdot |x_\alpha^{(l)}\rangle + \sum_{\alpha=1}^{N_d} d_\alpha^{(l)} l \cdot \overleftrightarrow{P}_\alpha^{(l)} \cdot |x_\alpha^{(l)}\rangle$$
$$= -\frac{1}{E_0} \cdot \left\{ |e_\theta^{inc.}\rangle^{(l)} + diag[\tan\alpha_i] \cdot |e_r^{inc.}\rangle^{(l)} \right\} \tag{4.133}$$

$$\sum_{\alpha=1}^{N_d} a_\alpha^{(l)} l \cdot \overleftrightarrow{Q}_\alpha^{(l)} \cdot |x_\alpha^{(l)}\rangle + \sum_{\alpha=1}^{N_d} b_\alpha^{(l)} \overleftrightarrow{R}_\alpha^{(l)} \cdot |x_\alpha^{(l)}\rangle$$
$$+ \sum_{\alpha=1}^{N_d} c_\alpha^{(l)} l \cdot \overleftrightarrow{S}_\alpha^{(l)} \cdot |x_\alpha^{(l)}\rangle + \sum_{\alpha=1}^{N_d} d_\alpha^{(l)} \overleftrightarrow{T}_\alpha^{(l)} \cdot |x_\alpha^{(l)}\rangle = \frac{1}{E_0} \cdot |e_\phi^{inc.}\rangle^{(l)} \tag{4.134}$$

$$-\frac{k_s}{k_0} \cdot \sum_{\alpha=1}^{N_d} a_\alpha^{(l)} l \cdot \overleftrightarrow{N}_\alpha^{(l)} \cdot |x_\alpha^{(l)}\rangle + \frac{k_s}{k_0} \cdot \sum_{\alpha=1}^{N_d} b_\alpha^{(l)} \overleftrightarrow{M}_\alpha^{(l)} \cdot |x_\alpha^{(l)}\rangle$$
$$- \sum_{\alpha=1}^{N_d} c_\alpha^{(l)} l \cdot \overleftrightarrow{P}_\alpha^{(l)} \cdot |x_\alpha^{(l)}\rangle + \sum_{\alpha=1}^{N_d} d_\alpha^{(l)} \overleftrightarrow{O}_\alpha^{(l)} \cdot |x_\alpha^{(l)}\rangle$$
$$= -\frac{\omega\mu_0}{k_0} \cdot \frac{1}{E_0} \cdot \left\{ |h_\theta^{inc.}\rangle^{(l)} + diag[\tan\alpha_i] \cdot |h_r^{inc.}\rangle^{(l)} \right\} \tag{4.135}$$

$$\frac{k_s}{k_0} \cdot \sum_{\alpha=1}^{N_d} a_\alpha^{(l)} \overleftrightarrow{R}_\alpha^{(l)} \cdot |x_\alpha^{(l)}\rangle - \frac{k_s}{k_0} \cdot \sum_{\alpha=1}^{N_d} b_\alpha^{(l)} l \cdot \overleftrightarrow{Q}_\alpha^{(l)} \cdot |x_\alpha^{(l)}\rangle$$
$$+ \sum_{\alpha=1}^{N_d} c_\alpha^{(l)} \overleftrightarrow{T}_\alpha^{(l)} \cdot |x_\alpha^{(l)}\rangle - \sum_{\alpha=1}^{N_d} d_\alpha^{(l)} l \cdot \overleftrightarrow{S}_\alpha^{(l)} \cdot |x_\alpha^{(l)}\rangle$$
$$= -\frac{\omega\mu_0}{k_0} \cdot \frac{1}{E_0} \cdot |h_\phi^{inc.}\rangle^{(l)} \tag{4.136}$$

with

$$\overleftrightarrow{M}_\alpha^{(l)} = {}^{int.}\overleftrightarrow{\Pi}_\alpha^{\theta_e^{(l)}} + diag[\tan\alpha_i] \cdot {}^{int.}\overleftrightarrow{\Pi}_\alpha^{r^{(l)}} \tag{4.137}$$

$$\overleftrightarrow{N}_\alpha^{(l)} = -{}^{int.}\overleftrightarrow{\Pi}_\alpha^{\theta_m^{(l)}} \tag{4.138}$$

$$\overleftrightarrow{O}_\alpha^{(l)} = -\left[{}^{s}\overleftrightarrow{\Pi}_\alpha^{\theta_e^{(l)}} + diag[\tan\alpha_i] \cdot {}^{s}\overleftrightarrow{\Pi}_\alpha^{r^{(l)}} \right] \tag{4.139}$$

$$\overleftrightarrow{P}_{\alpha}^{(l)} = {}^{s}\overleftrightarrow{\Pi}_{\alpha}^{\theta_m^{(l)}} \tag{4.140}$$

$$\overleftrightarrow{Q}_{\alpha}^{(l)} = {}^{int.}\overleftrightarrow{\Pi}_{\alpha}^{\phi_e^{(l)}} \tag{4.141}$$

$$\overleftrightarrow{R}_{\alpha}^{(l)} = -{}^{int.}\overleftrightarrow{\Pi}_{\alpha}^{\phi_m^{(l)}} \tag{4.142}$$

$$\overleftrightarrow{S}_{\alpha}^{(l)} = -{}^{s}\overleftrightarrow{\Pi}_{\alpha}^{\phi_e^{(l)}} \tag{4.143}$$

$$\overleftrightarrow{T}_{\alpha}^{(l)} = {}^{s}\overleftrightarrow{\Pi}_{\alpha}^{\phi_m^{(l)}} \quad . \tag{4.144}$$

Again, equations (4.133)–(4.136) can be transformed into the form

$$\begin{aligned} &\overleftrightarrow{A}^{(l)} \circ \vec{x}^{t^{(l)}} = \vec{I}_{inc.}^{(l)} \\ &\vec{x}^{(l)} = \left(\vec{a}^{(l)}, \vec{b}^{(l)}, \vec{c}^{(l)}, \vec{d}^{(l)}\right) \ , \end{aligned} \tag{4.145}$$

where the coefficient matrix is of the size $(4N_d \times 4N_d)$.

In contrast to (4.64), the coefficient matrix in (4.145) is only a function of the geometry and the size parameter. It does not depend on the scatterer orientation with respect to the incident field. On the other hand, $\vec{I}_{inc.}^{(l)}$ is determined only by the l-th expansion coefficients of the incident field according to (4.103)–(4.108).

By equations (4.64) and (4.145), which represent the central relations of the DMF in cylindrical and spherical co-ordinates, the scattering problem on dielectric particles with non-separable boundaries is solved. In the last section of this chapter we want to discuss an iteration scheme that results in a more stable numerical algorithm.

4.3 The Iterative Discretized Mie-Formalisms

The determination of the expansion coefficients of the internal and scattered field by means of equations (4.64) and (4.145), respectively, is in principle possible but has a restricted range of applicability due to numerical problems. Investigations of ellipsoidal scatterers with aspect ratios $\leq 1.5:1$, where aspect ratio means the ratio of the largest to the smallest scatterer dimension, have shown that a discretization in $0.7°$ – steps leads to convergent results. This corresponds to a discretization number of $N_d \approx 250$ which is also the number of expansion coefficients. The resulting coefficient matrix is actually small in comparison to FD/FE methods but large enough to have negative effects

on computing time and memory capacity. An increasing number of discretization lines produces additionally the problem of an ill-conditioned coefficient matrix for which more sophisticated algorithms such as the Singular Value Decomposition have to be applied. Scatterers with larger aspect ratios can hardly be treated by using equations (4.64) and (4.145). These are essentially the problems from which some of the methods mentioned in the introduction suffer, and which can lead to a rather strong limitation in the range of application.

On the other hand it is known from the Mie theory that the number of scattered field expansion coefficients, which has to be taken into account in order to achieve a convergent result, depends mainly on the size parameter under consideration. There are only three coefficients sufficient in the Rayleigh region, for instance. We can observe a similar behavior for nonseparable geometries. The differential scattering cross-sections of an ellipsoid with $a = 3\,\mathrm{mm}$, $b = 2\,\mathrm{mm}$, $\epsilon_s = 2.0$, and $f = 10\,\mathrm{GHz}$ (this corresponds to a size parameter of $k_0 a = 0.628$) are shown in Fig. 9. There we assumed plane wave incidence along the axis of symmetry. The definition of the scattering quantities will be discussed in the next chapter. Very stable results are obtained in considering only five coefficients in the field expansion (4.111)–(4.113). The use of more expansion terms shows only minute changes in the curves. The first ten expansion coefficients are given in Table 1. It is seen that they become very rapidly smaller. In practice, however, 250 coefficients are computed. Therefore, the question arises if this behavior can be taken into account. Indeed, this can be done. For this, let us return to the expressions (4.34)–(4.53) and (4.111)–(4.132), respectively. Now the sum is no longer running from 1 to N_d, but it is stopped at a certain *ncut* where *ncut* represents a convergency parameter still to be determined. Inserting of these expressions into the corresponding continuity conditions yields

$$\sum_{\alpha=1}^{ncut} a_\alpha \overleftrightarrow{M}_\alpha \cdot |x_\alpha\rangle + \sum_{\alpha=1}^{ncut} c_\alpha \overleftrightarrow{O}_\alpha \cdot |x_\alpha\rangle = -|\tilde{e}_z^{inc.}\rangle_{TE/TM} \tag{4.146}$$

$$\sum_{\alpha=1}^{ncut} a_\alpha \overleftrightarrow{Q}_\alpha \cdot |x_\alpha\rangle + \sum_{\alpha=1}^{ncut} b_\alpha \overleftrightarrow{R}_\alpha \cdot |x_\alpha\rangle + \sum_{\alpha=1}^{ncut} c_\alpha \overleftrightarrow{S}_\alpha \cdot |x_\alpha\rangle$$
$$+ \sum_{\alpha=1}^{ncut} d_\alpha \overleftrightarrow{T}_\alpha \cdot |x_\alpha\rangle = -|\tilde{e}_{\phi,r}^{inc.}\rangle_{TE/TM} \tag{4.147}$$

i	c(i)	d(i)
1	– 3.005 – j 4.98 E–2	– 0.1465 + j 3.47 E–4
2	– 2.8 E–4 +j 5.21 E–2	– 8.8 E–5 – j 8.65 E–3
3	– 4.29 E–3 – j 7.54 E–5	– 2.24 E–4 + j 9.18 E–6
4	4.76 E–7 + j 9.39 E–5	– 3.92 E–7 – j 8.88 E–6
5	– 4.6 E–6 – j 1.04 E–7	– 2.12 E–7 + j 2.23 E–8
6	1.8 E–9 + j 9.2 E–8	– 5.9 E–10 – j 5.96 E–9
7	– 3.16 E–9 – j 1.03 E–10	– 1.26 E–10 + j 2.66 E–11
8	2.2 E–12 + j 5.62 E–11	– 5.23 E–13 – j 2.67 E–12
9	– 1.5 E–12 – j 7. E–14	– 5. E–14 + j 2. E–14
10	1.52 E–15 + j 2.34 E–14	– 3.13 E–16 – j 8.1 E–16

Table 1. Expansion coefficients of the scattered field.

$$-\left(\frac{k_s}{k_0}\right)\cdot\sum_{\alpha=1}^{ncut} b_\alpha \overleftrightarrow{M}_\alpha\cdot|x_\alpha\rangle - \sum_{\alpha=1}^{ncut} d_\alpha \overleftrightarrow{O}_\alpha\cdot|x_\alpha\rangle = -|\tilde{h}_z^{inc.}\rangle_{TE/TM} \quad (4.148)$$

$$-\left(\frac{k_s}{k_0}\right)\cdot\sum_{\alpha=1}^{ncut} a_\alpha \overleftrightarrow{R}_\alpha\cdot|x_\alpha\rangle + \left(\frac{k_s}{k_0}\right)\cdot\sum_{\alpha=1}^{ncut} b_\alpha \overleftrightarrow{Q}_\alpha\cdot|x_\alpha\rangle - \sum_{\alpha=1}^{ncut} c_\alpha \overleftrightarrow{T}_\alpha\cdot|x_\alpha\rangle$$
$$+\sum_{\alpha=1}^{ncut} d_\alpha \overleftrightarrow{S}_\alpha\cdot|x_\alpha\rangle = -|\tilde{h}_{\phi,r}^{inc.}\rangle_{TE/TM} \quad (4.149)$$

$$|\tilde{e}_z^{inc.}\rangle_{TE/TM} = \frac{1}{E_0}\cdot e^{-jhz}\cdot|e_z^{inc.}\rangle_{TE/TM} \quad (4.150)$$

$$|\tilde{e}_{\phi,r}^{inc.}\rangle_{TE/TM} = \frac{j}{E_0}\cdot e^{-jhz}\cdot\{|e_\phi^{inc.}\rangle_{TE/TM} + diag[\tan\alpha_i]\cdot|e_r^{inc.}\rangle_{TE/TM}\} \quad (4.151)$$

$$|\tilde{h}_z^{inc.}\rangle_{TE/TM} = \frac{\omega\mu_0}{E_0 k_0}\cdot e^{-jhz}\cdot|h_z^{inc.}\rangle_{TE/TM} \quad (4.152)$$

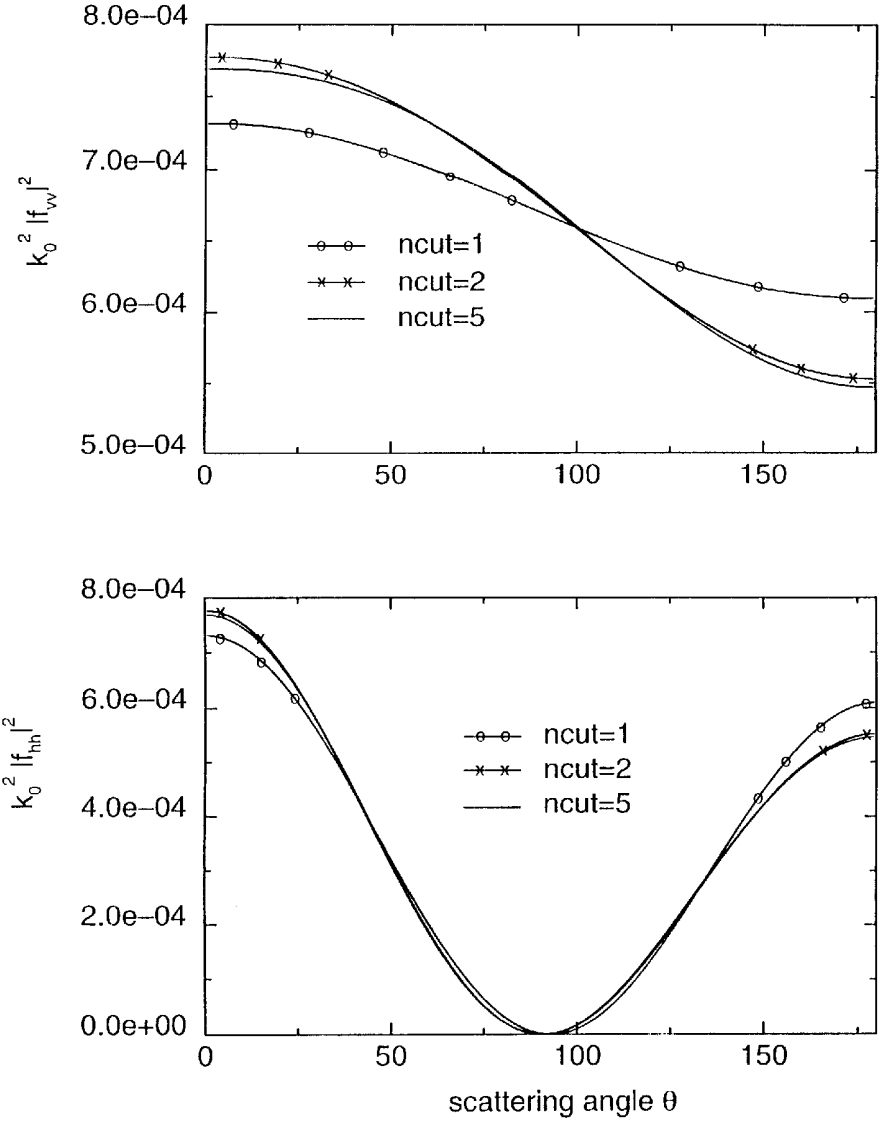

Figure 9. Differential scattering cross-sections (vv - and hh -polarization) taking $ncut$ expansion coefficients into account.

$$|\tilde{h}^{inc.}_{\phi,r}\rangle_{TE/TM} = \frac{j\omega\mu_0}{E_0 k_0}\cdot e^{-jhz}\cdot\{|h^{inc.}_{\phi}\rangle_{TE/TM} + diag[\tan\alpha_i]\cdot|h^{inc.}_{r}\rangle_{TE/TM}\} \quad (4.153)$$

in the case of NIC, and

$$\sum_{\alpha=1}^{ncut} a^{(l)}_{\alpha}\overleftrightarrow{M}^{(l)}_{\alpha}\cdot|x^{(l)}_{\alpha}\rangle + \sum_{\alpha=1}^{ncut} b^{(l)}_{\alpha} l\cdot\overleftrightarrow{N}^{(l)}_{\alpha}\cdot|x^{(l)}_{\alpha}\rangle + \sum_{\alpha=1}^{ncut} c^{(l)}_{\alpha}\overleftrightarrow{O}^{(l)}_{\alpha}\cdot|x^{(l)}_{\alpha}\rangle + \sum_{\alpha=1}^{ncut} d^{(l)}_{\alpha} l\cdot\overleftrightarrow{P}^{(l)}_{\alpha}\cdot|x^{(l)}_{\alpha}\rangle = -|\tilde{e}^{inc.}_{\theta,r}\rangle^{(l)} \quad (4.154)$$

$$\sum_{\alpha=1}^{ncut} a^{(l)}_{\alpha} l\cdot\overleftrightarrow{Q}^{(l)}_{\alpha}\cdot|x^{(l)}_{\alpha}\rangle + \sum_{\alpha=1}^{ncut} b^{(l)}_{\alpha}\overleftrightarrow{R}^{(l)}_{\alpha}\cdot|x^{(l)}_{\alpha}\rangle + \sum_{\alpha=1}^{ncut} c^{(l)}_{\alpha} l\cdot\overleftrightarrow{S}^{(l)}_{\alpha}\cdot|x^{(l)}_{\alpha}\rangle + \sum_{\alpha=1}^{ncut} d^{(l)}_{\alpha}\overleftrightarrow{T}^{(l)}_{\alpha}\cdot|x^{(l)}_{\alpha}\rangle = |\tilde{e}^{inc.}_{\phi}\rangle^{(l)} \quad (4.155)$$

$$-\frac{k_s}{k_0}\cdot\sum_{\alpha=1}^{ncut} a^{(l)}_{\alpha} l\cdot\overleftrightarrow{N}^{(l)}_{\alpha}\cdot|x^{(l)}_{\alpha}\rangle + \frac{k_s}{k_0}\cdot\sum_{\alpha=1}^{ncut} b^{(l)}_{\alpha}\overleftrightarrow{M}^{(l)}_{\alpha}\cdot|x^{(l)}_{\alpha}\rangle - \sum_{\alpha=1}^{ncut} c^{(l)}_{\alpha} l\cdot\overleftrightarrow{P}^{(l)}_{\alpha}\cdot|x^{(l)}_{\alpha}\rangle + \sum_{\alpha=1}^{ncut} d^{(l)}_{\alpha}\overleftrightarrow{O}^{(l)}_{\alpha}\cdot|x^{(l)}_{\alpha}\rangle = -|\tilde{h}^{inc.}_{\theta,r}\rangle^{(l)} \quad (4.156)$$

$$\frac{k_s}{k_0}\cdot\sum_{\alpha=1}^{ncut} a^{(l)}_{\alpha}\overleftrightarrow{R}^{(l)}_{\alpha}\cdot|x^{(l)}_{\alpha}\rangle - \frac{k_s}{k_0}\cdot\sum_{\alpha=1}^{ncut} b^{(l)}_{\alpha} l\cdot\overleftrightarrow{Q}^{(l)}_{\alpha}\cdot|x^{(l)}_{\alpha}\rangle + \sum_{\alpha=1}^{ncut} c^{(l)}_{\alpha}\overleftrightarrow{T}^{(l)}_{\alpha}\cdot|x^{(l)}_{\alpha}\rangle - \sum_{\alpha=1}^{ncut} d^{(l)}_{\alpha} l\cdot\overleftrightarrow{S}^{(l)}_{\alpha}\cdot|x^{(l)}_{\alpha}\rangle = -|\tilde{h}^{inc.}_{\phi}\rangle^{(l)} \quad (4.157)$$

$$|\tilde{e}^{inc.}_{\theta,r}\rangle^{(l)} = \frac{1}{E_0}\cdot\{|e^{inc.}_{\theta}\rangle^{(l)} + diag[\tan\alpha_i]\cdot|e^{inc.}_{r}\rangle^{(l)}\} \quad (4.158)$$

$$|\tilde{e}^{inc.}_{\phi}\rangle^{(l)} = \frac{1}{E_0}\cdot|e^{inc.}_{\phi}\rangle^{(l)} \quad (4.159)$$

$$|\tilde{h}^{inc.}_{\theta,r}\rangle^{(l)} = \frac{\omega\mu_0}{E_0 k_0}\cdot\{|h^{inc.}_{\theta}\rangle^{(l)} + diag[\tan\alpha_i]\cdot|h^{inc.}_{r}\rangle^{(l)}\} \quad (4.160)$$

$$|\tilde{h}^{inc.}_{\phi}\rangle^{(l)} = \frac{\omega\mu_0}{E_0 k_0}\cdot|h^{inc.}_{\phi}\rangle^{(l)} \quad (4.161)$$

for NAS. Accordingly, we have '$4N_d$' equations to determine '$4\,ncut$' coefficients. Since we intend to choose $ncut$ much smaller than N_d,

there are more equations than unknowns. To remove this overdetermination the continuity conditions are multiplied from the left by $\langle x_\beta|$ and $\langle x_\beta^{(l)}|$, respectively, where β runs from 1 to $ncut$. In this way, a uniquely determined system of the size $(4\,ncut \times 4\,ncut)$ is obtained. The resulting inhomogeneities at the right hand side represent the expansion coefficients of the incident field components if expanded in terms of the eigenvectors $|x_\alpha\rangle$ and $|x_\alpha^{(l)}\rangle$, respectively, i.e., we obtain

$$|\tilde{e}_z^{inc.}\rangle_{TE/TM} = \sum_{\alpha=1}^{ncut} e_{z_\alpha}^{(TE/TM)} \cdot |x_\alpha\rangle \tag{4.162}$$

$$|\tilde{e}_{\phi,r}^{inc.}\rangle_{TE/TM} = \sum_{\alpha=1}^{ncut} e_{\phi,r_\alpha}^{(TE/TM)} \cdot |x_\alpha\rangle \tag{4.163}$$

$$|\tilde{h}_z^{inc.}\rangle_{TE/TM} = \sum_{\alpha=1}^{ncut} h_{z_\alpha}^{(TE/TM)} \cdot |x_\alpha\rangle \tag{4.164}$$

$$|\tilde{h}_{\phi,r}^{inc.}\rangle_{TE/TM} = \sum_{\alpha=1}^{ncut} h_{\phi,r_\alpha}^{(TE/TM)} \cdot |x_\alpha\rangle \tag{4.165}$$

with

$$e_{z_\alpha}^{(TE/TM)} = \langle x_\alpha|\tilde{e}_z^{inc.}\rangle_{TE/TM} \tag{4.166}$$

$$e_{\phi,r_\alpha}^{(TE/TM)} = \langle x_\alpha|\tilde{e}_{\phi,r}^{inc.}\rangle_{TE/TM} \tag{4.167}$$

$$h_{z_\alpha}^{(TE/TM)} = \langle x_\alpha|\tilde{h}_z^{inc.}\rangle_{TE/TM} \tag{4.168}$$

$$h_{\phi,r_\alpha}^{(TE/TM)} = \langle x_\alpha|\tilde{h}_{\phi,r}^{inc.}\rangle_{TE/TM} \tag{4.169}$$

as expansion coefficients of the incident field in cylindrical co-ordinates with respect to the ϕ-dependence, and

$$|\tilde{e}_{\theta,r}^{inc.}\rangle^{(l)} = \sum_{\alpha=1}^{ncut} e_{\theta,r_\alpha}^{(l)} \cdot |x_\alpha^{(l)}\rangle \tag{4.170}$$

$$|\tilde{e}_{\phi}^{inc.}\rangle^{(l)} = \sum_{\alpha=1}^{ncut} e_{\phi_\alpha}^{(l)} \cdot |x_\alpha^{(l)}\rangle \tag{4.171}$$

$$|\tilde{h}_{\theta,r}^{inc.}\rangle^{(l)} = \sum_{\alpha=1}^{ncut} h_{\theta,r_\alpha}^{(l)} \cdot |x_\alpha^{(l)}\rangle \tag{4.172}$$

$$|\tilde{h}_{\phi}^{inc.}\rangle^{(l)} = \sum_{\alpha=1}^{ncut} h_{\phi_\alpha}^{(l)} \cdot |x_{\alpha}^{(l)}\rangle \tag{4.173}$$

with

$$e_{\theta,r_\alpha}^{(l)} = \langle x_{\alpha}^{(l)} | \tilde{e}_{\theta,r}^{inc.} \rangle^{(l)} \tag{4.174}$$

$$e_{\phi_\alpha}^{(l)} = \langle x_{\alpha}^{(l)} | \tilde{e}_{\phi}^{inc.} \rangle^{(l)} \tag{4.175}$$

$$h_{\theta,r_\alpha}^{(l)} = \langle x_{\alpha}^{(l)} | \tilde{h}_{\theta,r}^{inc.} \rangle^{(l)} \tag{4.176}$$

$$h_{\phi_\alpha}^{(l)} = \langle x_{\alpha}^{(l)} | \tilde{h}_{\phi}^{inc.} \rangle^{(l)} \tag{4.177}$$

as expansion coefficients of the incident field in spherical co-ordinates with respect to the θ-dependence. By using the definition

$$\overleftrightarrow{Z}_{\alpha\beta} = \left\{ \langle x_\beta | \overleftrightarrow{Z}_{\alpha} | x_\alpha \rangle \; ; \quad \alpha, \beta = 1, \ldots, ncut \right\} , \tag{4.178}$$

where $\overleftrightarrow{Z}_{\alpha} = \overleftrightarrow{M}_{\alpha}, \overleftrightarrow{O}_{\alpha}, \overleftrightarrow{Q}_{\alpha}, \overleftrightarrow{R}_{\alpha}, \overleftrightarrow{S}_{\alpha}, \overleftrightarrow{T}_{\alpha}$, according to (4.58)–(4.63), and

$$\overleftrightarrow{Z}_{\alpha\beta}^{(l)} = \left\{ \langle x_\beta^{(l)} | \overleftrightarrow{Z}_{\alpha}^{(l)} | x_\alpha^{(l)} \rangle \; ; \quad \alpha, \beta = 1, \ldots, ncut \right\} , \tag{4.179}$$

where $\overleftrightarrow{Z}_{\alpha}^{(l)} = \overleftrightarrow{M}_{\alpha}^{(l)}, \overleftrightarrow{N}_{\alpha}^{(l)}, \overleftrightarrow{O}_{\alpha}^{(l)}, \overleftrightarrow{P}_{\alpha}^{(l)}, \overleftrightarrow{Q}_{\alpha}^{(l)}, \overleftrightarrow{R}_{\alpha}^{(l)}, \overleftrightarrow{S}_{\alpha}^{(l)}, \overleftrightarrow{T}_{\alpha}^{(l)}$, according to (4.137)–(4.144), respectively, the following equation system for NIC in cylindrical co-ordinates can be derived

$$\begin{pmatrix} \overleftrightarrow{M}_{\alpha\beta} & \overleftrightarrow{0} & \overleftrightarrow{O}_{\alpha\beta} & \overleftrightarrow{0} \\ \overleftrightarrow{Q}_{\alpha\beta} & \overleftrightarrow{R}_{\alpha\beta} & \overleftrightarrow{S}_{\alpha\beta} & \overleftrightarrow{T}_{\alpha\beta} \\ \overleftrightarrow{0} & -\frac{k_s}{k_0}\overleftrightarrow{M}_{\alpha\beta} & \overleftrightarrow{0} & -\overleftrightarrow{O}_{\alpha\beta} \\ -\frac{k_s}{k_0}\overleftrightarrow{R}_{\alpha\beta} & \frac{k_s}{k_0}\overleftrightarrow{Q}_{\alpha\beta} & -\overleftrightarrow{T}_{\alpha\beta} & \overleftrightarrow{S}_{\alpha\beta} \end{pmatrix} \circ \begin{pmatrix} \vec{a} \\ \vec{b} \\ \vec{c} \\ \vec{d} \end{pmatrix}$$

$$= \begin{pmatrix} -\vec{e_z}^{(TE/TM)} \\ -\vec{e_{\phi,r}}^{(TE/TM)} \\ -\vec{h_z}^{(TE/TM)} \\ \vec{h_{\phi,r}}^{(TE/TM)} \end{pmatrix} , \tag{4.180}$$

and for NAS in spherical co-ordinates we get

$$\begin{pmatrix} \overleftrightarrow{M}^{(l)}_{\alpha\beta} & l\overleftrightarrow{N}^{(l)}_{\alpha\beta} & \overleftrightarrow{O}^{(l)}_{\alpha\beta} & l\overleftrightarrow{P}^{(l)}_{\alpha\beta} \\ l\overleftrightarrow{Q}^{(l)}_{\alpha\beta} & \overleftrightarrow{R}^{(l)}_{\alpha\beta} & l\overleftrightarrow{S}^{(l)}_{\alpha\beta} & \overleftrightarrow{T}^{(l)}_{\alpha\beta} \\ -\frac{k_s}{k_0} l\overleftrightarrow{N}^{(l)}_{\alpha\beta} & \frac{k_s}{k_0}\overleftrightarrow{M}^{(l)}_{\alpha\beta} & -l\overleftrightarrow{P}^{(l)}_{\alpha\beta} & \overleftrightarrow{O}^{(l)}_{\alpha\beta} \\ \frac{k_s}{k_0}\overleftrightarrow{R}^{(l)}_{\alpha\beta} & -\frac{k_s}{k_0} l\overleftrightarrow{Q}^{(l)}_{\alpha\beta} & \overleftrightarrow{T}^{(l)}_{\alpha\beta} & -l\overleftrightarrow{S}^{(l)}_{\alpha\beta} \end{pmatrix} \circ \begin{pmatrix} \vec{a}^{(l)} \\ \vec{b}^{(l)} \\ \vec{c}^{(l)} \\ \vec{d}^{(l)} \end{pmatrix}$$

$$= \begin{pmatrix} -\vec{e}^{(l)}_{\theta,r} \\ \vec{e}^{(l)}_{\phi} \\ -\vec{h}^{(l)}_{\theta,r} \\ -\vec{h}^{(l)}_{\phi} \end{pmatrix} . \tag{4.181}$$

In contrast to the equation systems (4.64) and (4.145), we have to consider now the two convergency parameters N_d and $ncut$. The accuracy in calculating the several matrix elements $z_{\alpha\beta}$ depends decisively on N_d, independent of the chosen value for $ncut$. $ncut$ itself determines the number of expansion terms in (3.31)–(3.34) and (3.62)–(3.65). It will be favorable to determine N_d first at a fixed $ncut$. Then, $ncut$ can be increased until a convergent result is achieved. The convergency criteria will be discussed in more detail in chapter 6 dealing with the application of the DMF to various scatterer geometries. Of course, the dependence on the azimuthal modes has additionally to be considered in the case of NAS, where the convergency with respect to N_d and $ncut$ must be newly investigated for every mode.

The iterative DMF described here represents a method of moments scheme [59] in which the inhomogeneous equation system is given by the continuity conditions of the tangential field components. Corresponding to the relations (3.31)–(3.34) and (3.62)–(3.65) for the Debye potentials, the eigenvectors calculated by means of the Method of Lines are used as basis as well as weighting vectors. This special choice is known as the Galerkin method which has the advantage of ensuring energy conservation and reciprocity for each approximate solution [55]. The coefficient matrix formed by the scalar products (4.178) and (4.179) exhibits a non-diagonal form, in general. But, if the separable limiting cases are considered again (sphere and circular cylinder at

perpendicular incidence) a diagonal matrix is obtained from which the known expressions (4.28), (4.29) and (4.82), (4.83) can be derived.

We will see in chapter 6 that, indeed, $ncut$ can chosen to be much smaller than N_d in most of the applications. Due to this, the iterative DMF represents a numerically very stable algorithm that is able to treat particles at larger size parameters without any problems. Next, the scattering quantities and their calculation within the framework of the DMF are discussed.

5. DEFINITION OF SCATTERING PARAMETERS

The scattering problem has been solved with the determination of the unknown coefficients a_i and b_i for the internal and c_i and d_i for the scattered field by means of the equation (4.180) in cylindrical and (4.181) in spherical co-ordinates. The total electromagnetic field can be readily calculated at any point inside and outside the scatterer. However, the calculation of scattering cross-sections from the known fields is of more practical interest because they allow a direct comparison between theory and experiment. In investigating the convergence, the differential scattering cross-sections are more appropriate than the integral scattering quantities because of their higher sensitivity. Therefore, we will mainly concentrate on the differential scattering quantities in our numerical considerations. First we want to discuss the general definitions and relations.

The differential scattering cross-section in spherical co-ordinates for any finite obstacle is defined by [3, 60]

$$\frac{d\sigma(\theta,\phi)}{d\Omega} = \lim_{r\to\infty} r^2 \frac{\vec{E}^s(r,\theta,\phi)\cdot[\vec{E}^s(r,\theta,\phi)]^*}{\vec{E}^{inc.}(r,\theta,\phi)\cdot[\vec{E}^{inc.}(r,\theta,\phi)]^*} \ . \tag{5.1}$$

In the far field region, the scattered field of any finite particle represents an outgoing spherical wave of the form

$$\vec{E}^s(r,\theta,\phi) = \vec{E}_0^s(\theta,\phi)\cdot\frac{e^{jk_0r}}{r} \ . \tag{5.2}$$

$\vec{E}_0^s$ denotes the complex scattering amplitude vector that contains all information about the scattering process. On the other hand, an infinitely extended cylinder with an arbitrarily shaped cross-section causes a scattered field which is in the far field region given by

$$\vec{E}^s(r,\phi,z) = \vec{E}_0^s(\phi,z)\cdot\frac{e^{jk_0r}}{\sqrt{r}} \ . \tag{5.3}$$

Because of the different r-dependence it is more meaningful to define the differential scattering cross-section as follows [49, 61–64]:

$$\frac{d\sigma(\phi,z)}{d\Omega} = \lim_{r\to\infty} r \frac{\vec{E}^s(r,\phi,z)\cdot[\vec{E}^s(r,\phi,z)]^*}{\vec{E}^{inc.}(r,\phi,z)\cdot[\vec{E}^{inc.}(r,\phi,z)]^*} \ . \tag{5.4}$$

Considering in all cases a plane wave as the incident field, i.e.,

$$\vec{E}^{inc.}(\vec{r}) = \vec{E}_0^{inc.}\cdot e^{j\vec{k}_0\cdot\vec{r}} \ , \tag{5.5}$$

one obtains for the differential scattering cross-sections (5.1) and (5.4)

$$\frac{d\sigma}{d\Omega} = \frac{|\vec{E}_0^s|^2}{|\vec{E}_0^{inc.}|^2} \ . \tag{5.6}$$

Equation (5.6) shows that, a main problem in scattering theory is the determination of the complex scattering amplitude $\vec{E}_0^s$.

In order to describe the polarization behavior of the scatterer, both, the incident and the scattered field are decomposed with respect to a reference plane into two components which are perpendicular to each other and perpendicular to the propagation direction. For finite objects, the reference plane is usually chosen to be the scattering plane that is determined by the wave vectors of the incident and of the scattered field $\vec{k}_0 = k_0\cdot\hat{e}_{inc.}$ and $\vec{k}_0^s = k_0\cdot\hat{e}_s$ [60]. $\hat{e}_{inc.}$ and $\hat{e}_s$ are unit vectors in the incident and the scattered propagation direction. The infinitely extended cylinder requires another representation which will be discussed in detail in chapter 5.1. The polarization of a field is referred to as either vertical (v) if its $\vec{E}$-vector stands perpendicularly on the reference plane, or horizontal (h) if it lies in this plane. Consequently we get (see, e.g., [3])

$$\vec{E}^{inc.}(\vec{r}) = \left[\hat{v}_{inc.}\cdot E_v^{inc.} + \hat{h}_{inc.}\cdot E_h^{inc.}\right]\cdot e^{j\vec{k}_0\cdot\vec{r}} \tag{5.7}$$

and

$$\vec{E}^s(\vec{r}) = \hat{v}_s\cdot E_v^s + \hat{h}_s\cdot E_h^s \ . \tag{5.8}$$

Here, $\hat{v}$ and $\hat{h}$ denote unit vectors of the vertical and horizontal field components, respectively, resulting from the decomposition. In general, each polarization component of the scattered field depends on

both components of the incident field. This fact can be expressed by a scattering amplitude matrix $\overleftrightarrow{F}$ which is for a finite obstacle defined by [3, 15, 18, 60]

$$\begin{pmatrix} E_v^s(r,\theta,\phi) \\ E_h^s(r,\theta,\phi) \end{pmatrix} = \frac{e^{jk_0 r}}{r} \cdot \begin{pmatrix} f_{vv}(\theta,\phi) & f_{vh}(\theta,\phi) \\ f_{hv}(\theta,\phi) & f_{hh}(\theta,\phi) \end{pmatrix} \cdot \begin{pmatrix} E_v^{inc.} \\ E_h^{inc.} \end{pmatrix} . \quad (5.9)$$

For infinitely extended cylinders we have

$$\begin{pmatrix} E_v^s(r,\phi,z) \\ E_h^s(r,\phi,z) \end{pmatrix} = \frac{e^{jk_0 r}}{\sqrt{r}} \cdot \begin{pmatrix} f_{vv}(\phi,z) & f_{vh}(\phi,z) \\ f_{hv}(\phi,z) & f_{hh}(\phi,z) \end{pmatrix} \cdot \begin{pmatrix} E_v^{inc.} \\ E_h^{inc.} \end{pmatrix} . \quad (5.10)$$

A comparison of equations (5.2), (5.3) and (5.8)–(5.10) yields the relation between the scattering amplitude vector $\vec{E}_0^s$ and the scattering amplitude matrix $\overleftrightarrow{F}$ that holds for finite particles as well as for infinitely extended cylinders.

$$\vec{E}_0^s = \hat{v}_s \cdot (f_{vv} E_v^{inc.} + f_{vh} E_h^{inc.}) + \hat{h}_s \cdot (f_{hv} E_v^{inc.} + f_{hh} E_h^{inc.}) \quad (5.11)$$

From equations (5.5) and (5.7) we can immediately see that the amplitude of the incident field is given by

$$\vec{E}_0^{inc.} = \hat{v}_{inc.} \cdot E_v^{inc.} + \hat{h}_{inc.} \cdot E_h^{inc.} . \quad (5.12)$$

Inserting the scattered and the incident field amplitudes (5.11) and (5.12) into equation (5.6) for the differential scattering cross-section and considering only one linear polarized incident field component $\hat{\alpha}_{inc.} \cdot E_\alpha^{inc.}$ yield the following expression:

$$\frac{d\sigma}{d\Omega} = |f_{\alpha\alpha}|^2 + |f_{\beta\alpha}|^2 , \quad \alpha, \beta = v, h \quad \text{and} \quad \beta \neq \alpha . \quad (5.13)$$

In a scattering experiment on a single particle, each term of the right hand side of (5.13) can be measured separately by use of polarizing filters, for instance. Thus, one may define polarimetric differential scattering cross-sections as follows [65].

$$\frac{d\sigma_{\alpha\beta}}{d\Omega} = |f_{\alpha\beta}|^2 , \quad \alpha, \beta = v, h \quad (5.14)$$

These differential scattering cross-sections can be directly compared with the intensity functions given in [15, 17, 28].

Other interesting quantities that characterize the scattering process on a finite obstacle are the total cross-sections σ_{sca}, σ_{ext}, and σ_{abs} of the scattering, extinction and absorption. σ_{sca} is obtained by integrating (5.13) over the solid angle $d\Omega$. The extinction cross-section σ_{ext} describes the sum of absorption and scattering and can be calculated from the scattering amplitude in forward direction by means of the optical theorem [58, 60, 66, 67].

$$\sigma_{ext} = A \cdot \xi_{ext} = \frac{4\pi}{k_0} \cdot \mathrm{Im} f_{\alpha\alpha}(\theta = 0) \tag{5.15}$$

α indicates the polarization state of the incident field (v or h). ξ_{ext} is referred to as the extinction efficiency and A denotes the particle cross-sectional area projected onto a plane perpendicular to the incident beam [18]. Instead of this area, a spherical cross-section is frequently used in calculating the efficiency of non-spherical particles, i.e.,

$$A = \pi \cdot a^2 \ . \tag{5.16}$$

a represents a characteristic dimension of the particle (often the largest or smallest dimension). Finally, the difference between σ_{ext} and σ_{sca} yields the absorption cross-section σ_{abs}.

From the discussion given above it is seen that, the problem to be solved now is the calculation of the scattering amplitude matrix $\overleftrightarrow{F}$ from the known scattered field. In the next chapters, this will be done in cylindrical and spherical co-ordinates.

5.1 Polarimetric Differential Scattering Cross-sections in Cylindrical Co-ordinates

The scattered field components of an infinitely extended cylinder with an arbitrarily shaped cross-section are given by equations (4.34)–(4.36). Because of the special dependence on the tilt angle of the incident field we introduce the new radial variable

$$\tilde{r} = r \cdot \cos\delta \tag{5.17}$$

in the following considerations. Since all scattering quantities discussed in chapter 5 are defined in the far field region, $(\lim_{\tilde{r}\to\infty})$ has to be applied to the scattered field. By using the expressions (4.40)–(4.42) and the

asymptotic expression of the Hankel function for large arguments [68] one obtains

$$|e_z^s\rangle = E_0 \cdot \sqrt{\frac{2}{\pi}} \cdot \cos^2\delta \cdot e^{jhz} \cdot diag\left\{\frac{e^{jk_0\tilde{r}_i}}{\sqrt{k_0\tilde{r}_i}}\right\} \cdot \sum_{\alpha=1}^{ncut} c_\alpha \cdot e^{-j(\nu_\alpha\cdot\frac{\pi}{2}+\frac{\pi}{4})} \cdot |x_\alpha\rangle \tag{5.18}$$

$$|e_r^s\rangle = -\tan\delta \cdot |e_z^s\rangle \tag{5.19}$$

$$|e_\phi^s\rangle = -E_0 \cdot \sqrt{\frac{2}{\pi}} \cdot \cos\delta \cdot e^{jhz} \cdot diag\left\{\frac{e^{jk_0\tilde{r}_i}}{\sqrt{k_0\tilde{r}_i}}\right\} \cdot \sum_{\alpha=1}^{ncut} d_\alpha \cdot e^{-j(\nu_\alpha\cdot\frac{\pi}{2}+\frac{\pi}{4})} \cdot |x_\alpha\rangle \tag{5.20}$$

with $i = 1, \ldots, N_d$. Note that all terms vanishing stronger than $(\sqrt{\tilde{r}})^{-1}$ have been omitted in the far field approximation.

A comparison between (5.3) and (5.18)–(5.20) shows that the scattering amplitude is mainly characterized by the discretized ϕ-dependence. The separation factor e^{jhz} holds for any infinitely long cylinder, independent of the cross-section shape. From (5.18)–(5.20) we can furthermore see that, for a fixed time and perpendicular incidence $(\delta = 0)$ the surfaces of constant phases $(k_0 \cdot r = const.)$ are circular cylinders. In the more general case of oblique incidence the surfaces of constant phases $(k_0 \cdot r \cdot \cos\delta + k_0 \cdot z \cdot \sin\delta = const.)$ are cones with an half-angle δ. Since the propagation direction $\vec{k}_0^s$ stands perpendicularly on the phase surfaces, the scattered radiation itself propagates along the surface of a cone with an apical angle $(180° - 2\delta)$ [17, 18].

In order to calculate the scattering amplitude matrix $\overleftrightarrow{F}$ from the scattered field (5.18)–(5.20), one has to define certain reference planes to decompose the incident and the scattered field into vertical and horizontal components. In contrast to NIC, any finite particle produces an outgoing spherical wave of the kind (5.2) in the far field. For these particles, the reference plane is usually chosen to be the scattering plane determined by the incident and the scattered wave vector $\vec{k}_0$ and $\vec{k}_0^s$. The finite obstacle can be randomly oriented with respect to the incident field. Furthermore, the observation direction $\vec{k}_0^s$ may also be chosen randomly. In dealing with infinitely long cylinders, this concept fails, however, because we do not have outgoing spherical

waves, and the case that $\vec{k}_0$ and $\vec{k}_0^s$ are pointing along the cylinder axis is impossible. In these directions, there can not exist an incident field impinging on the particle and a scattered field leaving the particle. Moreover, the observation direction is related to the incident wave vector. Thus, $\vec{k}_0^s$ can not be chosen randomly for a given incident field.

Bohren and Huffman [18] proposed a scheme that allows the introduction of a scattering amplitude matrix $\overleftrightarrow{F}$ and the representation of the scattered field in the form (5.10) also for infinitely long cylinders. They defined two reference planes, one for the incident and one for the scattered field (see Fig. 10). The reference plane of the incident field is formed by the cylinder axis and the incident wave vector $\vec{k}_0 = k_0 \cdot \hat{e}_{inc.}$ whereas that for the scattered field is given by the cylinder axis and the scattered wave vector $\vec{k}_0^s = k_0 \cdot \hat{e}_s$. Then, the ϕ-dependence of the scattering amplitude which is characteristic for each cylinder can simply be recorded by rotating the scattering reference plane around the cylinder axis.

First we want to define horizontal and vertical field components of the scattered field with respect to the scattering reference plane on the cone discussed above. Since electromagnetic waves are transverse waves, the horizontal and vertical component at $\phi = \text{constant}$ are given by (see Fig. 11)

$$|e_h^s\rangle = \cos\delta \cdot |e_z^s\rangle - \sin\delta \cdot |e_r^s\rangle \tag{5.21}$$

$$|e_v^s\rangle = -|e_\phi^s\rangle \ . \tag{5.22}$$

Next we decompose the incident field (4.8)–(4.16) into a horizontal and a vertical component with respect to the incident reference plane. Without loss of generality the reference plane is chosen to be at $\phi = 0^\circ$. Thus, the incident field is obtained in the following form:

TE:

$$^{(TE)}E_r^{inc.} = {}^{(TE)}E_z^{inc.} = 0 \tag{5.23}$$

$$^{(TE)}E_\phi^{inc.} = E_0 \cdot e^{jhz} \cdot e^{-jk_0\tilde{r}} \tag{5.24}$$

TM:

$$^{(TM)}E_\phi^{inc.} = 0 \tag{5.25}$$

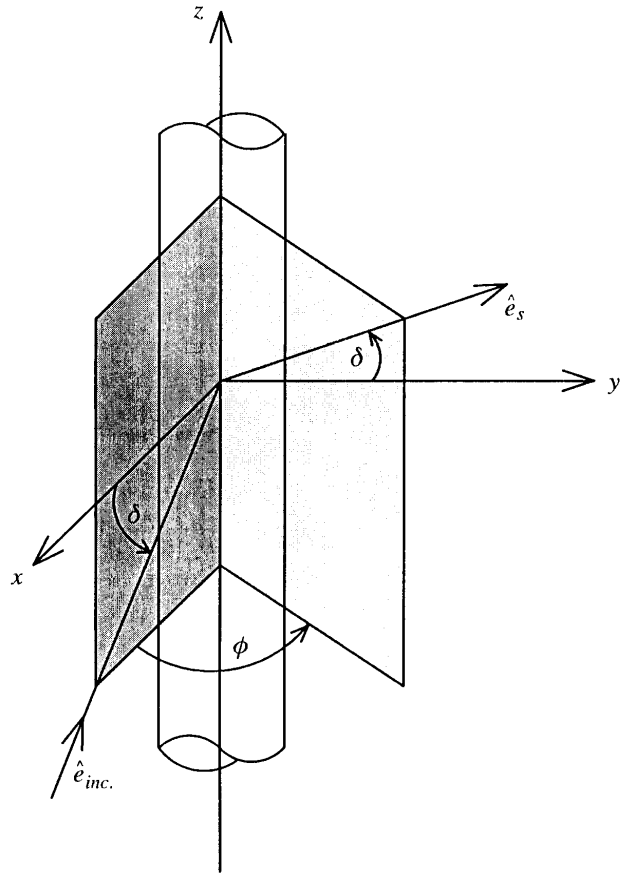

Figure 10. Reference planes for the infinitely extended cylinder.

$$ {}^{(TM)}E_r^{inc.} = E_0 \cdot \sin\delta \cdot e^{jhz} \cdot e^{-jk_0\tilde{r}} \tag{5.26} $$

$$ {}^{(TM)}E_z^{inc.} = E_0 \cdot \cos\delta \cdot e^{jhz} \cdot e^{-jk_0\tilde{r}} \tag{5.27} $$

In the incident TE case, only a field component perpendicular to the reference plane remains whereas the TM case exhibits only components in this plane. This makes it possible to define the horizontally polarized field component from the incident TM field and the vertical component from the TE field. As it was also done for the scattered field, the horizontal component is taken from the projection of the TM-contributions into the plane perpendicular to the propagation direction. Using (5.7) and considering that the factor $e^{-jk_0\tilde{r}}$ has to be

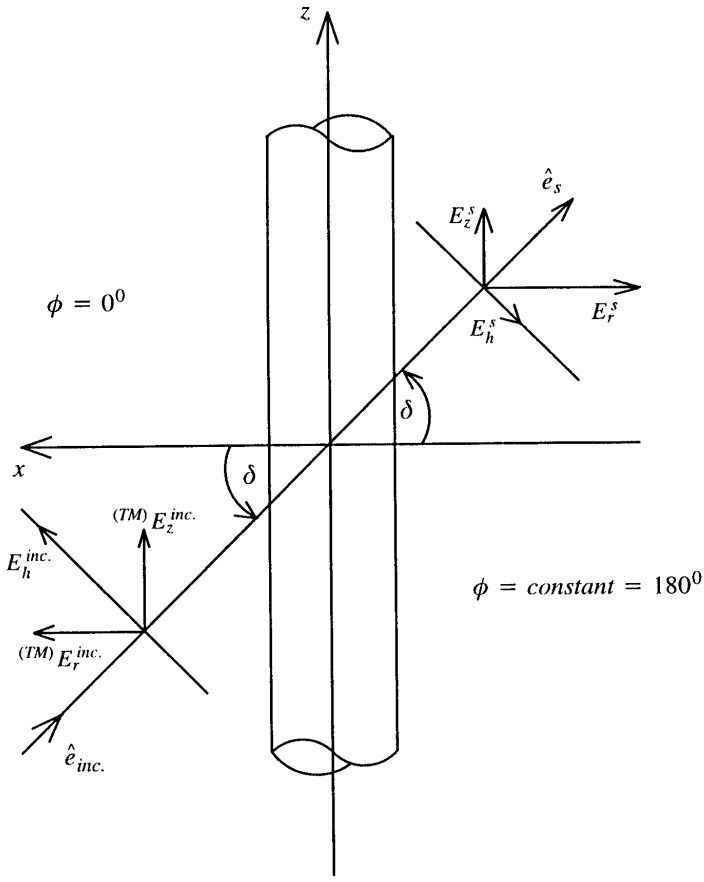

Figure 11. Definition of the horizontally polarized components of the incident and the scattered field for an infinitely extended cylinder. Here, the reference plane of the scattered field is considered at $\phi = 180°$.

separated provide

$$E_h^{inc.} = [\cos\delta \cdot {}^{(TM)}E_z^{inc.} + \sin\delta \cdot {}^{(TM)}E_r^{inc.}] \cdot e^{jk_0\tilde{r}} = E_0 \cdot e^{jhz} \quad (5.28)$$

$$E_v^{inc.} = {}^{(TE)}E_\phi^{inc.} \cdot e^{jk_0\tilde{r}} = E_0 \cdot e^{jhz} \ . \quad (5.29)$$

The magnitude of the horizontally and the vertically polarized incident field component is equal. $\hat{v}_{inc.} \cdot E_v^{inc.}$ and $\hat{h}_{inc.} \cdot E_h^{inc.}$ are, however, perpendicular to each other.

Now we are able to derive a relation between the scattered and the incident field of the kind (5.10). Inserting the vertical and horizontal components of the scattered and the incident field into (5.10) provides the elements of the scattering amplitude matrix on one discretization line.

$$f_{hh,i} = \sqrt{\frac{2}{\pi k_0}} \cdot \cos\delta \cdot \sum_{\alpha=1}^{ncut} c_\alpha^{(h)} \cdot e^{-j(\nu_\alpha \cdot \frac{\pi}{2} + \frac{\pi}{4})} \cdot x_{\alpha,i} \tag{5.30}$$

$$f_{hv,i} = \sqrt{\frac{2}{\pi k_0}} \cdot \cos\delta \cdot \sum_{\alpha=1}^{ncut} c_\alpha^{(v)} \cdot e^{-j(\nu_\alpha \cdot \frac{\pi}{2} + \frac{\pi}{4})} \cdot x_{\alpha,i} \tag{5.31}$$

$$f_{vh,i} = \sqrt{\frac{2}{\pi k_0}} \cdot \cos\delta \cdot \sum_{\alpha=1}^{ncut} d_\alpha^{(h)} \cdot e^{-j(\nu_\alpha \cdot \frac{\pi}{2} + \frac{\pi}{4})} \cdot x_{\alpha,i} \tag{5.32}$$

$$f_{vv,i} = \sqrt{\frac{2}{\pi k_0}} \cdot \cos\delta \cdot \sum_{\alpha=1}^{ncut} d_\alpha^{(v)} \cdot e^{-j(\nu_\alpha \cdot \frac{\pi}{2} + \frac{\pi}{4})} \cdot x_{\alpha,i} \tag{5.33}$$

$$i = 1, \ldots, N_d$$

$x_{\alpha,i}$ represents the i-th component belonging to the eigenvector $|x_\alpha\rangle$. The coefficients $c_\alpha^{(h)}$ and $d_\alpha^{(h)}$ are those obtained from (4.180) by using the incident TM field whereas $c_\alpha^{(v)}$ and $d_\alpha^{(v)}$ are calculated in the TE case. Within the DMF the relation (5.10) holds on each discretization line. Furthermore it can be seen that the elements of the scattering amplitude matrix have the dimension $\sqrt{\text{length}}$. This is due to the fact that the scattered field of an infinitely extended cylinder decreases with $1/\sqrt{\tilde{r}}$ in the far field. The polarimetric differential scattering cross-sections (5.14) for infinitely long cylinders are therefore of the dimension 'length' in contrast to finite particles the cross-sections of which have the dimension 'area'. In order to compare our results with the intensity functions given in [15, 17, 28] the factor $\sqrt{\frac{2}{\pi k_0}}$ is replaced by $\left(\sqrt{x_{1,1} \cdot \sqrt{N_d}}\right)^{-1}$ in the amplitudes (5.30)–(5.33).

5.2 Polarimetric Differential Scattering Cross-sections in Spherical Co-ordinates

In the general case of oblique incidence the scattered field (4.111)–(4.113) of NAS is calculated in the particle frame $\{x, y, z\}$ in which the

z-axis coincides with the symmetry axis of the particle (see Fig. 8). In this co-ordinate system one makes use of the rotational symmetry of the scatterer in deriving the characteristic equation system of the DMF. On the other hand, the scattering quantities discussed in the beginning of this chapter are defined in the laboratory frame $\{X^L, Y^L, Z^L\}$. The transformation of the scattered field from the particle frame into the laboratory frame is done by inverting (4.91), i.e.,

$$\begin{pmatrix} \hat{x} \\ \hat{y} \\ \hat{z} \end{pmatrix} = \overleftrightarrow{A}_E \cdot \begin{pmatrix} \hat{X}^L \\ \hat{Y}^L \\ \hat{Z}^L \end{pmatrix} \tag{5.34}$$

with

$$\overleftrightarrow{A}_E = \left(\overleftrightarrow{A}_E^{-1} \right)^T . \tag{5.35}$$

Note that $\overleftrightarrow{A}_E^{-1}$ is given by (4.92). Since the radial variables of both systems are proportional to each other, as it can be seen below, the far field approximation of the scattered field can already be taken in the particle frame. By use of the asymptotic expression of the Hankel function for large arguments [68] in the Eqs. (4.117)–(4.121) we obtain

$$|e_r^s\rangle = |0\rangle \tag{5.36}$$

$$|e_\theta^s\rangle = E_0 \cdot \sqrt{\frac{2}{\pi}} \cdot diag\left\{ \frac{e^{j\rho_{0_i}}}{\rho_{0_i}} \right\} \cdot \sum_l e^{jl\phi} \cdot \sum_{\alpha=1}^{ncut} e^{-j(\nu_\alpha^{(l)} \frac{\pi}{2} + \frac{\pi}{4})} \cdot \left(c_\alpha^{(l)} \cdot \frac{1}{2h_\theta} \cdot \overleftrightarrow{D}_c^{(l)} + j \cdot l \cdot d_\alpha^{(l)} \cdot diag\left\{ \frac{1}{\sin\theta_i} \right\} \right) \cdot |x_\alpha^{(l)}\rangle \tag{5.37}$$

$$|e_\phi^s\rangle = E_0 \cdot \sqrt{\frac{2}{\pi}} \cdot diag\left\{ \frac{e^{j\rho_{0_i}}}{\rho_{0_i}} \right\} \cdot \sum_l e^{jl\phi} \cdot \sum_{\alpha=1}^{ncut} e^{-j(\nu_\alpha^{(l)} \frac{\pi}{2} + \frac{\pi}{4})} \cdot \left(j \cdot l \cdot c_\alpha^{(l)} \cdot diag\left\{ \frac{1}{\sin\theta_i} \right\} - d_\alpha^{(l)} \cdot \frac{1}{2h_\theta} \cdot \overleftrightarrow{D}_c^{(l)} \right) \cdot |x_\alpha^{(l)}\rangle \tag{5.38}$$

$$i = 1, \ldots, N_d \ .$$

Now we are coming to the transformation of the scattered far field (5.37)–(5.38) from the particle frame into the laboratory frame. As it was already mentioned in chapter 4.2.2, the scattering plane is chosen to be the $X^L Z^L$-plane, i.e., we consider the incident and the scattered field only at $\Phi^L = 0$ and $\Phi^L = \pi$. Consequently, all terms

in the transformation with $\sin\Phi^L$ vanish. The relations between the variables $\{r,\theta,\phi\}$ of the particle frame and those of the laboratory frame $\{R^L,\Theta^L,\Phi^L\}$ are given by [28]

$$\phi = \arctan\left(\frac{y}{x}\right) \tag{5.39}$$

$$\theta = \arctan\left[\sqrt{(x^2+y^s)}/z\right] \tag{5.40}$$

$$r = \frac{z}{cos\left\{\arctan\left[\sqrt{(x^2+y^s)}/z\right]\right\}} \tag{5.41}$$

with

$$\begin{aligned} x &= R^L\cdot(-\sin\Theta^L\cdot\cos\Phi^L\cdot\cos\Phi_p\cdot\cos\Theta_p+\cos\Theta^L\cdot\sin\Theta_p)\\ y &= R^L\cdot\sin\Theta^L\cdot\cos\Phi^L\cdot\sin\Phi_p \\ z &= R^L\cdot(\sin\Theta^L\cdot\cos\Phi^L\cdot\cos\Phi_p\cdot\sin\Theta_p+\cos\Theta^L\cdot\cos\Theta_p)\ . \end{aligned} \tag{5.42}$$

It is immediately seen that θ and ϕ are independent of R^L, and $r = const.\cdot R^L$, The constant is determined by the particle orientation $\{\Theta_p,\Phi_p\}$ and the observation point $\{\Theta^L,\Phi^L\}$. The field components (5.37) and (5.38) can be directly transformed into the laboratory frame at the scattering plane by means of

$$\begin{aligned} |e^s_{R^L}\rangle &= \alpha_{R^L}\cdot|e^s_\theta\rangle+\beta_{R^L}\cdot|e^s_\phi\rangle\\ |e^s_{\Theta^L}\rangle &= \alpha_{\Theta^L}\cdot|e^s_\theta\rangle+\beta_{\Theta^L}\cdot|e^s_\phi\rangle\\ |e^s_{\Phi^L}\rangle &= \alpha_{\Phi^L}\cdot|e^s_\theta\rangle+\beta_{\Phi^L}\cdot|e^s_\phi\rangle \end{aligned} \tag{5.43}$$

with

$$\begin{aligned} \alpha_{R^L} &= \sin\Theta^L\cdot\cos\Phi^L\cdot(\sin\Phi_p\cdot\cos\theta\cdot\sin\phi\\ &\quad-\cos\Phi_p\cdot\cos\Theta_p\cdot\cos\theta\cdot\cos\phi-\cos\Phi_p\cdot\sin\Theta_p\cdot\sin\theta)\\ &\quad+\cos\Theta^L\cdot(\sin\Theta_p\cdot\cos\theta\cdot\cos\phi-\cos\Theta_p\cdot\sin\theta)\\ \beta_{R^L} &= \sin\Theta^L\cdot\cos\Phi^L\cdot(\sin\Phi_p\cdot\cos\phi+\cos\Phi_p\cdot\cos\Theta_p\cdot\sin\phi)\\ &\quad-\cos\Theta^L\cdot\sin\Theta_p\cdot\sin\phi \end{aligned} \tag{5.44}$$

$$\begin{aligned} \alpha_{\Theta^L} &= \cos\Theta^L\cdot\cos\Phi^L\cdot(\sin\Phi_p\cdot\cos\theta\cdot\sin\phi\\ &\quad-\cos\Phi_p\cdot\cos\Theta_p\cdot\cos\theta\cdot\cos\phi-\cos\Phi_p\cdot\sin\Theta_p\cdot\sin\theta)\\ &\quad+\sin\Theta^L\cdot(\cos\Theta_p\cdot\sin\theta-\sin\Theta_p\cdot\cos\theta\cdot\sin\phi)\\ \beta_{\Theta^L} &= \cos\Theta^L\cdot\cos\Phi^L\cdot(\sin\Phi_p\cdot\cos\phi+\cos\Phi_p\cdot\cos\Theta_p\cdot\sin\phi)\\ &\quad+\sin\Theta^L\cdot\sin\Theta_p\cdot\sin\phi \end{aligned} \tag{5.45}$$

$$\begin{aligned}\alpha_{\Phi^L} &= -\cos\Phi^L \cdot (\cos\Phi_p \cdot \cos\theta \cdot \sin\phi \\ &\quad + \sin\Phi_p \cdot \cos\Theta_p \cdot \cos\theta \cdot \cos\phi + \sin\Phi_p \cdot \sin\Theta_p \cdot \sin\theta) \\ \beta_{\Phi^L} &= -\cos\Phi^L \cdot (\cos\Phi_p \cdot \cos\phi - \sin\Phi_p \cdot \cos\Theta_p \cdot \sin\phi)\ .\end{aligned} \tag{5.46}$$

The transformation of the scattered far field (5.37)–(5.38) of the particle frame provides initially a $|e^s_{R^L}\rangle$-component in (5.43). On the other hand it is known that the scattered far field of any arbitrarily shaped finite particle represents an outgoing spherical wave with a vanishing radial component in each arbitrarily chosen spherical co-ordinate system. Indeed, inserting (5.42) into (5.44) and using (5.39)–(5.40) yield

$$\alpha_{R^L} = \beta_{R^L} = 0 \tag{5.47}$$

so that $|e^s_{R^L}\rangle = |0\rangle$. Furthermore, one can show [28] that

$$\begin{aligned}\alpha_{\Theta^L} &= \beta_{\Phi^L} \\ \alpha_{\Phi^L} &= -\beta_{\Theta^L}\ .\end{aligned} \tag{5.48}$$

Therefore, the far field approximation of the scattered field in the laboratory frame in the scattering plane reads as follows:

$$\begin{aligned}|e^s_{\Theta^L}\rangle &= \beta_{\Phi^L} \cdot |e^s_\theta\rangle + \beta_{\Theta^L} \cdot |e^s_\phi\rangle \\ |e^s_{\Phi^L}\rangle &= \beta_{\Phi^L} \cdot |e^s_\phi\rangle - \beta_{\Theta^L} \cdot |e^s_\theta\rangle\ .\end{aligned} \tag{5.49}$$

For the further discussion we define the functions

$$\begin{aligned}f^{(l)}_{\theta,i}(\theta^{dis}_i) &= \sum_{\alpha=1}^{ncut} e^{-j(\nu^{(l)}_\alpha \frac{\pi}{2}+\frac{\pi}{4})} \cdot \left(c^{(l)}_\alpha \cdot \frac{1}{2h_\theta} \cdot \overleftrightarrow{D}^{(l)}_c \cdot |x^{(l)}_\alpha\rangle \right. \\ &\quad \left. + j \cdot l \cdot d^{(l)}_\alpha \cdot diag\left\{ \frac{1}{\sin\theta^{dis}_n} \right\} \cdot |x^{(l)}_\alpha\rangle \right)_{\theta^{dis}_i}\end{aligned} \tag{5.50}$$

$$\begin{aligned}f^{(l)}_{\phi,i}(\theta^{dis}_i) &= \sum_{\alpha=1}^{ncut} e^{-j(\nu^{(l)}_\alpha \frac{\pi}{2}+\frac{\pi}{4})} \cdot \left(j \cdot l \cdot c^{(l)}_\alpha \cdot diag\left\{ \frac{1}{\sin\theta^{dis}_n} \right\} \cdot |x^{(l)}_\alpha\rangle \right. \\ &\quad \left. - d^{(l)}_\alpha \cdot \frac{1}{2h_\theta} \cdot \overleftrightarrow{D}^{(l)}_c \cdot |x^{(l)}_\alpha\rangle \right)_{\theta^{dis}_i} \\ &\qquad (i,n) = 1,\ldots,N_d\end{aligned} \tag{5.51}$$

so that (5.37) and (5.38) provide

$$e^s_{\theta,i}(r_i,\theta_i^{dis},\phi) = E_0 \cdot \sqrt{\frac{2}{\pi}} \cdot \frac{e^{jk_0r_i}}{k_0r_i} \cdot \sum_l e^{jl\phi} \cdot f^{(l)}_{\theta,i}(\theta_i^{dis}) \qquad (5.52)$$

$$e^s_{\phi,i}(r_i,\theta_i^{dis},\phi) = E_0 \cdot \sqrt{\frac{2}{\pi}} \cdot \frac{e^{jk_0r_i}}{k_0r_i} \cdot \sum_l e^{jl\phi} \cdot f^{(l)}_{\phi,i}(\theta_i^{dis}) \qquad (5.53)$$

$$i = 1,\ldots,N_d \ .$$

In the above expressions, the index 'dis' is introduced in order to indicate that the particle frame angle θ_i^{dis} results from the discretization scheme (3.40) and (3.43), respectively. As we will see later, the functions $f^{(l)}_{\theta,i}(\theta_i^{dis})$ and $f^{(l)}_{\phi,i}(\theta_i^{dis})$ are important in calculating the elements of the scattering amplitude matrix.

Since $f^{(l)}_{\theta,i}(\theta_i^{dis})$ and $f^{(l)}_{\phi,i}(\theta_i^{dis})$ are given only at certain discrete angles θ_i^{dis} within the DMF, the calculation of the scattering amplitudes in the laboratory frame is more complicated than known from the T-matrix method which allows the field calculation in the particle frame directly at those points resulting from the variable transformation (5.39)–(5.42). For the determination of these functions as well as of the coefficients β_{Θ^L} and β_{Φ^L} we proceed as follows. First we choose a fixed particle orientation $\{\Theta_p,\Phi_p\}$, some discrete laboratory frame angles $\{\Theta_m^L,\Phi_m^L\}$ and calculate the corresponding particle frame angles $\{\theta_m^{tr},\phi_m^{tr}\}$ by means of (5.39)–(5.42). It has to be mentioned that the choice of Φ_m^L is already done by the above defined scattering plane. The index 'tr' is to indicate that these angles result from a transformation. For a given orientation $\{\Theta_p,\Phi_p\}$ of the particle, any angle θ_m^{tr} differs, in general, from any angle θ_i^{dis}, $i = 1,\ldots,N_d$. This makes an interpolation or extrapolation of the functions $f^{(l)}_{\theta,i}(\theta_i^{dis})$ and $f^{(l)}_{\phi,i}(\theta_i^{dis})$ necessary in order to get $f^{(l)}_{\theta,m}(\theta_m^{tr})$ and $f^{(l)}_{\phi,m}(\theta_m^{tr})$. The accuracy of the interpolation or extrapolation depends on the number N_d of the discretization lines. An increasing N_d decreases the error. In the applications we will see that this procedure does not lead to numerical problems. The functions obtained in this way are then multiplied by the factor $e^{jl\phi_m^{tr}}$ and inserted into the modified equations (5.52) and (5.53). Performing the summation over l results in the interpolated far field components and $e^s_{\theta,m}(r_m,\theta_m^{tr},\phi_m^{tr})$ and $e^s_{\phi,m}(r_m,\theta_m^{tr},\phi_m^{tr})$ in the particle frame belonging to the chosen set of variables $\{\Theta_p,\Phi_p;\Theta_m^L,\Phi_m^L\}$. The coefficients β_{Θ^L} and β_{Φ^L} are

also calculated by use of the angles $\{\theta_m^{tr}, \phi_m^{tr}\}$. Due to the interpolation procedure, an arbitrary number n_d of observation points $\{\Theta_m^L, \Phi_m^L\}$ $m = 1, \ldots, n_d$, can be chosen, i.e., we are now independent of the original discretization of the DMF. In this way, the dimension of each scattered field component (5.49) becomes n_d instead of N_d.

Finally we are dealing with the horizontally and vertically polarized components of the scattered and the incident field in the laboratory frame with respect to the scattering plane. Because of the restriction to this plane in calculating the field (5.49) we can immediately define

$$\begin{aligned} |e_h^s\rangle &= |e_{\Theta^L}^s\rangle \\ |e_v^s\rangle &= |e_{\Phi^L}^s\rangle \ . \end{aligned} \tag{5.54}$$

On the other hand, the incident electric field decomposed into a vertical and a horizontal component with respect to the scattering plane is already given by equations (4.87) and (4.89). Corresponding to (5.7), the amplitude of both components is simply E_0. We determine the elements of the scattering amplitude matrix (5.9) by means of the equations (5.49)–(5.54). On each fixed Θ_m^L we have

$$f_{h\gamma,m} = \sqrt{\frac{2}{\pi}} \cdot \frac{1}{k_0} \cdot \sum_l \exp(jl\phi_m^{tr}) \cdot \left[\beta_{\phi^L} \cdot f_{\theta,\gamma,m}^{(l)}(\theta_m^{tr}) + \beta_{\theta^L} \cdot f_{\phi,\gamma,m}^{(l)}(\theta_m^{tr})\right] \tag{5.55}$$

$$f_{v\gamma,m} = \sqrt{\frac{2}{\pi}} \cdot \frac{1}{k_0} \cdot \sum_l \exp(jl\phi_m^{tr}) \cdot \left[\beta_{\phi^L} \cdot f_{\phi,\gamma,m}^{(l)}(\theta_m^{tr}) - \beta_{\theta^L} \cdot f_{\theta,\gamma,m}^{(l)}(\theta_m^{tr})\right] \tag{5.56}$$

with $m = 1, \ldots, n_d$ and $\gamma = (v, h)$ .In these equations,the functions $f_{\theta,v,m}^{(l)}(\theta_m^{tr})$ and $f_{\phi,v,m}^{(l)}(\theta_m^{tr})$ denote those functions $f_{\theta,m}^{(l)}(\theta_m^{tr})$ and $f_{\phi,m}^{(l)}(\theta_m^{tr})$ calculated by means of the coefficients $c_{\alpha,v}^{(l)}$ and $d_{\alpha,v}^{(l)}$ if using the vertically polarized incident field. In the other case, the coefficients $c_{\alpha,h}^{(l)}$ and $d_{\alpha,h}^{(l)}$ coming from the horizontally polarized incident field are taken to calculate $f_{\theta,h,m}^{(l)}(\theta_m^{tr})$ and $f_{\phi,h,m}^{(l)}(\theta_m^{tr})$.

Due to the interpolation or extrapolation the angles Θ_m^L can be fixed only to those points where we want to know the scattering behavior of the particle. In this way we can directly take the angle $\Theta_1^L = 0°$ to calculate the extinction cross-section by means of the optical theorem (5.15) for any particle orientation. Otherwise, the uncomfortable

task would be to find a discretization that gives the scattering pattern at the desired angles Θ_m^L.

Finally it should be noted that we multiply the polarimetric differential scattering cross-sections (5.14) of the NAS by k_0^2 in all following calculations. In this way, these cross-sections become dimensionless and comparable with the results of other authors.

6. APPLICATIONS

In this chapter, numerical results obtained with the iterative DMF are presented and discussed. For the numerical computation double precision accuracy has been used, throughout. This will allow us to deal with size parameters up to 100. With this range of applicability we are able to bridge the gap between the resonant region and the geometric optics approximation for certain structures. This is demonstrated for the infinitely extended cylinder with an hexagonal cross-section. The result shows the well-known 22° halo which has been observed only within ray-tracing techniques, so far. Additionally, a comparison with the corresponding circular cylinder at the same size parameter will enable us to estimate the validity of an assumption underlying the hybrid techniques presently developed for scattering calculations. The convergence behavior of the polarimetric differential scattering cross-sections with respect to the number of discretization lines (N_d) and to the number of expansion contributions ($ncut$) is of our main interest. Whenever possible, the results have been compared with those of other methods, especially with T-matrix computations and with the separation of variable method. These comparisons demonstrate the accuracy and usefulness of the proposed method. As already mentioned in chapter 4, the reproduction of the known results for spheres and infinitely extended circular cylinders are of special importance for the DMF. These cases are treated first.

6.1 Circular Cylinders and Spheres

Scattering of a plane wave impinging perpendicularly on a infinitely extended circular cylinder ($\delta = 0^\circ$) has been already solved in 1881 by Lord Rayleigh and is discussed in detail in [15], for instance. The generalization to the case of oblique incidence ($\delta \neq 0^\circ$) has been given in this century only [16, 17, 69]. Although practitioners are mostly interested in finite cylinders, the infinitely extended cylinder can be

used in some cases as an approximation of sufficiently long cylinders. Figures 12 and 13 show the differential scattering behavior of a circular cylinder for different tilt angles. In all the following figures concerning cylinders, $\phi = 0°$ refers to the forward and $\phi = 180°$ to the back scattering direction. In Figs. 12 and 13, a size parameter of $k_0 r = 5$ is chosen which is beyond the Rayleigh limit. If using 30 discretization lines in $[0, 2\pi]$ and a parameter of $ncut = 15$, convergency is achieved, i.e., if increasing N_d by 100 and $ncut$ by 5, the changes in the differential scattering cross-sections are generally below 0.5% for each value of ϕ. Our results obtained with the DMF are in excellent agreement with the results given in [17, 64, 70]. For perpendicular incidence (Fig. 13a) Eqs. (4.28) and (4.29) have been used to calculate the scattering coefficients. In this case no cross-polarization contributions will appear, in contrast to oblique incidence for which the horizontal-vertical and vertical-horizontal contributions are identical if dealing with circular cylinders. If we look at the results for increasing tilt angles another interesting feature can be seen. The oscillations typical for the resonance region become fewer and fewer, and the scattering behavior is approaching that of a dipole. This is due to the argument ρ_0 in the Hankel functions which contains a $\cos\delta$-dependence. Therefore, an increasing value of δ from $0°$ to $90°$ acts like a reduction in frequency.

In the literature there are very few calculations for size parameters above 20. To demonstrate that the DMF is able to deal with this region, the differential scattering cross-sections for a circular cylinder at perpendicular incidence and at a size parameter of $k_0 r = 100$ are given in Fig. 14. Reaching those values will allow a comparison with ray-tracing techniques [21, 71]. In our example, convergent results have been achieved with $N_d = 4000$ and $ncut = 240$ which is accompanied by a much higher numerical effort. In the logarithmic scale, a remarkable splitting into a shadowed ($\phi = 0°$–$90°$) and an illuminated region ($\phi = 90°$–$180°$) can be observed, each of which reveals a different scattering behavior. That of the shadowed region is what we know from the geometric optics approximation while in the illuminated area the typical oscillations of the resonance region appear. It's exactly this behavior which gives the justification for the hybrid techniques developed for scattering on non-separable objects [72]. These methods start from an appropriate splitting of the scatterer into different regions in which different approximations hold. As we will see later, this splitting

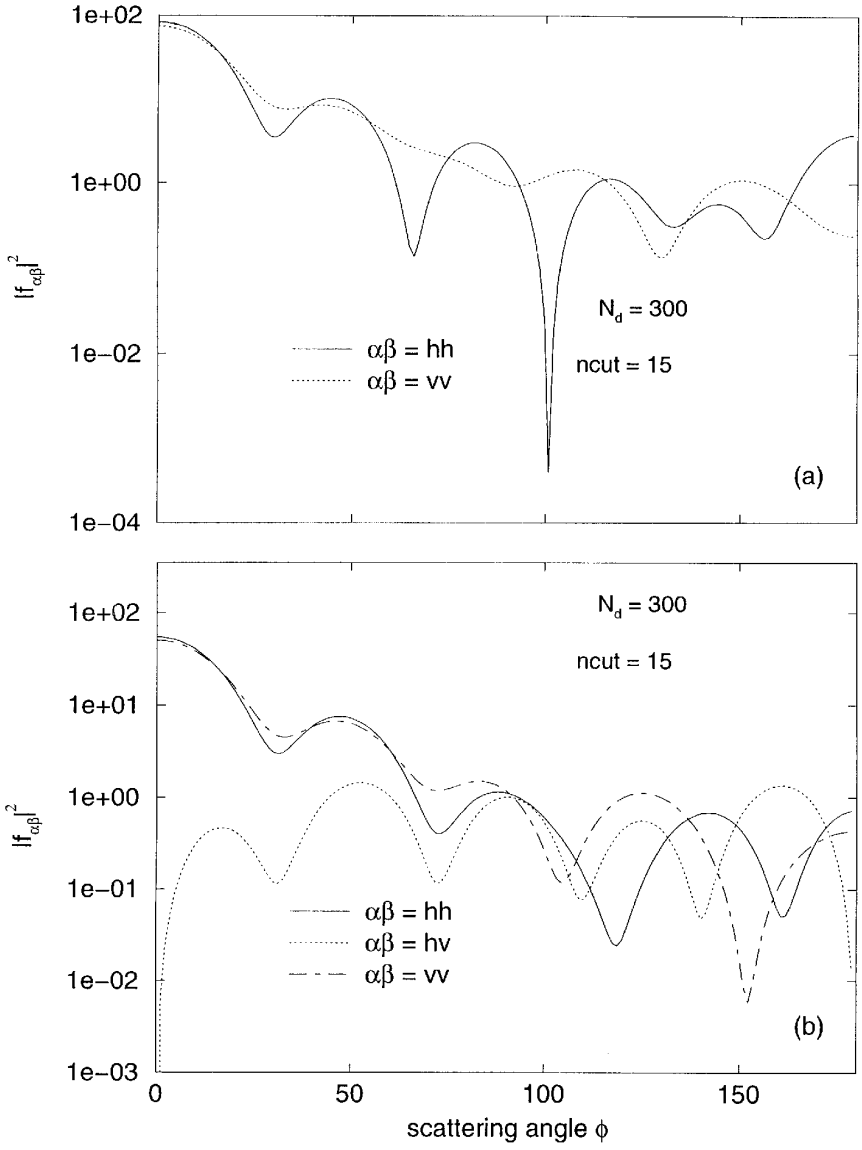

Figure 12. Differential scattering behavior of a circular cylinder with r = 3 mm, f = 79.5775 GHz ($k_0 r = 5$) and $\epsilon_s = 2.1316$: (a) tilt angle $\delta = 0°$, (b) tilt angle $\delta = 30°$.

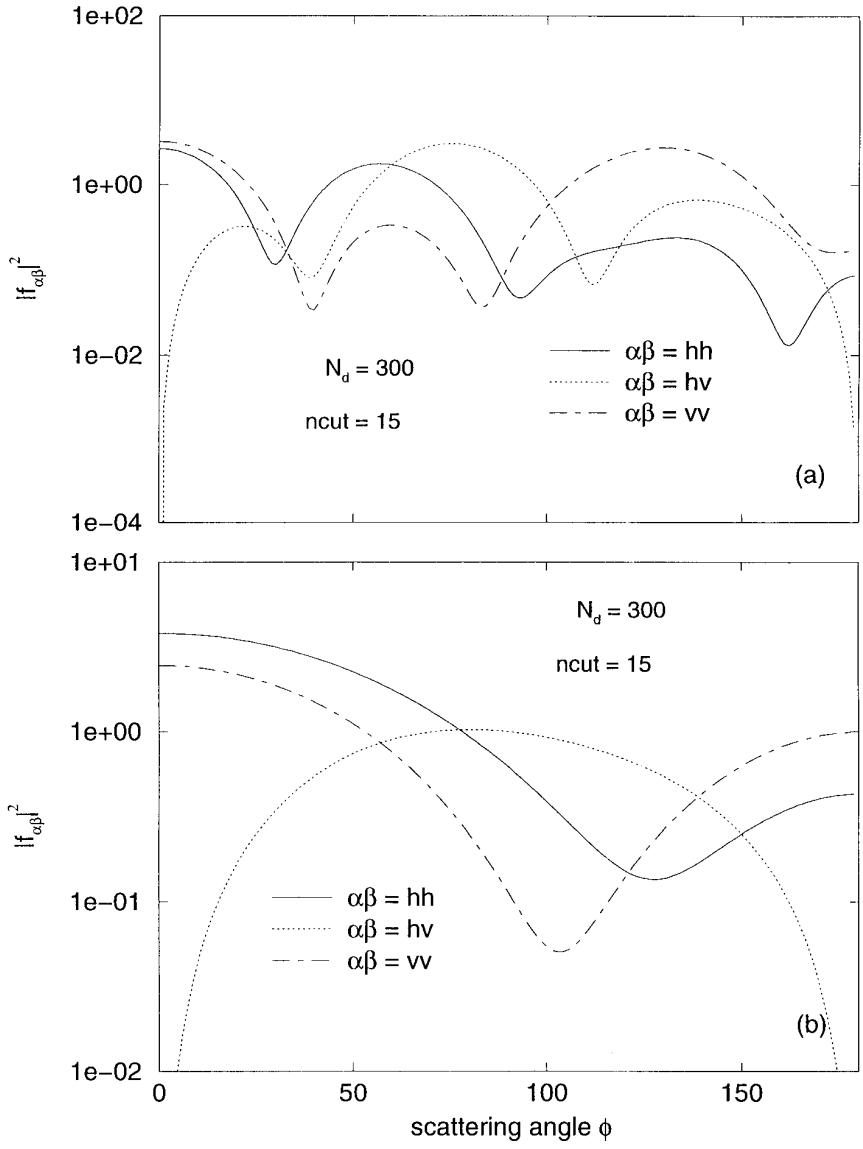

Figure 13. Same as Fig. 12, but for (a) tilt angle $\delta = 60°$ and (b) tilt angle $\delta = 80°$.

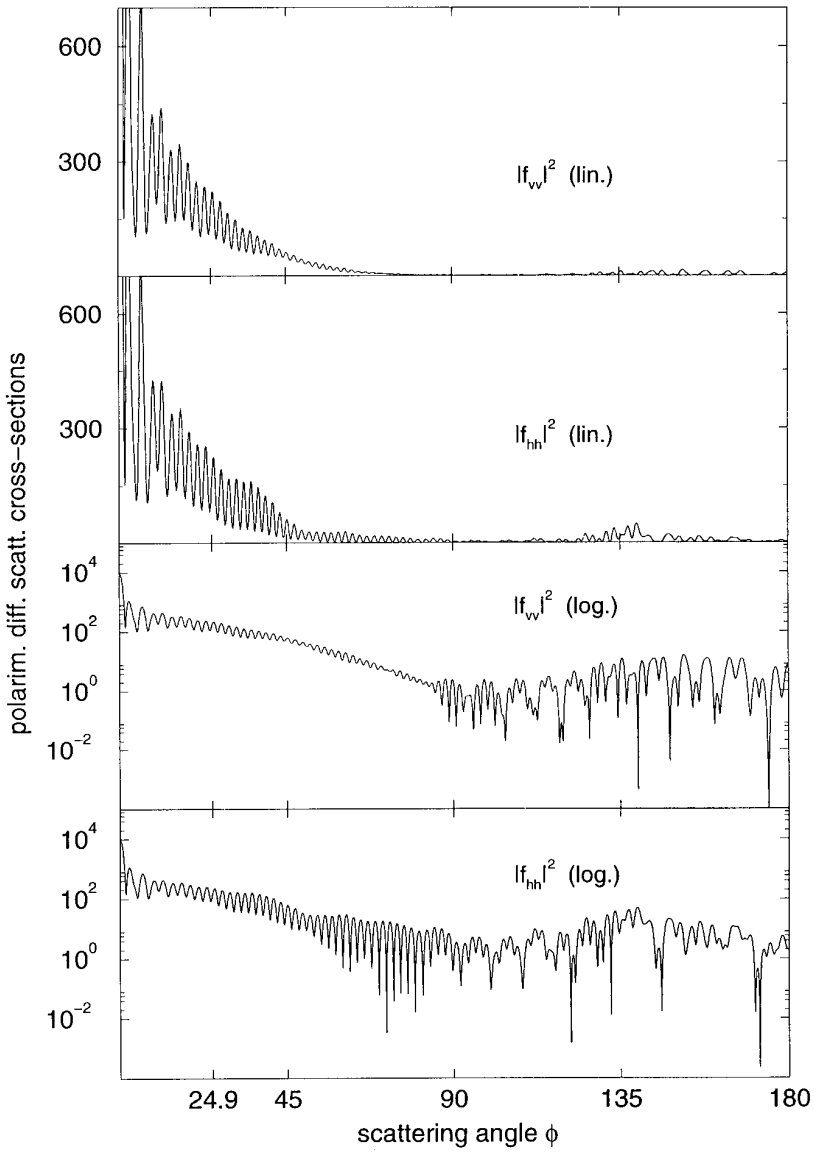

Figure 14. Differential scattering behavior of a circular cylinder with $r = 3$ mm, $f = 1591.55$ GHz $(k_0 r = 100)$ and $\epsilon_s = 1.721$ in both, linear and logarithmic scale. Number of discretization lines: $N_d = 4000$. Number of expansion coefficients: $ncut = 240$.

becomes questionable when dealing with non-circular cross-sections.

At the end of this section we want to treat a dielectric sphere in the Rayleigh and resonance region (Fig. 15). If the orientation is given by $\Theta_p = \Phi_p = 0°$, Eqs. (4.82) and (4.83) have been used to calculate the scattering coefficients. For the size parameter of $k_0 r = 0.628$, the interval $[0, \pi]$ is discretized with 150 lines, and for $k_0 r = 6.28$, 300 discretization lines are needed to reach convergency (including the down spikes). In Table 2, the corresponding extinction efficiencies calculated with the DMF and the Mie theory are given.

	DMF	MIE
$k_0 r = 0.628$	0.163	0.163
$k_0 r = 6.28$	2.520	2.514

Table 2. Extinction efficiencies of the dielectric sphere discussed in Fig. 15. Results are obtained with the iterative DMF and Mie theory.

If we repeat the same calculation but for the orientation $\Theta_p = \Phi_p = 45°$, then we have to solve the equation system (4.181). To reproduce the results given in Fig. 15, 4 and 8 azimuthal modes are necessary for the lower and higher size parameter, while the numbers of N_d and $ncut$ remain unchanged.

In the examples discussed above, the origin of the co-ordinate system has been put into the point of symmetry to make the boundary surface a separable one. A first step into non-spherical and non-circular scattering consists in shifting the origin. From the mathematical point of view, the spherical (circular) boundary becomes non-spherical (non-circular). But this shift is washed out in the differential scattering behavior since it appears only as a phase factor. Therefore, from the physical point of view, the scattering is still that of a sphere or circular cylinder. To proof this we have shifted the sphere of Fig. 15 by 0.5 mm along the positive z-axis. If increasing the number of discretization lines by 150 and $ncut$ by 7, the results are exactly the same. This demonstrates that the shifted but separable boundary surface provides an ideal test case for the numerical procedure, and it is suitable for the production of appropriate initial values for N_d and $ncut$ if dealing

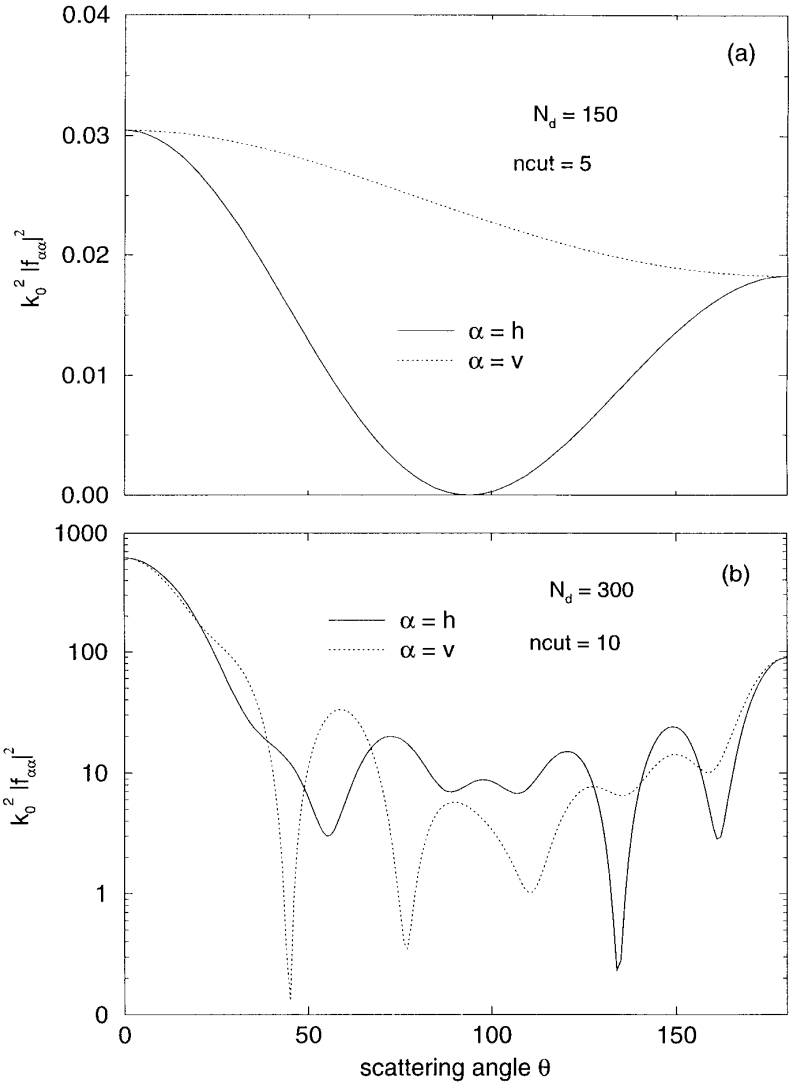

Figure 15. Differential scattering behavior of a sphere with $r = 3$ mm and $\epsilon_s = 5.0$ at two different size parameters: (a) $f = 10$ GHz $(k_0 r = 0.628)$ σ_{ext} (Mie) $= 0.163$, σ_{ext} (DMF) $= 0.1627$ (To reproduce this result for $\Theta_p = \Phi_p = 45°$, 4 azimuthal modes are needed). (b) $f = 100$ GHz $(k_0 r = 6.28)$ σ_{ext} (Mie) $= 2.514$, σ_{ext} (DMF) $= 2.524$ (To reproduce this result for $\Theta_p = \Phi_p = 45°$, 8 azimuthal modes are needed).

with real non-separable scatterers. For example, if we want to calculate the scattering behavior of a spheroid having an aspect ratio of 2:1 and a certain size parameter, first we perform the calculation for the sphere at the same size parameter and permittivity. This is followed by shifting the sphere along the z-axis until an aspect ratio of 2:1 is reached. Now we have to increase N_d and $ncut$ to reproduce the former results. These values of N_d and $ncut$ are the initial values to deal with the spheroid. In most of the cases considered in this paper, these initial values produce results which are accurate enough for practical applications.

6.2 Non-circular Cylinder

Let us now consider a cylinder with an elliptical cross-section at a size parameter of $k_0 a = 5$. The aspect ratio of the cross-section is $1.5 : 1$. The results for different tilt angles are shown in Figs. 16 and 17. Convergency has been achieved with $N_d = 300$ and $ncut = 25$ for each of the tilt angles. In contrast to the circular cylinder, if looking at oblique incidence, the horizontal-vertical and vertical-horizontal cross-polarization contributions differ from each other (compare Fig. 17). Thus, a measurement of these contributions allows a distinction between circular and non-circular cross-sections. This difference vanishes for increasing tilt angles, i.e., if approaching the dipole behavior.

In Table 3 the back scattering cross-sections are given for elliptical cylinders of different aspect ratios and size parameters. The results are compared with a surface integral method discussed in [64]. The calculations within the DMF have been performed with $N_d = 350$ and $ncut = 20$. A good correspondence has been obtained.

Hexagonal cylinders present basic models for ice crystals in cirrus clouds. To get an understanding of how do they affect the radiation balance of clouds an understanding of their scattering behavior in different frequency regions is necessary [73–78]. The ray-tracing technique in the geometric optics limit is the mostly used method to deal with those structures [79, 80] at higher size parameters but, it's still questionable if this method can be applied to intermediate size parameters between the resonance region and the geometric optics limit [71, 81, 82]. With the following examples we want to demonstrate that the DMF can be successfully applied to analyze those structures in the intermediate size parameter range. The discretization scheme has to be chosen in such a manner that no discretization line is located exactly

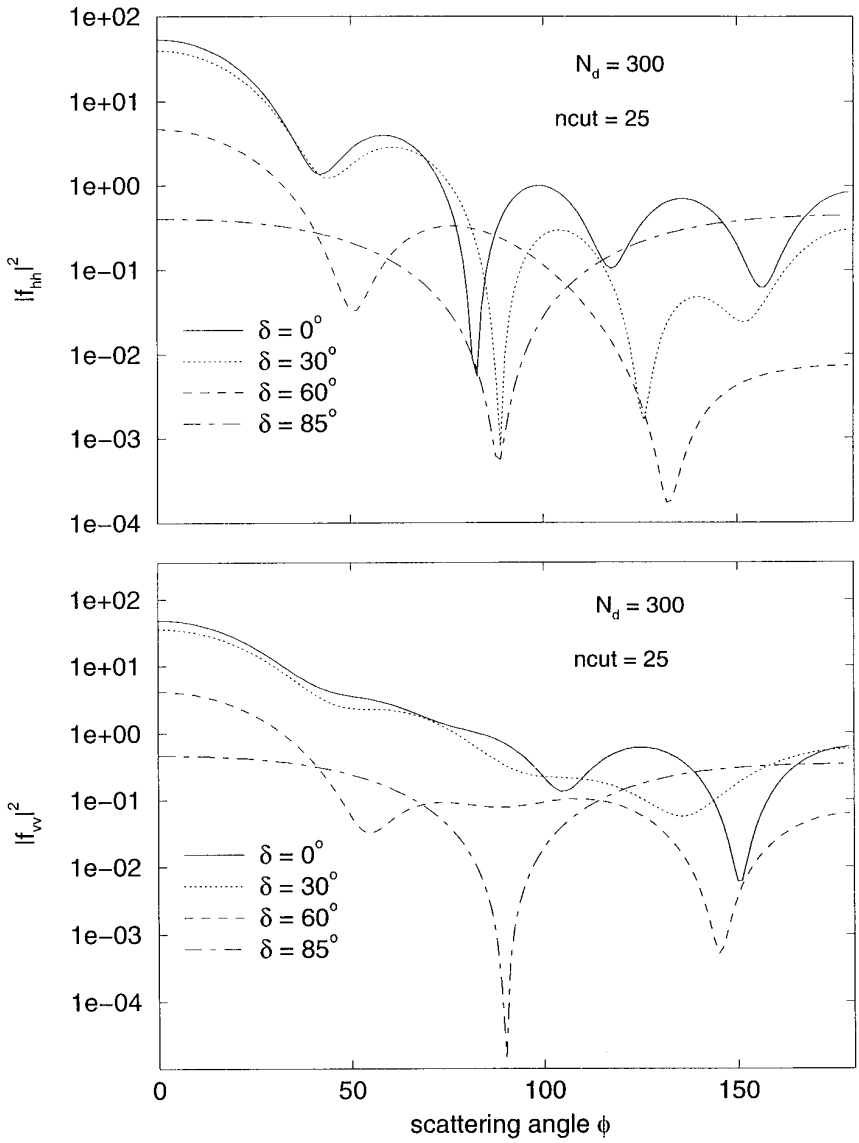

Figure 16. Differential scattering cross-sections (hh- and vv-polarization) of an elliptical cylinder with $a = 3$ mm, $b = 2$ mm, $f = 79.5775$ GHz $(k_0 a = 5)$ and $\epsilon_s = 2.1316$ at different tilt angles.

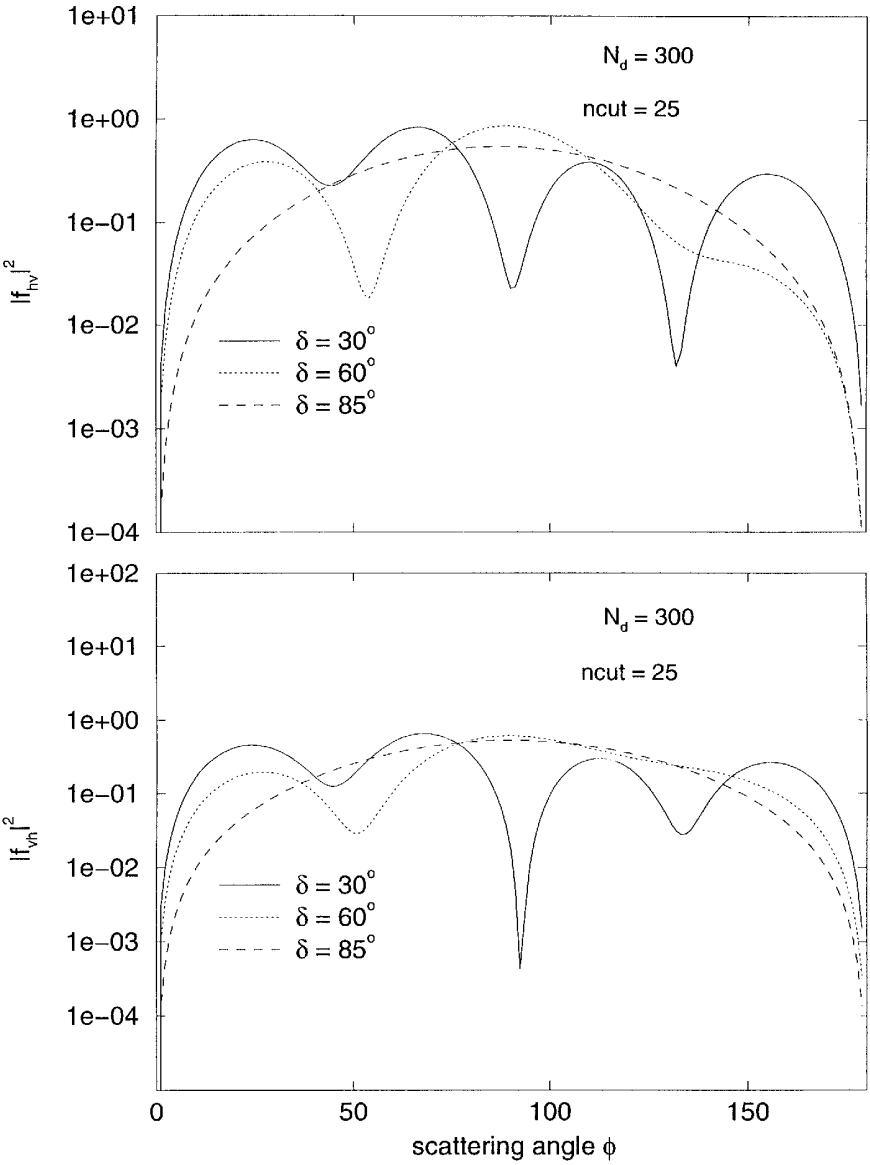

Figure 17. Same as Fig. 16, but for vh- and hv-polarization.

k_0a	a [mm]	b [mm]	σ_{BCS} / DMF this paper	σ_{BCS} / SIE [64]
1.0	4.7713	3.6959	0.120	0.11
1.5	7.1570	6.4897	0.057	0.06
2.0	9.5427	9.0530	0.563	0.57
2.5	11.9284	11.5403	0.237	0.22
3.0	14.3140	13.9923	1.220	1.22

Table 3. Backscattering cross-sections of an ellipsoidal particle ($\epsilon_s = 2.0$, $f = 10$ GHz) at different aspect ratios and size parameters.

on an edge, due to the singularity of the electromagnetic field in this point. In this way, the dielectric edge is smoothed. Nevertheless we get a convergent result if increasing the number of discretization lines, i.e., if approaching the edge more and more. In Fig. 18, the results are given for a hexagonal cross-section with equal sides at a size parameter of $k_0a = 100$ in a linear and logarithmic scale. We can see remarkable differences to the results depicted in Fig. 14 for the circular analogue. The circular cylinder has only a sharp peak in the forward direction while in the hexagonal case the well-known halo can be observed at an angle of $24.9°$ in both polarizations. It is caused by the plane faces of the hexagonal cross-section. The angle of the halo is a consequence of the permittivity and the angle of incidence in the xy-plane used in our example. From Fig. 19 we can take that, the halo already appears at a size parameter of $k_0a = 40$ but, at this size parameter it is overlapped by the oscillations typical for the resonance region. Additionally we can see that, if performing an orientation averaging with respect to the angle of incidence in the xy-plane, the halo is shifted toward the $22°$. To achieve convergency we have used $N_d = 3999$ and $ncut = 240$ for the results in Fig. 18. The results of Fig. 19 are obtained with $N_d = 1099$ and $ncut = 160$. Of course, the numerical effort increases drastically for these calculations.

There is another interesting behavior in Fig. 18 which is not seen in the circular case. For the hexagonal cylinder we can find no splitting into a shadowed and illuminated region. Over the whole scattering range a behavior can be observed which is that of the resonance region. As a consequence it seems to be difficult to find an appropriate splitting

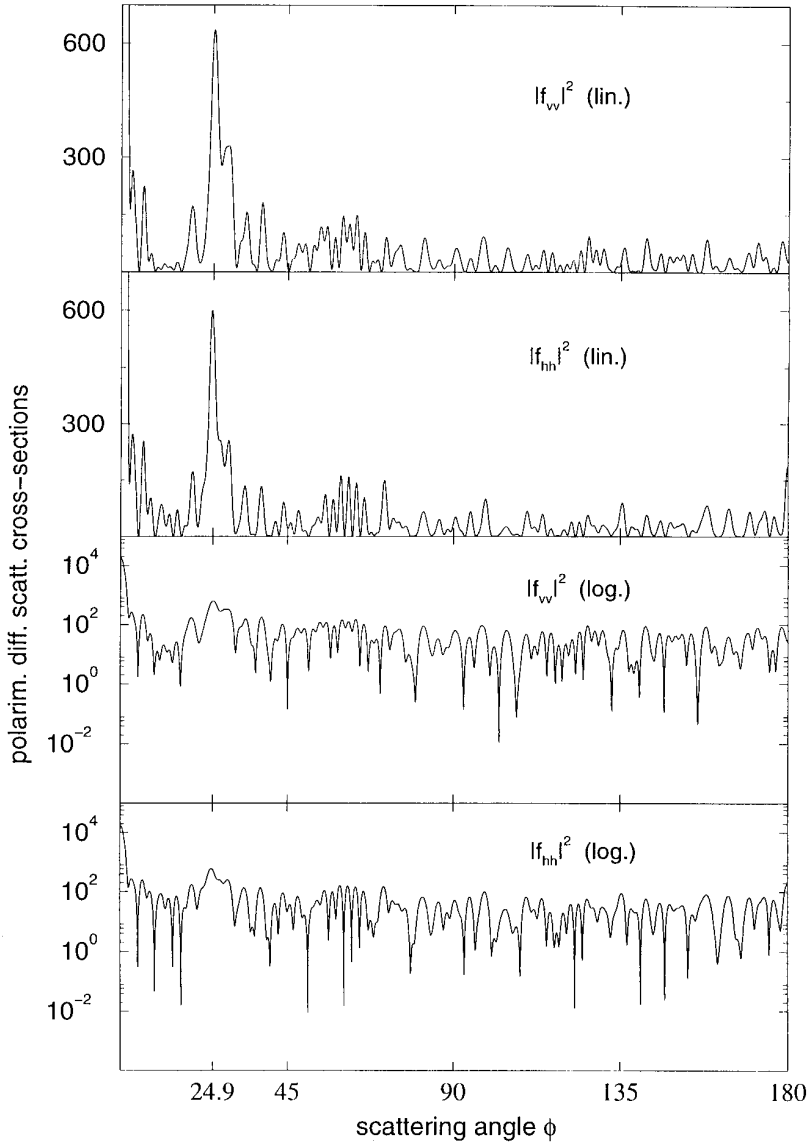

Figure 18. Differential scattering behavior of a hexagonal cylinder with $a = 3$ mm, $f = 1591.55$ GHz $(k_0 a = 100)$ and $\epsilon_s = 1.721$ in both, linear and logarithmic scale. Number of discretization lines: $N_d = 3999$. Number of expansion coefficients: $ncut = 240$. Please note the halo effect at $24.9°$.

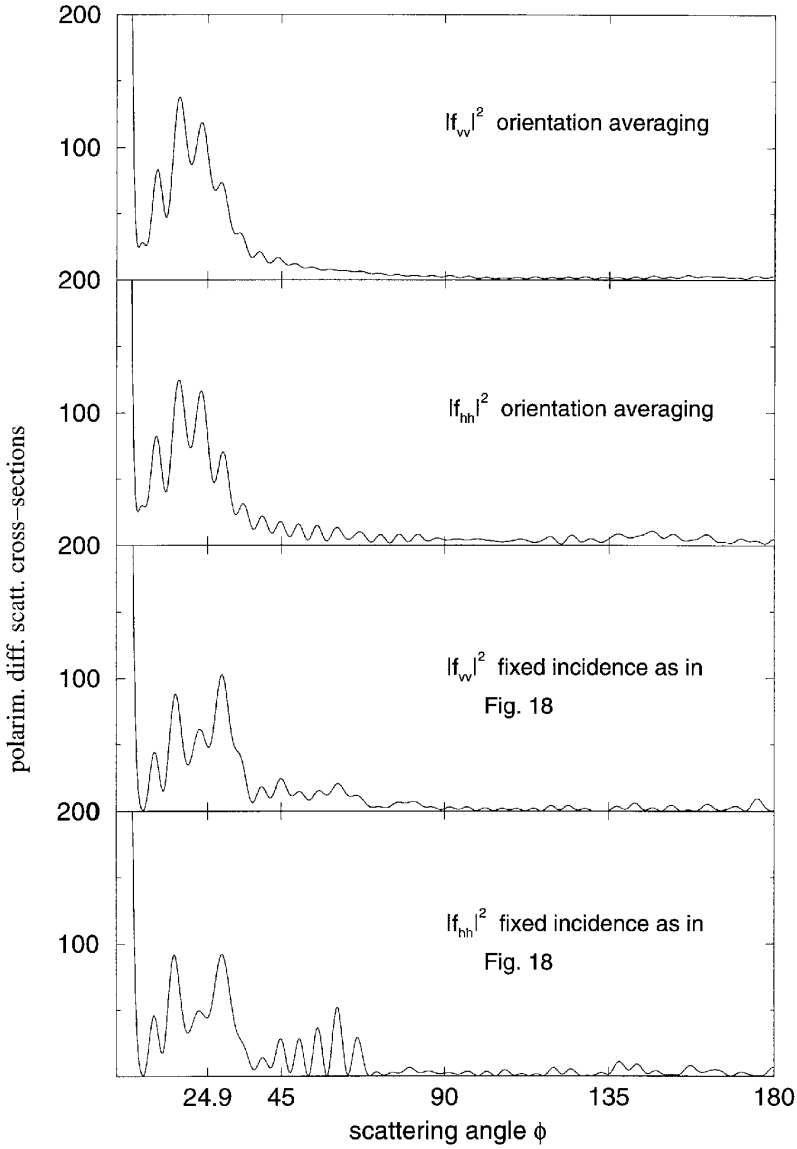

Figure 19. Same as Fig. 18, but for $f = 636.62$ GHz $(k_0 a = 40)$. The first two pictures show the effect of orientation averaging with respect to the incidence in the xy-plane. Number of discretization lines: $N_d = 1099$. Number of expansion coefficients: $ncut = 160$.

for the hybrid methods if they are applied to non-separable scattering problems.

6.3 Axisymmetric Scatterers

In this last section we want to give some examples for oblate and prolate spheroids and for Chebyshev particles. The results for ellipsoidal particles can be compared with the calculations of the separation of variable method carefully performed by Asano and Yamamoto [83]. This provides another possibility to estimate the accuracy of our numerical procedure. In Fig. 20, the differential scattering cross-sections are presented for ellipsoidal particles with an aspect ratio of 2:1 for both, prolate and oblate geometries. An incident field propagating along the axis of symmetry is assumed. The results obtained with the DMF agree very well with those of [83]. In our calculations it has been proved that the numerical effort is higher for the oblate spheroid than for the prolate one. The differences between both structures are most obvious in the back scattering region. Especially at $\theta = 120^\circ$ the vertically polarized differential scattering coefficient of the oblate spheroid is much higher than that of the prolate spheroid. A similar behavior can be observed at higher size parameters.

Fig. 21 shows the scattering characteristics of an prolate spheroid (aspect ratio 2:1) at a size parameter of $k_0 a = 10$ in different orientations. Exactly the same case has been considered by Barber and Hill in [28] with the T-matrix approach. The correspondence with our results is very good for both, the differential scattering cross-sections and the extinction efficiencies. If we look at the orientations of $\Theta_p = \Phi_p = 0^\circ$ and 90°, no cross-polarization contributions exist due to the symmetry of these scattering configurations. For the different orientations (except $\Theta_p = \Phi_p = 0^\circ$) 7 azimuthal modes are needed.

Finally, an example for Chebyshev particles is discussed. This geometry plays an important role in the modelling of hydrometeors and atmospheric aerosols [1]. Therefore, this structure has been considered systematically by Wiscombe and Mugnai with the T-matrix method [84–87]. Due to convergency problems for a deformation parameter of $\epsilon = 0.2$, their calculations are restricted to an upper limit of $k_0 r = 5$ in size parameter. No problems occur within the DMF if we go beyond this value although the numerical effort increases drastically (see Fig. 22). After determining the initial values as discussed above, N_d and $ncut$ have been increased stepwise until the differences between

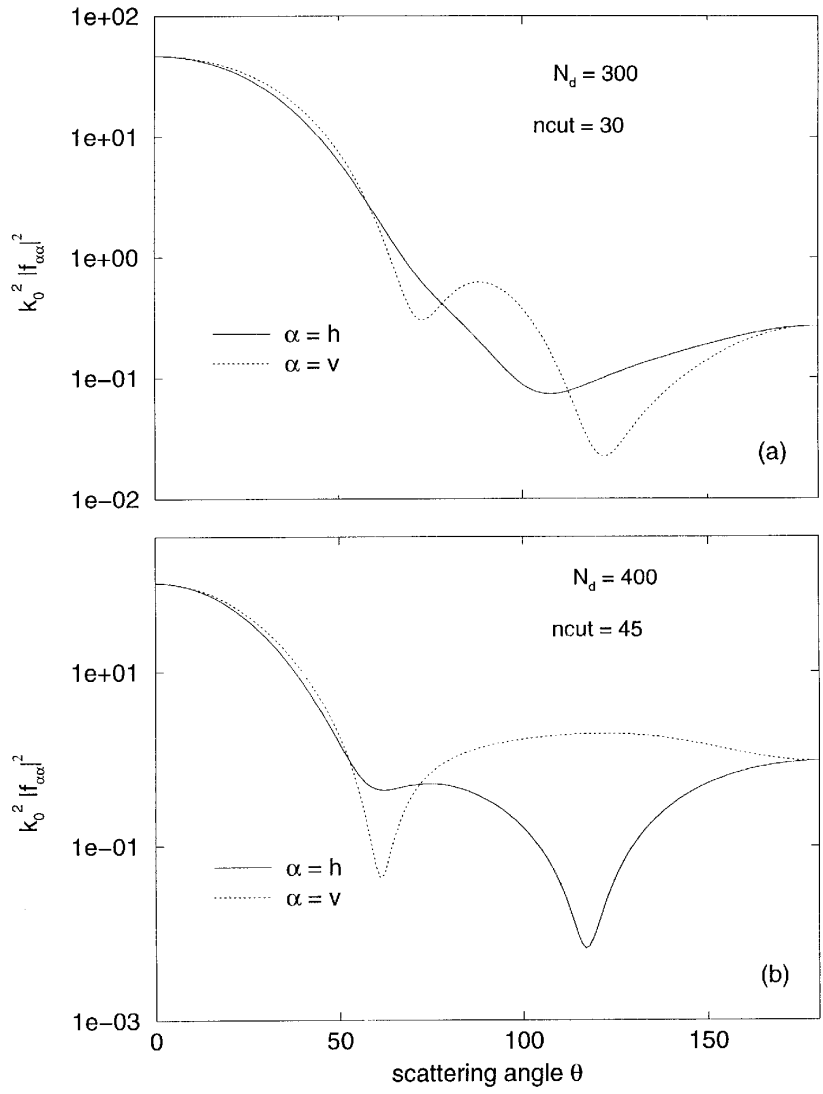

Figure 20. Differential scattering behavior of a prolate and oblate spheroid with $\epsilon_s = 1.7689$ at a frequency of $f = 73.46$ GHz and for incidence along the axis of symmetry $(\Theta_p = \Phi_p = 0°)$: (a) prolate spheroid with $a = 3$ mm, $b = 1.5$ mm. $\sigma_{sca} = 0.878$. (b) oblate spheroid with $a = 1.5$ mm, $b = 3$ mm. $\sigma_{sca} = 1.0605$.

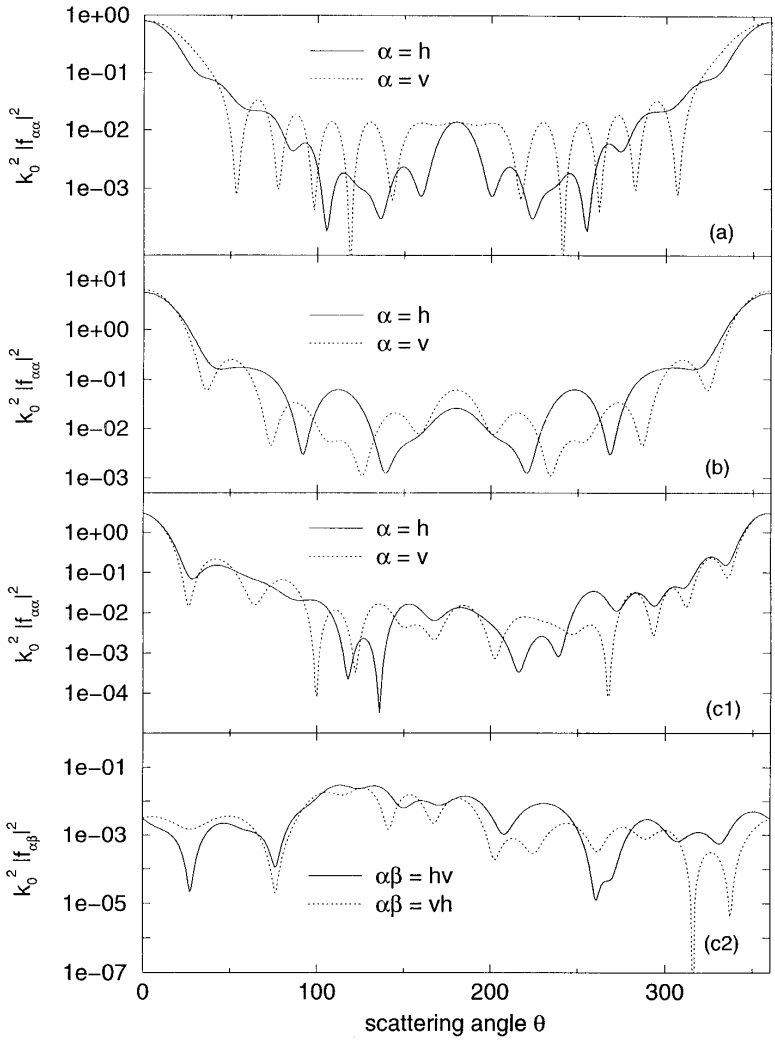

Figure 21. Differential scattering behavior of a prolate spheroid with $a = 3$ mm, $b = 1.5$ mm and $\epsilon_s = 2.25$ at $f = 159.155$ GHz ($k_0 a = 10$). Independent of the orientation, the discretization parameters are $N_d = 700$ and $ncut = 45$. (a) $\Theta_p = \Phi_p = 0°$: σ_{ext} (DMF) $= 0.518$, σ_{ext} (B/H in [28]) $= 0.519$. (b) $\Theta_p = \Phi_p = 90°$: σ_{ext} (DMF) $= 1.645$, σ_{ext} (B/H in [28]) $= 1.647$. (c1) $\Theta_p = \Phi_p = 45°$: σ_{ext} (DMF) $= 1.138$, σ_{ext} (B/H in [28]) $= 1.14$. (c2) orientation as in (c1), but for hv- and vh-polarization.

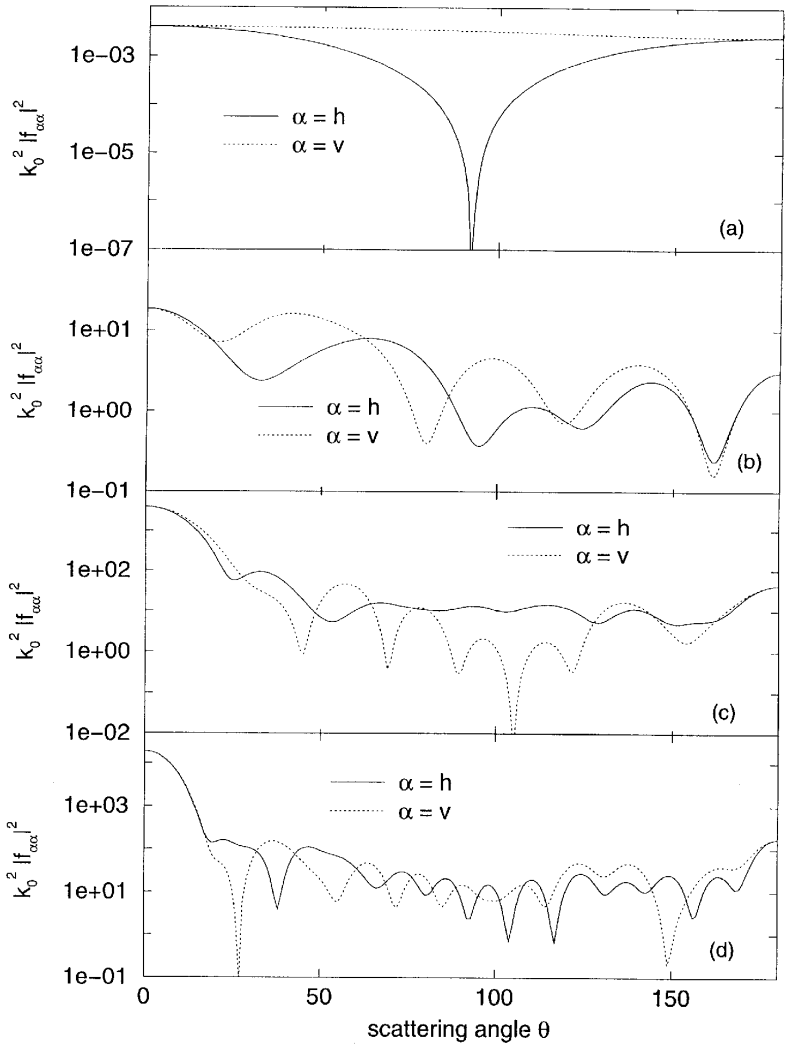

Figure 22. Differential scattering behavior of a Chebyshev particle of second order with $r_{sph} = 3$ mm, $\epsilon_s = 5.0$ and $\epsilon = 0.2$ at different size parameters: (a) $f = 7.9577$ GHz $(k_0 r_{sph} = 0.5)$, $N_d = 300$ and $ncut = 10$. $\sigma_{ext} = 0.0355$. (b) $f = 79.577$ GHz $(k_0 r_{sph} = 5)$, $N_d = 300$ and $ncut = 15$. $\sigma_{ext} = 0.66$. (c) $f = 159.155$ GHz $(k_0 r_{sph} = 10)$, $N_d = 500$ and $ncut = 50$. $\sigma_{ext} = 2.504$. (d) $f = 232.5$ GHz $(k_0 r_{sph} = 15)$, $N_d = 600$ and $ncut = 65$. $\sigma_{ext} = 2.508$.

two steps following each other become less than 0.5% over the whole scattering range from 0° to 180°.

7. CONCLUSION

In this paper, a new method for the analysis of plane wave scattering on axisymmetric objects and infinitely extended cylinders with non-circular cross-sections has been discussed. This method is called the Discretized Mie-Formalism and is based on a transformation of the corresponding Helmholtz equations into uncoupled systems of ordinary differential equations depending only on the radial co-ordinate. These systems can be solved by taking the regularity and the radiation condition analytically into account. Thus, the final calculation is reduced to the scatterers surface. The decoupling of the equation systems has been achieved by means of the so-called Method of Lines. The algebraic eigenvectors of this mathematical tool to solve partial differential equations have been used, furthermore, as a functional basis for the expansion of the Debye potentials and the electromagnetic field components, respectively. Therefore, the DMF looks very similar to what is known from the Mie theory for separable geometries. The validity of the Rayleigh hypothesis from the point of view of the DMF can be clarified.

The DMF in its direct form has a restricted range of applicability due to the fact that the coefficient matrix of the final characteristic equation system becomes very large and ill-conditioned for higher size parameters. To overcome this difficulty an iterative version of the DMF has been derived which is based on a Method of Moment scheme. For this, the above mentioned eigenvectors serve as both, basis and weighting functions. The resulting equation system is much more stable and smaller than that of the direct method. The iterative DMF is able to analyze scattering for size parameters up to 100. This makes it possible to estimate approximate methods like the geometric optics approximation and hybrid techniques, for instance.

The DMF as it is discussed in this paper uses a one-dimensional discretization scheme. If one is interested in non-axisymmetric scatterers, a two-dimensional discretization must be chosen. This is possible but accompanied by much higher numerical efforts.

For further considerations, the expansions of the Debye potentials given in Eqs. (3.31)–(3.34) and (3.62)–(3.65), respectively, are of special importance. This expansion is valid no matter whether we look

at a separable or non-separable boundary value problem. It should be possible to use such an expansion for the derivation of the corresponding Green's function. This would allow us to switch to the integral representation of non-spherical scattering. As a result, different approximations will become possible (approximations within a Born series, for instance). Additionally, the relations between our approach and that of the Extended Boundary Condition Method will become more clearly. As we have already discussed, the coefficient matrix of our characteristic equation system reveals some similar features which are known from the T-matrix of the EBCM.

Since the way of solution in plane wave scattering is very similar to other electromagnetic field problems (guided waves, antenna problems, ...), these future considerations should be of general interest.

REFERENCES

1. Schuerman, D. W. (ed.), *Light Scattering by Irregularly Shaped Particles,* Plenum Press, New York, 1980.
2. Ulaby, F. T., R. K. Moore, and A. K. Fung, *Microwave Remote Sensing,* Vols. 1–3, Artech House, Norwood, 1986.
3. Tsang, L., J. A. Kong, and R. T. Shin, *Theory of Microwave Remote Sensing,* John Wiley and Sons, New York, 1985.
4. Asrar, G., *Theory and Application of Optical Remote Sensing,* John Wiley and Sons, New York, 1989.
5. Kondratyev, K. Y., V. V. Kozoderov, and O. I. Smotky, *Remote Sensing of the Earth from Space,* Springer Verlag, Moskau, 1992.
6. Chandrasekhar, S., *An Introduction to the Study of Stellar Structures,* Univ. of Chicago Press, Chicago, 1939.
7. Giese, R. H., K. Weiss, R. H. Zerull, and T. Ono, "Large fluffy particles: a possible explanation of the optical properties of interplanetary dust," *Astron. and Astrophys.,* Vol. 65, p. 265, 1978.
8. Greenberg, J. M., "Interstellar dust," in *Cosmic Dust,* A. J. M. McDonnell (ed.), John Wiley and Sons, London, 1978.
9. Bickel, W. S., M. E. Stafford, "Biological particles as irregularly shaped scatterers," in [1], p. 299, 1980.
10. Regan, J. F., J. A. Parrish, *The Science of Photomedicine,* Plenum Press, New York, 1982.
11. Hofle, W., "Backscatter factor and scattering loss of spatially large defects in single-mode fibres, *Frequenz,* Vol. 47, p. 226, 1993.
12. Mie, G., "Beiträge zur Optik trüber Medien, speziell kolloidaler Metallösungen," *Ann. Phys.,* Vol. 25, p. 377, 1908.

13. Debye, P., "Der Lichtdruck auf Kugeln von beliebigem Material," *Ann. Phys.,* Vol. 30, p. 57, 1909.
14. Lord Rayleigh, "On the electromagnetic theory of light," *Phil. Mag.,* Vol. 12, p. 81, 1881.
15. Van de Hulst, H. C., *Light Scattering by Small Particles,* John Wiley and Sons, New York, 1957.
16. Wait, J. R., *Electromagnetic Radiation from Cylindrical Structures,* Pergamon Press, London, 1959.
17. Kerker, M., *The Scattering of Light,* Academic Press, New York, 1969.
18. Bohren, C. F., D. R. Huffman, *Absorption and Scattering of Light by Small Particles,* John Wiley and Sons, New York, 1983.
19. Flatau, P. J., G. L. Stephens, B. T. Draine, "Light scattering by rectangular solids in the discrete dipole approximation," *J. Opt. Soc. Am.,* Vol. A7, p. 593, 1990.
20. Draine, B. T., P. J. Flatau, "The discrete dipole approximation for scattering calculations," *J. Opt. Soc. Am.,* Vol. A11, p. 1491, 1994.
21. Wendling, P., R. Wendling, and H. K. Weickmann, "Scattering of solar radiation by hexagonal ice crystals," *Appl. Optics,* Vol. 18, p. 2663, 1979.
22. Macke, A., "Modellierung der optischen Eigenschaften von Cirruswolken," Dissertation, GKSS - Forschungszentrum Geesthacht, Geesthacht, 1994.
23. Yeh, C., "Perturbation approach to the diffraction of electromagnetic waves by arbitrarily shaped dielectric obstacles," *Phys. Rev.,* Vol. 135, No. 5A, p. 193, 1964.
24. McDonald, B. H., A. Wexler, "Finite-element solution of unbounded field problems," *IEEE-MTT,* Vol. 20, p. 841, 1972.
25. Kunz, K. S., R. J. Luebbers, *Finite-Difference Time Domain Method for Electromagnetics,* CRC Press, Boca Raton, 1993.
26. Waterman, P. C., "Matrix formulation of electromagnetic scattering," *Proc. IEEE,* Vol. 53, p. 805, 1965; "Symmetry, unitarity, and geometry in electromagnetic scattering, *Phys. Rev.,* Vol. D3, p. 825, 1971.
27. Barber, P., and C. Yeh, "Scattering of electromagnetic waves by arbitrarily shaped dielectric bodies," *Appl. Optics,* Vol. 14, p. 2864, 1978.
28. Barber, P., and S. C. Hill, *Light Scattering by Particles: Computational Methods,* World Scientific, Singapore, 1990.

29. Mishchenko, M. I., and L. D. Travis, "Light scattering by polydispersions of randomly oriented spheroids with sizes comparable to wavelengths of observations," *Appl. Optics,* Vol. 33, p. 7206, 1994.
30. Mishchenko, M. I., L. D. Travis, and D. W. Mackowski, "T-Matrix computations of light scattering by nonspherical particles: A review," *JQSRT,* Vol. 55, p. 535, 1996.
31. Mullin, C. R., R. Sandburg, and C. O Velline, "A numerical technique for the determination of scattering cross sections of infinite cylinders of arbitrary geometrical cross section," *IEEE-AP,* Vol. 12, p. 141, 1965.
32. Wiscombe, W. J., and A. Mugnai, *Single Scattering from Nonspherical Chebyshev Particles,* NASA Reference Publ. 1157, 1986.
33. Morrison, J. A., and M. J. Cross, "Scattering of a plane electromagnetic wave by axisymmetric raindrops," *Bell Syst. Tech. J.,* Vol. 53, p. 955, 1974.
34. Al-Rizzo, H. M., and J. M. Tranquilla, "Electromagnetic scattering from dielectrically coated axisymmetric objects using the generalized point-matching technique," *J. Comp. Phys.,* Vol. 119, p. 342, 1995.
35. Rother, T., and K. Schmidt, "The discretized Mie-formalism – a novel algorithm to treat scattering on axisymmetric particles," *J. Electrom. Waves and Appl.,* Vol. 10, p. 273, 1996.
36. Rother, T., and K. Schmidt, "The discretized Mie-formalism for plane wave scattering by dielectric cylinders," *J. Electrom. Waves and Appl.,* Vol. 10, p. 697, 1996.
37. Rother, T., and K. Schmidt, "The discretized Mie-formalism for plane wave scattering on dielectric objects with non-separable geometries," *JQSRT,* Vol. 55, p. 615, 1996.
38. Pregla, R., and W. Pascher, "Method of lines," in *Numerical Techniques for Microwave and Millimeter Wave Passive Structures,* T. Itoh (ed.), John Wiley and Sons, New York 1989.
39. Rogge, U., and R. Pregla, "Method of lines for the analysis of striploaded optical waveguides," *J. Opt. Soc. Am.,* Vol. B8, p. 459, 1991.
40. Pregla, R., "About the nature of the method of lines," *AEU,* Vol. 41, p. 386, 1987.
41. Dreher, A., and R. Pregla, "Full-wave analysis of radiating planar resonators with the method of lines," *IEEE-MTT,* Vol. 41, p. 1363, 1993.
42. Dreher, A., and T. Rother, "New aspects of the method of lines," *IEEE-Microwave and Guided Wave Letters,* Vol. 5, p. 408, 1995.

43. Petit, R., and M. Cadilhac, "Sur la diffraction d'une onde plane par un reseau infiniment conducteur," *C. R. Acad. Sci.,* Ser. B 262(7), p. 468, 1966.
44. Millar, R. F., "On the Rayleigh hypothesis in scattering problems," *Electron. Letters,* Vol. 5, p. 416, 1969.
45. Bates, R., "Rayleigh hypothesis, the extended boundary condition and point matching," *Electron Letters,.* Vol. 5, p. 654, 1969.
46. Millar, R. F., and R. Bates, "On the legitimacy of an assumption underlying the point-matching method," *IEEE-MTT,* Vol. 18, p. 325, 1970.
47. Millar, R. F., "The Rayleigh hypothesis and a related least-squares solution to scattering problems for periodic surfaces and other scatterers," *Radio Science,* Vol. 8, p. 785, 1973.
48. Voronovich, A. G., *Wave Scattering from Rough Surfaces,* Springer-Verlag, Berlin, 1994.
49. Harrington, R. F., *Time-Harmonic Electromagnetic Fields,* McGraw Hill, New York, 1961.
50. Kong, J. A., *Electromagnetic Wave Theory,* John Wiley and Sons, New York, 1985.
51. Sommerfeld, A., *Partielle Differentialgleichungen der Physik,* Akademische Verlagsgesellschaft, Leipzig, 1958.
52. Morse, P. M., and H. Feshbach, *Methods of Theoretical Physics,* McGraw Hill, New York, 1953.
53. Stratton, J. A., *Electromagnetic Theory,* McGraw Hill, New York, 1941.
54. Fick, E., *Einfuhrung in die Grundlagen der Quantentheorie,* Geest und Portig K.-G., Leipzig, 1981.
55. Wang, J. J. H., *Generalized Moment Methods in Electromagnetics,* John Wiley and Sons, New York 1991.
56. Xiao, S., and R. Vahldieck, "Solution of the Helmholtz equation with the method of lines in cylindrical coordinates," *IEEE AP-S Intern. Symp.,* Seattle, USA, Vol. 3, p. 2104, 1994.
57. Wilkinson, J. H., *The Algebraic Eigenvalue Problem,* Oxford Univ. Press, Oxford 1965.
58. Born, M., and E. Wolf, *Principles of Optics,* Pergamon Press, Oxford, 1980.
59. Harrington, R. F., *Field Computation by Moment Methods,* Macmillan Comp., New York, 1968.
60. Newton, R. G., *Scattering Theory of Waves and Particles,* Springer-Verlag, New York, 1982.
61. Richmond, J. H., "Scattering by a dielectric cylinder of arbitrary cross section shape," *IEEE-AP,* Vol. 13, p. 334, 1965.

62. Ouda, M., and A. Sebak, "Scattering from lossy dielectric cylinders using a multifilament current model with impedance boundary conditions," *IEE-Proc. H,* Vol. 139, p. 429, 1992.
63. Yeh, C., "Backscattering cross section of a dielectric elliptical cylinder," *J. Opt. Soc. Am.,* Vol. 55, p. 309, 1965.
64. Wu, T. K., and L. L. Tsai, "Scattering by arbitrarily cross-sectioned layered lossy dielectric cylinders," *IEEE-AP,* Vol. 25, p. 518, 1977.
65. Goedecke, G. H., and S. G. O'Brien, "Scattering by irregular inhomogeneous particles via the digitized green's function algorithm," *Appl. Optics,* Vol. 27, p. 2431, 1988.
66. Ishimaru, A., *Wave Propagation and Scattering in Random Media,* Vol. 1: *Single Scattering and Transport Theory,* Academic Press, San Diego, 1978.
67. Nieto-Vesperinas, M., *Scattering and Diffraction in Physical Optics,* John Wiley and Sons, New York, 1991.
68. Abramowitz, M., and I. A. Stegun (eds.): *Pocketbook of Mathematical Functions,* Verlag Harri Deutsch, Frankfurt/Main 1984.
69. Burberg, R., "Die Beugung elektromagnetischer Wellen am unendlich langen Kreiszylinder," *Z. Naturforschg.,* Vol. 11a, p. 800, 1956.
70. Kerker, M., D. Cooke, W. A. Farone, and R. A. Jacobsen, "Electromagnetic scattering from an infinite circular cylinder at oblique incidence," *J. Opt. Soc. Am.,* Vol. 56, p. 487, 1966.
71. Macke, A., M. I. Mishchenko, K. Muinonen, and B. E. Carlson, "Scattering of light by large nonspherical particles: ray tracing approximation versus T-Matrix method," *Optics Lett.,* Vol. 20, p. 1934, 1995.
72. Jacobus, U., and F. M. Landstorfer, "Improved PO-MM hybrid formulation for scattering from three-dimensional perfectly conducting bodies of arbitrary shape," *IEEE-AP,* Vol. 43, p. 162, 1995.
73. Magono, C., and C. W. Lee, "Meteorological classification of natural snow crystals," *J. of the Faculty of Science of the Hokkaido Univ.,* Vol. 2, p. 321, 1966.
74. Ono, A., "The shape and riming properties of ice crystals in natural clouds," *J. Atmos. Sci.,* Vol. 26, p. 138, 1969.
75. Auer, A. H., Jr., and D. L. Veal, "The dimensions of ice crystals in natural clouds," *J. Atmos. Sci.,* Vol. 27, p. 919, 1970.
76. Kinne, S., and K. N. Liou, "The effects of the nonsphericity and size distribution of ice crystals on the radiative properties of cirrus clouds," *Atm. Res.,* Vol. 24, p. 273, 1989.

77. Kuik, F., J. F. de Haan, and J. W. Hovenier, "Single scattering of light by circular cylinders," *Appl. Optics,* Vol. 33, p. 4906, 1994.
78. Stammes, P., "Light Scattering Properties of Aerosols and the Radiation inside a Planetary Atmosphere," Dissertation (Ph.D), Freie Universitat Amsterdam, 1989.
79. Takano, Y., and K. N. Liou, "Solar radiative transfer in cirrus clouds, Part 1: Single scattering and optical properties of hexagonal ice crystals," *J. Atmos. Sci.,* Vol. 46, p. 3, 1989.
80. Takano, Y., and K. N. Liou, "Radiative transfer in cirrus clouds, Part 3: Light scattering by irregular ice crystals," *J. Atmos. Sci.,* Vol. 52, p. 818, 1995.
81. Yang, P., and K. N. Liou, "Light scattering by hexagonal ice crystals: comparison of finite-difference time domain and geometric optics models," *J. Opt. Soc. Am. A,* Vol. 12, p. 162, 1995.
82. Yang, P., and K. N. Liou, "Finite-difference time domain method for light scattering by small ice crystals in three-dimensional space," *J. Opt. Soc. Am. A,* Vol. 13, p. 2072, 1996.
83. Asano, S., and G. Yamamoto, "Light scattering by a spheroidal particle," *Appl. Optics,* Vol. 14, p. 29, 1975.
84. Mugnai, A., and W. J. Wiscombe, "Scattering of radiation by moderately nonspherical particles," *J. Atmos. Science,* Vol. 37, p. 1291, 1980.
85. Mugnai, A., and W. J. Wiscombe, "Scattering from nonspherical Chebyshev particles: 1. cross sections, single-scattering albedo, asymmetry factor, and backscattered fraction," *Appl. Optics,* Vol. 25, p. 1235, 1985.
86. Mugnai, A., and W. J. Wiscombe, "Scattering from nonspherical Chebyshev particles: 2. means of angular scattering patterns," *Appl. Optics,* Vol. 27, p. 2405, 1988.
87. Mugnai, A., and W. J. Wiscombe, "Scattering from nonspherical Chebyshev particles: 3. variability in angular scattering patterns," *Appl. Optics,* Vol. 28, p. 3061, 1989.